NONDESTRUCTIVE DAMAGE DETECTION BY SIMULTANEOUS IDENTIFICATION OF STIFFNESS AND DAMPING

A Dissertation

by

SANG SU HYUNG

Submitted to the Office of Graduate Studies of
Texas A&M University
in partial fulfillment of the requirements for the degree of

DOCTOR OF PHILOSOPHY

December 2007

Major Subject: Civil Engineering

NONDESTRUCTIVE DAMAGE DETECTION BY SIMULTANEOUS IDENTIFICATION OF STIFFNESS AND DAMPING

A Dissertation

by

SANG SU HYUNG

Submitted to the Office of Graduate Studies of
Texas A&M University
in partial fulfillment of the requirements for the degree of

DOCTOR OF PHILOSOPHY

Approved by:

Chair of Committee,	Norris Stubbs
Committee Members,	Joseph Bracci
	Lynn Beason
	Robert Bolton
Head of Department,	David Rosowsky

December 2007

Major Subject: Civil Engineering

ABSTRACT

Nondestructive Damage Detection by Simultaneous Identification of Stiffness and Damping. (December 2007)

Sang Su Hyung,

B.S., Seoul National University, Korea;

M.S., Seoul National University, Korea

Chair of Advisory Committee: Dr. Norris Stubbs

The objective of this study is to develop a nondestructive damage evaluation methodology that can identify simultaneously both stiffness and damping changes in a structure. Two approaches are used to meet the stated objectives. First, a method is developed on the basis of the conservation of total energy; second, the other method utilizes the acceleration-structural parameters (stiffness and damping) sensitivities. The total energy in a system consists of the sum of the kinetic energy, the potential energy, and the dissipated energy. In the second approach, a baseline structure is first identified. A baseline structure is defined to be a structural system having a similar dynamic response to the existing structure with no damage. In this study, natural frequencies and modal damping values are used to identify the baseline structure.

The performance of the developed methodology is validated using several numerical experiments; Two classes of structures are considered here: (1) a high-rise building modeled as shear beams and (2) a two-span continuous beam structure. In the shear beam model of the structure, the damping damage is simulated by increasing the Newtonian dash pot constant which models the dissipation at the damaged story. For the two-span continuous beam structure, it is assumed that damping of the undamaged structure can be modeled using a proportional damping matrix. The damping matrix of the damaged structure is modeled as the combination of a proportional damping matrix

of the undamaged structure and a stiffness proportional damping matrix of the damaged element.

Three damage cases are investigated for each of the two structures considered here. Only one element experiences damping damage for the first damage scenario. In the second damage scenario, both stiffness damage and damping damage are simulated with different severities in one element of the model. In the third damage scenario, two elements are simulated with stiffness damage and damping damage, to verify whether or not the developed methodology works for multi-damage cases.

The proposed method is modified to use mode shapes and the modified proposed method is applied to experimental data to identify stiffness damage in a R/C structure.

ACKNOWLEDGEMENTS

I would like to give thanks to Dr. Norris Stubbs, my advisor, who served as chairman of my committee, for all his guidance, invaluable help, continuous encouragement, and unceasing generosity throughout my studies at Texas A&M. I could not have succeeded in my study at Texas A&M without his help. It was an honor to have him as my advisor. He showed me the model of the professor that I would like to pursue. I also would like to thank the other members of my committee: I thank Dr. Joseph Bracci for his helpful discussion and instruction. His experimental data was really valuable for this study. I would like to express my thanks to Dr. Lynn Beason for his advice. I worked with him as a T.A. for more than 3 semesters. I enjoyed the humor and friendship we shared. I thank Dr. Robert Bolton for his sincere support.

I am really indebted to my brothers. They were always worried about me and my family and gave me encouragement and invaluable help. I really thank my parents and parents in-law. I can not express my thanks enough for their help and their prayers. My wife and I are very excited to see them soon. We prayed, do pray and will continue to pray for them.

I have received the most invaluable gifts in the world during my study at Texas A&M, Chae-eun and Chae-rin, my two daughters. The joy they give me is immeasurable. I really, really, two reallys are not enough, thank my wife Yoona Ko for her understanding, patience, and sacrifices. I give her my sincere love and thank.

I thank and praise God for his grace and what he gives me and has done through and for me.

TABLE OF CONTENTS

Page

TABLE OF CONTENTS (continued)

Page

TABLE OF CONTENTS (continued)

Page

LIST OF TABLES

Page

LIST OF TABLES (continued)

LIST OF TABLES (continued)

Page

LIST OF TABLES (continued)

Page

LIST OF FIGURES

Page

LIST OF FIGURES (continued)

Page

LIST OF FIGURES (continued)

Page

LIST OF FIGURES (continued)

Page

LIST OF FIGURES (continued)

Page

LIST OF FIGURES (continued)

Page

1 INTRODUCTION

1.1 STATEMENT OF THE PROBLEM

The accumulation of damage in a structural member can cause structural failure. Structural failure of a civil engineering structure can endanger human lives and result in huge economic losses. Consequently, it is very important to check periodically the integrity of the structure to avoid the collapse of the structure. Nondestructive Damage Evaluation (NDE) involves, among other things, locating and estimating severities of damage in a structure without compromising the integrity of the structure. By combining the technique of NDE with periodical monitoring, a check of the integrity of the structure can be accomplished.

Even if structures were designed and constructed very carefully, they can still be exposed to such environmental hazards as earthquakes, wind, aging, and higher service loads than those used in the design. Therefore, damage can occur in any structure. The location of a damaged element and its severity can be estimated by NDE. NDE can be applied to both structures which are suspected to have sustained damage or structures in which the consequencies of failure are very severe.

The ultimate goal of NDE is to locate and estimate the severity of damage as soon as possible after the damage has occurred in a structure. Many studies have been conducted to locate stiffness damage using the changes of modal parameters, especially mode shape vectors and natural frequencies. However, very few research studies have attempted to identify, simultaneously, changes in stiffness and damping characteristics of the elements of a structure. According to previous studies, if the changes of damping characteristics can be detected, damaged elements in the structure may be localized at an earlier stage, compared to stiffness damage, and consequently premature structural failure may be avoided.

This dissertation follows the style and format of the *ASCE Journal of Structural Engineering*.

The correction of the damaged element when damage is very small may result in a significant reduction in repair costs and the other unwanted consequencies of failure.

This study deals with damage detection approaches which can identify, simultaneously, changes in stiffness and damping characteristics in a structure.

1.2 BACKGROUND

1.2.1 Overview

Damage may be defined as any change introduced into a system that yields unwanted performance of the system (Doebling et al. 1998). Currently available NDE methods can be categorized into local methods and global methods. Local methods examine the structure one piece at a time. Local methods include visual inspection, acoustic emission, ultrasonic, radiography, eddy current, and magnetic particle inspections (Bray and McBride 1992).

Global damage detection methods usually examine the changes in vibration characteristics of the structure (Doebling et al. 1998). The basic idea behind vibration-based damage detection is that changes in physical properties are reflected in modal parameters such as natural frequencies, mode shapes, and modal damping values. On the basis of their performance, these global methods can be classified into four levels of damage detection. The four levels are (Rytter 1993): (1) Level I – determination of whether damage is present in the structure; (2) Level II – Level I plus the determination of the location of damaged elements; (3) Level III – Level II plus the severity estimation of the damaged elements; and (4) Level IV – Level III plus the evaluation of the impact of the damage on the performance of structure.

Two general approaches are available for global damage detection: (1) “the Response-based approach”, which relates the response data directly to the damage; and (2) “the Model-based approach”, which updates structural parameters of an initial finite element model of the structure so that the analytical responses and measured responses are close in some optimal way. The Response-based approach is relatively fast and inexpensive, while the Model-based approach is expensive and time-consuming.

However, the Model-based approach can detect damaged elements and estimate the damage in a single iteration, based on the updated parameters. In this study, Level III model-based damage detection models are proposed.

1.2.2 NDE Methods Based on System Identification

System Identification is the process of selecting a model of a system from a specified class of models, to which the system under study is most equivalent, based on input and output data (Zadeh 1962). The process of system identification consists of three main steps: (1) defining a model and planning experiments to measure the response of the system (model selection and testing); (2) Estimating the unknown parameters of the model, using the defined model and the measured response (parameter estimation); and (3) validating and refining the model (model validation and model updating).

Here, the term model is defined as a representation of a system that contains information of that system in a usable form. Usually, the construction of a model begins with the application of basic physical laws of the process under study. The construction of a model is equivalent to mapping from a data set of input and output pairs to a set of potential models (Ljung 1988). Parameter estimation can be defined as the determination of the parameters that govern the behavior of a specific model, based on the assumption that the structure of the model is known (Eykhoff 1974). The essence of parameter estimation is to find the values of the model parameters that render the difference between the responses of the calibrated model and real structure a minimum. Model validation is defined as the refinement of an analytical model so that the response of the analytical model approaches the measured responses. For model validation, natural frequencies, mode shapes, or modal damping values obtained from modal testing can be compared with those from finite element models.

For the identification problem, incompleteness of the response measurements can give biased parameter estimations (Cottin 1998) and inadequacy of a mathematical model may yield discrepancy between modeling and reality (Yao 1998). In the field of structural engineering, finite element models are commonly used to build static and

dynamic numerical models of the subject structure. However, the identified model may not be correct if the model is not updated using results from modal testing (Juang 1994).

Currently available system identification techniques include Time Domain Identification Procedures, Perturbation Methods, Sensitivity Matrix Methods, Frequency Response Function Methods, and Static Measurement Methods. In Time Domain Identification Procedures, accelerations and excitation forces are assumed to be known for a given time interval, and displacements and velocities are obtained by integrating the accelerations with respect to time. For example, Agbabian et al.(1990) applied a time-domain identification procedure to identify structural parameters of a 3-DOF mechanical system. In that study, noise-polluted output measurements and the excitation were used to evaluate the procedure. The results were reported as a statistical estimation of parameters. In addition, Natke(1982), and Tomlinson(1985), identified the system matrices for a variety of nonlinear structural dynamic problems using time domain data.

Perturbation methods are also utilized to solve nonlinear differential equations. In perturbation methods, a solution that may depend on a presumed small quantity is assumed and the deviations of eigenvalues and eigenvectors between the analysis and the test are assumed to be relatively small. For example, Chen and Wada (1975) applied a matrix perturbation technique to update the response analysis based on the assumption that analytical eigenvalues and eigenvectors differ little from those of the equivalent experiment. Also, Sackman et al.(1983) used a perturbation method to determine modal properties of a structural system having attached light equipment and determined the dynamic response of the structural system to any excitation using the derived modal properties and mode superposition method.

The applications of sensitivity-type analyses have increased, since the measured natural frequencies can be numerically duplicated using updating techniques. For example, Collins et al.(1974) formulated a sensitivity type method to identify the structural parameters in a statistical sense using experimental measurements of the modal parameters (natural frequencies and mode shapes). The sensitivity matrix technique was extended to system identification and nondestructive damage detection

studies by Stubbs (1985). Later, Stubbs and Kim (1996) used the sensitivity method approach to identify baseline models of structures. In the latter method, sensitivity matrices relating the fractional changes in stiffness elements to the fractional changes of eigenvalues of the system were used to identify the stiffness of the baseline structure.

Most system identification techniques utilize modal parameters. To extract modal parameters, frequency response functions (FRF) must be generated. However, several methods do not use the frequency response function measurements directly. Lin and Ewins (1994) proposed a technique for model updating that use the measured frequency response functions directly. Also, Mottershead (1990) suggested a method that can identify structural parameters utilizing measured frequency responses and the least squares technique. In that study, a simply-supported beam model was employed to illustrate the validity of the suggested method.

In another approach, the static measurement method, measured deformations, which are induced by static loads such as a slowly moving truck on bridge or a slowly moving mass on a building, are used for the identification of the structural parameters. Hajela and Soerio (1990) used not only dynamic responses but also static displacements to simulate higher modes (which are difficult to measure). Banan et al (1994) identified the stiffness parameters using different number of static load cases and different numbers of measured displacements. Nam(2001) selected several criteria to define the accuracy of the responses of identified structures with respect to the measured responses: modal scale factor (MSF), modal assurance criterion (MAC), coordinate modal assurance criterion (COMAC), frequency domain assurance criterion (FDAC), and frequency response assurance criterion (FRAC). Note that COMAC and FRAC reflect the degree of correlation between the analytical responses and experimentally measured responses while MAC and FDAC can indicate the global agreement of the responses. Nam(2001) also utilized the following four criteria to evaluate the SID techniques: (1) Can the structural parameters be identified?; (2) How much computational effort is needed to implement the SID technique?; (3) How easily can the SID technique be applied to complex structural systems?; and (4) How accurate are the structural

parameters identified from the SID techniques? Based on these criteria, the sensitivity method was selected as the best system identification technique.

1.2.3 NDE Methods from Changes in Modal Parameters

Damage in a structure can cause various changes in the structural response such as frequency shifts, mode shape variation, and modal flexibility changes. The major existing NDE methods are listed in Table 1-1 (Kim 2002).

Table 1-1 Existing NDE Methods

Existing NDE Methods	Author	Year
Methods Utilizing Frequency Changes	Lifshitz	1969
Methods Utilizing Mode Shape Changes	Fox	1992
Methods Utilizing Mode Shape Curvature Changes	Pandey	1991
Methods Utilizing Strain Mode Shape Changes	Chance	1994
Methods Utilizing Strain Energy Changes	Stubbs	1992
Methods Utilizing Modal Flexibility Changes	Biswas	1994

The essential concept governing the early studies of vibration-based NDE is that changes in local stiffnesses can cause changes in eigenfrequencies. Lifshitz and Roten (1969) performed an experiment in which particle-filled resin specimens were subjected to a tensile loading superimposed with low amplitude longitudinal and torsional oscillations. They observed any potential changes of the dynamic moduli and natural frequency shift. Later, Adams et al. (1978) suggested a method based on receptance analysis to locate the damaged element and estimate the severity of the damage in a one dimensional axial member using vibration measurements made at single location on the structure.

Cawley and Adams (1979) used the sensitivity approaches to predict the location and magnitude of damage in a two dimensional plate structure. The sensitivity-based

Cawley and Adams's approach was extended and generalized by Stubbs (1985) and Stubbs and Osgueda (1990a, 1990b). Later, it was shown that the measured resonant frequencies might be dependent on the site's air temperature, humidity, mean air pressure, and mean rainfall on the previous day of the test day (Salawu 1997 and Farrar, et al. 2000). Given the changes in natural frequencies, usually only the presence of damage can be determined and the location of damage cannot be detected. If multiple frequency shifts are provided, the location of damage can be detected with the combination of changes in natural frequencies.

The use of mode shapes was suggested as a better approach to detect the location of damage compared to the use of only resonant frequencies (Fox 1992). However, it was shown that changes in the displacement mode shapes between the undamaged and damaged structure may not be localized in the damage region (Pandey et al. 1991; Yao et al. 1992). Pandey et al.(1991) performed numerical studies on cantilever beams and simple-supported beams. They suggested that the severity of damage in a structure can be estimated by the magnitude of changes in curvature of the mode shapes. They also checked natural frequencies, MAC, COMAC, and displacement mode shape to determine whether any of the proposed techniques could indicate the location of damage. However, only the mode shape curvature, which was obtained by central difference approximation of displacement mode shape, could locate the damage.

Wahap and Roeck (1999) suggested a Curvature damage factor which combined the differences in the curvature of the mode shape for all modes to one number for each measured point. This technique was demonstrated numerically with a simple beam and two-span continuous beam, and applied to a real structure, namely the Z24 bridge in Switzerland. Kramer et al.(1999) investigated the influence of the environment on the dynamic characteristics through the tests conducted on Z24 bridge.

Some researches suggested strain mode shape as a better indicator of damage rather than displacement mode shape. For example, Yao et al. (1992) showed that the exact location of damage could not be detected with displacement mode shapes in their experiment on a 5-story frame. In their experiment, strain mode shapes at or near the

damage location exhibited the largest change while strain mode shapes remote from the damage location remained unchanged. Chance et al. (1994) used strain mode shapes instead of curvature mode shapes, which are obtained through the differentiation of the displacement mode shapes for damage location. In their experiment, they used a crack device to simulate a fatigue crack, and showed that changes in strain mode shapes are most effective for fault detection. Chen and Swamidas (1994) also showed that the difference of strain mode shapes between a cracked and an uncracked plate could be used for the location of crack through FE analysis. They observed that the amplitude of strain FRF decreased as the crack depth was increased.

In some research studies, modal strain energy was used for damage detection. For example, the Damage Index (DI) method to locate and estimate the severity of damage in a structure using changes in the modal strain energy was proposed by Stubbs et al.(1992). This method is based on the assumption that the fractional modal strain energy of a potential damaged element is not changed for a small damage event. Stubbs et al.(1995) demonstrated the feasibility and practicality of this method by applying the procedure to a full-scale bridge. This method was expanded to perform damage detection without baseline modal parameters(Stubbs and Kim 1996). Petro et al. (1997) proposed a modal strain energy damage index based on a change rate in modal strain energy between undamaged and damaged structures. The authors showed that the changes in the modal strain energy estimated from mode shape can be used for location of damage, using modal test results on an aluminum plate. Carrasco et al. (1997) performed modal tests on a space truss structure with 18 different damage cases. In their studies, difference in modal strain energy, weighted by modal strain energy distribution for undamaged structure, was suggested for damage location. They recommended that for damage detection, lumping the modal strain energies at the nodes is better than observing the modal strain energy at the element level. Shi et al. (2000) showed that the modal strain energy change ratio can be used for damage location. The authors quantified damage with the sensitivity coefficient of Modal Strain Energy Change (MSEC) to damage and MSEC obtained from expanded damaged mode shape by

analytical undamaged mode shape. Nicholson and Alnefaie (2000) compared three indices for damage detection, the Strain Energy Damage Index(SEDI), SEDI2, and the Modal Moment Index(MMI). Among them, the Modal Moment Index showed the best performance for damage severity estimation. The MMI was based on the assumption that bending moment is not changed by damage and jumps sharply at the damaged location.

Modal flexibility changes were also used for damage detection. For example, Rubbin and Coppolono (1983) proposed a normalized flexibility parameter for monitoring offshore jacket platforms using ambient vibration responses. Pandey and Biswas(1994) developed an approach based on the changes in the flexibility matrix which is the inverse of the stiffness matrix for detecting damage in structures. The advantage of this method is that the flexibility matrix can be approximated with a few measurable lower modes. Toksoy and Aktan (1994) applied modal flexibility method to three-span reinforced-concrete high-way bridge. They demonstrated the sensitivity of modal flexibility to damage in RC slabs which were highly redundant. Aktan el al(1994) applied modal flexibility method to seven high-way bridges. They compared bridge deflections obtained from modal flexibility to measured deflections and verified the reliability of modal flexibility. Mayes(1995) proposed an algorithm (Structural Translation and Rotation Error Checking) and applied it to the I-40 bridge in Albuqueerque, New Mexico. In that experiment, better results were obtained with static flexibility data as compared with the predictions using individual mode shape.

1.2.4 Damping Damage Detection

Damping is one of the more important model parameters for the design and analysis of vibrating structures. However, unfortunately, it is impossible to identify all the mechanisms of damping that dissipate vibrational energy of actual structures. The damping coefficient cannot be calculated from the dimensions of the structure and the sizes of the structural elements and the damping coefficient varies with different environmental effects. Consequently, the damping of materials and structures are usually determined experimentally and represented in a highly idealized manner.

Lifshitz and Rotem(1969) showed that damping is more sensitive than the extensional (or torsional) modulus to damage. In their tests, a decrease of 8% to 14% in the dynamic moduli was observed with an increase of 40% in the logarithmic decrement. Tilly (1977) observed that damping values of highway bridges are influenced by the type of excitation and the amplitude of movement.

Savage and Hewlett(1978) observed that geometrically similar unstressed beams had significantly higher damping ratios than prestressed beams and hypothesized that the difference of damping ratio was caused by micro-cracking along the beam's length. In the cracked region, microscopic movement can cause friction between solid concrete and this friction can increase the damping ratio. In the prestressed beam, the microcracks were effectively closed up by the post-load and friction motion was reduced.

Dorn (1982) found that the changes in energy consumption can be used to characterize the damage. Variation in the damping properties was measured from the changes in energies supplied into the system which is always operated at its proper frequency. In Dorn's experiment, the fatigue strength was estimated rapidly with the changes in damping. Jeary and Ellis (1984) also suggested change in damping as a potential indicator of structural changes since damping changes may indirectly indicate small local stiffness change. When both frequencies and mode shapes are insensitive to damage, damping may be the only indicator of damage.

Tsai and Yang(1988) suggested that the damping matrix derived from system identification techniques could be used to detect the location of damage. Salane and Baldwin made tests on a single span bridge laboratory model and a full-scale highway bridge and concluded that changes in damping ratios indicate that structural changes had occurred. Hearn and Testa(1991) conducted tests on a steel frame subjected to sine wave load cycles and found sharp change in damping for each damage case. The same authors made tests on the transverse motion of wire ropes under constant tension and found that damping increased with damage.

Slastan and Pietrzko(1993) also reported a general increase in damping values after the initiation of cracks in reinforced concrete beams. Kawiecki (2001) applied

arrays of surface-bonded piezoelements to determine modal damping characteristics of a tested structure. A 0.5 mm thick Dyad 606 viscoelastic patch was used to simulate damage and different modal damping characteristics for the damaged structure were obtained from modal damping characteristics for the undamaged structure. The authors expected that this approach can be applied for structural health monitoring because structural or material damage is frequently associated with changes in damping.

1.3 LIMITATIONS OF CURRENT NDE TECHNIQUES

Although a very large number of NDE techniques have been developed, most of them are focused on the detection of stiffness damage. These methods are based on the assumption that stiffness changes cause modal parameter changes and damage can be detected only when stiffness parameters are changed. However, in the early stage of damage, stiffness parameters change very little, while damping characteristics may change more significantly. When local damping characteristics are changed, mode shapes do not change significantly. Furthermore, it is very difficult to measure the mode-shape differences. Thus, NDE methods using mode shapes or mode shape curvatures cannot be applied to damping damage detection. The same situation applies to the difference in natural frequencies. Among the three modal parameters available, modal damping values will experience the most obvious changes; however, modal damping values are global parameters, since they do not directly reflect local damping changes. Consequently, new NDE techniques which can detect the changes not only in stiffness parameters but also in damping characteristics are needed.

.

1.4 OBJECTIVES OF THIS WORK

The goal of this study is to develop a methodology to locate and estimate simultaneously the severity of both stiffness and damping damage in structures. This goal is accomplished by meeting the following four objectives:

1. Identify a selected baseline structure;

2. Develop a methodology to locate and estimate the severities of stiffness and damping damage in structural elements;
3. Validate the methodology using numerical simulations of high-rise building modeled as shear building;
4. Validate the methodology using numerical simulations of a two-span continuous beam structure.

1.5 SIGNIFICANCE OF THIS WORK

The study proposed here is important since not only stiffness change but also damping change can be detected, located, and sized. In NDE, the capability to detect and estimate damage as soon as possible after the damage has occurred in structure is a paramount task. For early detection of damage, more sensitive indicators of damage should be developed. Most current NDE techniques focus on the detection of stiffness damage. However, as we have argued earlier, damping changes may be more sensitive to damage than stiffness changes. Damping characteristics can be changed significantly while stiffness changes remain negligible. So, if both damping damage and stiffness damage can be detected, damage can be detected at an earlier stage and the documentation of such damage can lead to such desirable consequencies as the saving of lives, reduction of property losses, and a reduction in maintenance cost and business loss time.

In addition, the results of this study can be extended to the problem of estimating the integrity of dampers that have been incorporated to control the motion of critical structures. Recently, large-scale dampers have been used to decrease member design load demands and displacement demands. However, if the incorporated dampers are damaged, potentially catastrophic system failure may ensue in the structure. The proposed NDE method is expected to be applied to the estimation of the integrity of dampers incorporated in structure to dissipate energy.

2 DEVELOPMENT OF NDE METHODOLOGY BASED ON THE ENERGY CONSERVATION

2.1 INTRODUCTION

In previous studies, the data from modal space (such as mode shapes and eigenfrequencies) were used to locate and size stiffness-damaged element. However, in this study, the responses in the time domain (such as accelerations-time, velocities-time, and displacements-time) are used for the detection of damaged element and estimation of the severity. In this study, NDE methods based on the conservation of the total energy in a system which can simultaneously detect and estimate both of stiffness damaged elements and damping damaged elements are developed.

2.2 DERIVATION OF EQUATIONS FOR ENERGY CONSERVATION

The basic concept driving the proposed method is that the total energy in a system is constant for every time step in the response of the system. In any conservative elastic system, the sum of the potential and the kinetic energy is constant at any time step, whether the system is linear or nonlinear (Reddy, 1984). If damping is considered, dissipated energy also should be taken into consideration and the conservation of energy, including dissipated energy, can be expressed as

$$E_{pot} + E_{kin} + E_{diss} = \Phi = \text{const} \qquad \textbf{(2-1)}$$

Here, Φ represents for the total energy of the system. The model that will be considered in this development is shown in Fig. 2-1. The total potential energy of this system, E_{pot}, is given by

$$E_{pot}(t) = \sum_{j=1}^{NS} \frac{k_j}{2} \Delta x_j(t)^2 \qquad \textbf{(2-2)}$$

for a system with NS stiffness elements. The parameter k_j is the stiffness of jth element and Δx_j is the deformation experienced by jth element. The quantity E_{kin} is the total kinetic energy of the system and is given by

$$E_{kin} = \sum_{j=1}^{NM} \frac{m_j}{2} \dot{x}_j(t)^2 \qquad \textbf{(2-3)}$$

where NM is the number of lumped masses, and m_j and $\dot{x}_j$ are lumped mass and velocity of the jth DOF, respectively. The quantity E_{diss} is the total dissipated energy of the system and can be expressed as

$$E_{diss} = \sum_{j=1}^{ND} \int_{t_1}^{t_n} c_j \Delta\dot{x}_j(t)^2 \, dt \qquad \textbf{(2-4)}$$

where ND is the number of damping elements. c_j and $\Delta\dot{x}_j$ denote the damping coefficient and the velocity of the elongation of element j, respectively. Parameters t_1 and t_n are the first time when the observation was taken, and current time, respectively. Thus in expanded from, the equation for energy conservation is given by

$$\sum_{j=1}^{NS} \frac{k_j}{2} \Delta x_j(t)^2 + \sum_{j=1}^{NM} \frac{m_j}{2} \dot{x}_j(t)^2 + \sum_{j=1}^{ND} \int_{t_1}^{t_n} c_j \Delta\dot{x}_j(t)^2 \, dt = \Phi \qquad \textbf{(2-5)}$$

Since, responses are available only at discrete times, the above equation becomes

$$\sum_{j=1}^{NS} \frac{k_j}{2} {}^{n}\Delta x_j{}^2 + \sum_{j=1}^{NM} \frac{m_j}{2} {}^{n}\dot{x}_j{}^2 + \sum_{j=1}^{ND} \int_{t_1}^{t_n} c_j {}^{n}\Delta\dot{x}_j{}^2 dt = \Phi \qquad \textbf{(2-6)}$$

where superscript n denotes the nth readings.

To calculate kinetic energy, potential energy, and dissipated energy, displacements and velocities are needed. These values are obtained by numerical integration of the measured acceleration. Conceptually, the values could also be obtained from dedicated displacement and velocity sensors.

It is convenient to move the kinetic energy to the right-hand side of Equations (2.6) and the total energy to the left-hand side of Equation (2.6), since the kinetic energy is assumed as known and the total energy is assumed as unknown. Thus, Equation (2.6) becomes:

$$\sum_{j=1}^{NS} \frac{k_j}{2} {}^{n}\Delta x_j^{\,2} + \sum_{j=1}^{ND} \int_{t_1}^{t_n} c_j {}^{n}\Delta \dot{x}_j^{\,2} dt - \Phi = -\sum_{j=1}^{NM} \frac{m_j}{2} {}^{n}\dot{x}_j^{\,2} \qquad \textbf{(2-7)}$$

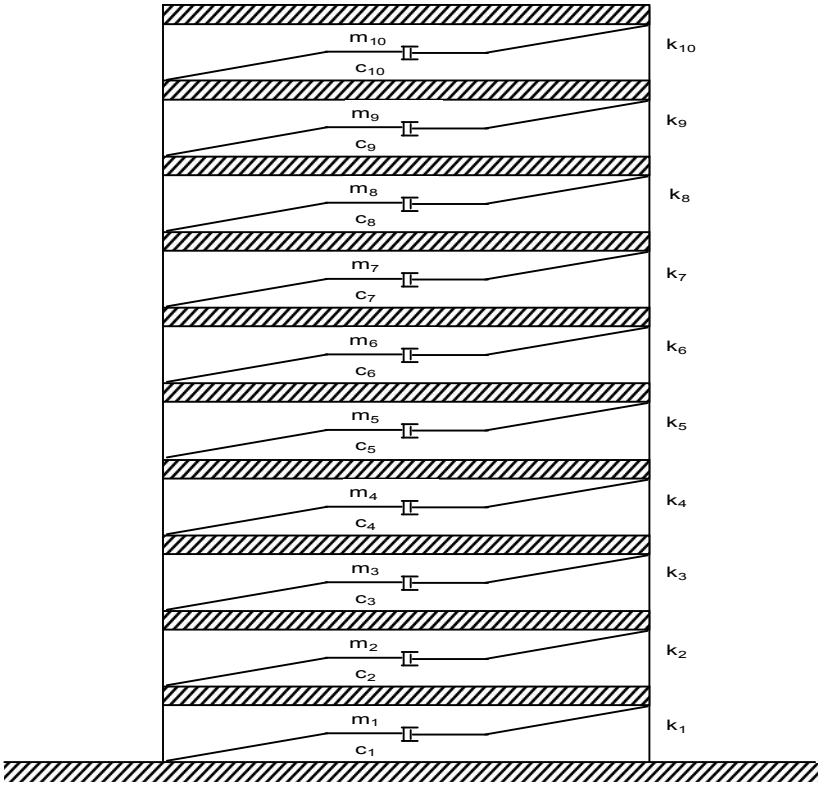

Fig. 2-1 Model of 10-Story Shear Building

2.3 DERIVATION OF EQUATIONS FOR IDENTIFICATION OF STIFFNESS AND DAMPING

The energy conservation equation can now be defined for any time step, and the resulting equations, evaluated for arbitrary time steps, can be expressed in matrix form as follows:

$$\begin{bmatrix} \frac{1}{2}\Delta x_1(t_{s1})^2 & \frac{1}{2}\Delta x_2(t_{s1})^2 & \cdots & \frac{1}{2}\Delta x_{NS}(t_{s1})^2 & \int_{t_1}^{t_{s1}}\Delta\dot{x}_1(t)^2dt & \int_{t_1}^{t_{s1}}\Delta\dot{x}_2(t)^2dt & \cdots & \int_{t_1}^{t_{s1}}\Delta\dot{x}_{ND}(t)^2dt & -1 \\ \frac{1}{2}\Delta x_1(t_{s2})^2 & \frac{1}{2}\Delta x_2(t_{s2})^2 & \cdots & \frac{1}{2}\Delta x_{NS}(t_{s2})^2 & \int_{t_1}^{t_{s2}}\Delta\dot{x}_1(t)^2dt & \int_{t_1}^{t_{s2}}\Delta\dot{x}_2(t)^2dt & \cdots & \int_{t_1}^{t_{s2}}\Delta\dot{x}_{ND}(t)^2dt & -1 \\ \vdots & \vdots & \vdots & \vdots & \vdots & \vdots & \vdots & \vdots & \vdots \\ \frac{1}{2}\Delta x_1(t_{sN})^2 & \frac{1}{2}\Delta x_2(t_{sN})^2 & \cdots & \frac{1}{2}\Delta x_{NS}(t_{sN})^2 & \int_{t_1}^{t_{sn}}\Delta\dot{x}_1(t)^2dt & \int_{t_1}^{t_{sn}}\Delta\dot{x}_2(t)^2dt & \cdots & \int_{t_1}^{t_{sn}}\Delta\dot{x}_{ND}(t)^2dt & -1 \end{bmatrix} \begin{Bmatrix} k_1 \\ k_2 \\ \vdots \\ k_{NS} \\ c_1 \\ c_2 \\ \vdots \\ c_{ND} \\ \Phi \end{Bmatrix} = \begin{Bmatrix} -\sum_{j=1}^{NM}\frac{m_j}{2}\dot{x}_j(t_{s1})^2 \\ -\sum_{j=1}^{NM}\frac{m_j}{2}\dot{x}_j(t_{s2})^2 \\ \vdots \\ -\sum_{j=1}^{NM}\frac{m_j}{2}\dot{x}_j(t_{sn})^2 \end{Bmatrix} \quad \textbf{(2-8)}$$

Let

$$\mathbf{\Lambda} = \begin{bmatrix} \frac{1}{2}\Delta x_1(t_{s1})^2 & \frac{1}{2}\Delta x_2(t_{s1})^2 & \cdots & \frac{1}{2}\Delta x_{NS}(t_{s1})^2 & \int_{t_1}^{t_{s1}}\Delta\dot{x}_1(t)^2dt & \int_{t_1}^{t_{s1}}\Delta\dot{x}_2(t)^2dt & \cdots & \int_{t_1}^{t_{s1}}\Delta\dot{x}_{ND}(t)^2dt & -1 \\ \frac{1}{2}\Delta x_1(t_{s2})^2 & \frac{1}{2}\Delta x_2(t_{s2})^2 & \cdots & \frac{1}{2}\Delta x_{NS}(t_{s2})^2 & \int_{t_1}^{t_{s2}}\Delta\dot{x}_1(t)^2dt & \int_{t_1}^{t_{s2}}\Delta\dot{x}_2(t)^2dt & \cdots & \int_{t_1}^{t_{s2}}\Delta\dot{x}_{ND}(t)^2dt & -1 \\ \vdots & \vdots & \vdots & \vdots & \vdots & \vdots & \vdots & \vdots & \vdots \\ \frac{1}{2}\Delta x_1(t_{sN})^2 & \frac{1}{2}\Delta x_2(t_{sN})^2 & \cdots & \frac{1}{2}\Delta x_{NS}(t_{sN})^2 & \int_{t_1}^{t_{sn}}\Delta\dot{x}_1(t)^2dt & \int_{t_1}^{t_{sn}}\Delta\dot{x}_2(t)^2dt & \cdots & \int_{t_1}^{t_{sn}}\Delta\dot{x}_{ND}(t)^2dt & -1 \end{bmatrix} \quad \textbf{(2-9)}$$

$$\mathbf{\Delta} = \begin{Bmatrix} k_1 \\ k_2 \\ \vdots \\ k_{NS} \\ c_1 \\ c_2 \\ \vdots \\ c_{ND} \\ \Phi \end{Bmatrix}, \text{and} \quad \mathbf{\beta} = \begin{Bmatrix} -\sum_{j=1}^{NM}\frac{m_j}{2}\dot{x}_j(t_{s1})^2 \\ -\sum_{j=1}^{NM}\frac{m_j}{2}\dot{x}_j(t_{s2})^2 \\ \vdots \\ -\sum_{j=1}^{NM}\frac{m_j}{2}\dot{x}_j(t_{sn})^2 \end{Bmatrix} \quad \textbf{(2-10)}$$

The above equation may be expressed as

$$\mathbf{\Lambda\Delta = \beta} \quad \textbf{(2-11)}$$

The unknowns, which are spring constants and damping coefficients and total energy can be obtained from the solution:

$$\boldsymbol{\Delta} = (\boldsymbol{\Lambda}^T \boldsymbol{\Lambda})^{-1} (\boldsymbol{\Lambda}^T \boldsymbol{\beta}) \quad \textbf{(2-12)}$$

Note that when the square matrix $\boldsymbol{\Lambda}^T \boldsymbol{\Lambda}$ is rank-deficient, the Moore-Penrose pseudoinverse can be used to get $\boldsymbol{\Delta}$.

2.4 OVERALL SOLUTION PROCEDURES

Based on the latter discussion, the overall identification of stiffness and damping can be achieved by the three steps described below:

Step 1: Velocities and displacements at each node of the existing structure are measured;

Step 2: Using estimated velocities and displacement, construct $\boldsymbol{\Lambda}$ and $\boldsymbol{\beta}$ given in Eq. 2-10; and

Step 3: Use the pseudo-inverse technique to solve for the stiffness parameters and damping parameters, in $\boldsymbol{\Delta} = (\boldsymbol{\Lambda}^T \boldsymbol{\Lambda})^{-1} (\boldsymbol{\Lambda}^T \boldsymbol{\beta})$, (Eq.2-12)

2.5 SUMMARY

In this section, the equation for energy conservation at each time step has been derived. Next an efficient solution procedure has been introduced to identify stiffness parameters and damping parameters simultaneously. Finally the overall procedure to solve for the stiffness parameters and damping coefficients has been summarized.

3 DEVELOPMENT OF NDE METHODOLOGY BASED ON THE SENSITIVITY APPROACH

3.1 INTRODUCTION

In this section, another NDE method to identify stiffness and damping parameters using the acceleration responses of the existing structure are developed. In this method, a baseline structure is first identified. The stiffness parameters and damping characteristics of the baseline structure are adjusted so that the simulated accelerations of baseline structure at selected points are close to the measured accelerations of the existing structure. The adjusted stiffness parameters and damping characteristics of the baseline structure are then forced to converge to those of the existing structure.

3.2 IDENTIFICATION OF BASELINE STRUCTURE

A baseline structure is defined to be a structural system that has a similar response to the existing structure under investigation but have no damage in the elements of the structure. In this study, natural frequencies and modal damping values are used to identify the baseline structure. The structural parameters of the baseline structure are updated so as to have similar natural frequencies and modal damping values with those of the existing structure. However, the mode shapes of the identified baseline structure may be different in the neighborhood of the flaw. The comparison of an existing structure and an identified baseline structure is shown in Fig. 3-1. Here, ω_i^*, ς_i^*, and Φ_i^* represent the ith natural frequency, ith modal damping value, and the ith mode shape vector, respectively, of the damaged structure. To identify the stiffness and damping characteristics of the baseline structure, the system identification methodology proposed by Stubbs and Kim (1996) is used. Only stiffness was treated in Stubbs and Kim's methodology, so that methodology is extended in this study to include also damping characteristics of the system

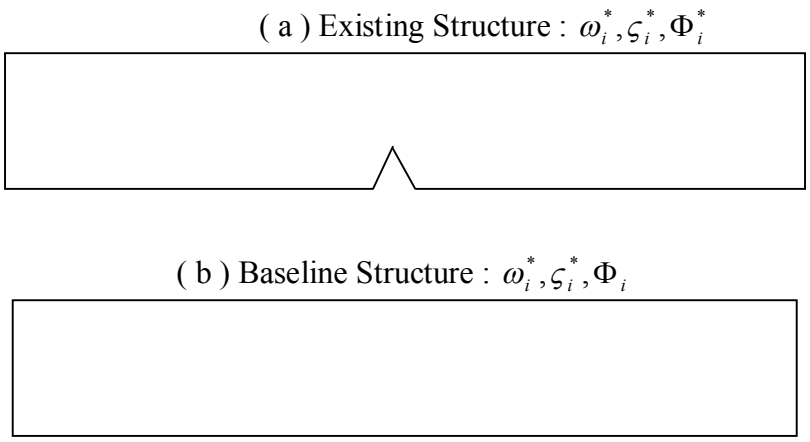

Fig. 3-1 Damaged Structure and Estimate of Baseline Structure

The driving concept behind the system identification methodology proposed by Stubbs and Kim (1996) is that the adjustment of stiffness for each element can be determined from a sensitivity matrix, F, and a fractional difference in eigenvalues vector, **Z**, by solving the system of equations $\boldsymbol{\alpha} = \mathbf{F}^{-1}\mathbf{Z}$. Here, α is a vector in which each component represents the fractional change of stiffness of each element. The updated stiffness of the baseline structure can be determined from α and an initially assumed stiffness by $k_j^* = k_j(1+\alpha_j)$. Here, k_j^* is the updated stiffness of the jth element of the baseline structure, and k_j is the initially assumed stiffness of the jth element of the baseline structure. If the number of available natural frequencies is M, and the number of elements is NE, **F** will be M x NE matrix, **Z** will be M x 1 column matrix and **α** will be NE x 1 column matrix. The reason **F** is called as sensitivity matrix is that each component of **F** represents the fractional change in the square of the natural frequency with respect to fractional change in the local stiffness. In the system identification procedure proposed by Stubbs and Kim (1996), **F**, **Z** and **α** were formulated for only natural frequencies and stiffness, but in this study, the analogous **F**, **Z** and **α** matrices are formulated to include also damping.

The sensitivity matrix **F** for stiffness can be determined as follows: first, M natural frequencies are obtained numerically from the FE (finite element) model with initially assumed stiffness and damping characteristics; second, the stiffness of the first

group of elements is changed by a known amount; third, M natural frequencies of FE model having the modified stiffness parameters but unchanged damping characteristics are computed numerically; fourth, the fractional changes of eigenfrequencies are computed; fifth, each row of the first column of the F matrix is obtained in the fourth process by the modified stiffness in the second process; and sixth, the above processes are repeated for all groups.

The Sensitivity matrix for damping can be determined by a similar process. The only differences are that damping characteristics instead of stiffness are modified in the second process, while stiffness parameters remain unchanged and modal damping values are used instead of eigenfrequencies in the third process. In this approach, it is assumed that elements of baseline structure can be categorized into a few groups; this assumption is reasonable since many elements in civil engineering structure have identical sectional properties and mechanical properties

If the number of available modes in which natural frequency and modal damping values can be measured is larger than the number of groups, the problem will be over-determined. If the number of groups is NG, the sensitivity matrix **F** will be M x NG matrix, **Z** will be M x 1, and $\boldsymbol{\alpha}$ will be NG x 1 vector.

The baseline structure can be identified by utilizing the following procedure:

1. Natural frequencies and modal dampings of the existing structure (the damaged structure) are measured (Mode shape will not be used for the identification of the baseline structure);
2. Based on information using as-built plans and field inspection, an initial estimate of the stiffness parameters and damping characteristics is made;
3. Natural frequencies and modal damping values are numerically generated from an FE model with the estimated stiffness parameters and damping characteristics;
4. Sensitivity matrix **F** relating fractional stiffness vector α to fractional eigenvalue vector **Z** is computed;
5. Using **F** and **Z**, the stiffness parameters are updated;
6. Step 4 and 5 are repeated until $\mathbf{Z} \cong \mathbf{0}$ or $\boldsymbol{\alpha} \cong \mathbf{0}$;

7. Senstivity matrix **F** relating fractional damping characteristics vector $\boldsymbol{\alpha}$ to fractional modal damping values vector **Z** with modified stiffness parameters are computed;
8. Using **F** and **Z**, damping characteristics are updated;
9. Steps 7 and 8 are repeated until $\mathbf{Z} \cong \mathbf{0}$ or $\boldsymbol{\alpha} \cong \mathbf{0}$ for modal damping values; and
10. Steps 3 ~ 9 are repeated until natural frequencies and modal damping values of the baseline structure are sufficiently close to those of the existing structure.

The converged FE model is the baseline structure. It has natural frequencies and modal damping values close to those of the existing structure, but no flaws or damage exist in the baseline structure.

3.3 IDENTIFICATION OF EXISTING STRUCTURE

The stiffness parameters and damping characteristics of the baseline structure are updated repeatedly until the differences between simulated accelerations of the baseline structure and simulated accelerations of the existing structure at measurement locations converge to zero. After repeated updates of stiffness parameters and damping characteristics, the baseline structure should converge to the existing structure. The existing structure can be identified by incorporating the following steps:

1. Accelerations at several pre-selected locations of the existing structure are simulated.
2. A baseline structure is generated using the process suggested in Section 3.2 and the accelerations at the selected points with existing structure are numerically simulated.
3. A Sensitivity matrix **F** for acceleration to stiffness parameters and damping characteristics at each time step is calculated for each time step.

   For the nth time step, the sensitivity matrix F will have the form:

$$\mathbf{F} = \begin{bmatrix} \frac{\partial a_1(t_n)}{\partial k_1} & \cdots & \frac{\partial a_1(t_n)}{\partial k_M} & \frac{\partial a_1(t_n)}{\partial c_1} & \cdots & \frac{\partial a_1(t_n)}{\partial c_N} \\ \vdots & \cdots & \vdots & \vdots & \cdots & \vdots \\ \frac{\partial a_m(t_n)}{\partial k_1} & \cdots & \frac{\partial a_m(t_n)}{\partial k_M} & \frac{\partial a_m(t_n)}{\partial c_1} & \cdots & \frac{\partial a_m(t_n)}{\partial c_N} \end{bmatrix} \quad \textbf{(3-1)}$$

Where k_M is Mth stiffness parameter, c_N is Nth damping parameter, and $a_m(t_n)$ is the acceleration at mth measurement location at nth time step. For each time step, sensitivity matrix can be made and they are stacked up, so if n time steps are available at m measurement points, and M stiffness parameters and N damping parameters are to be identified, sensitivity matrix **F** will be nm x (M+N) matrix.

4. A difference column matrix **Z,** of which each row is equivalent to the difference between the simulated accelerations of the existing structure and the simulated accelerations of the baseline structure at each time step, is built up. The difference column matrix at nth time step has the form:

$$\mathbf{Z} = \begin{Bmatrix} \tilde{a}_1(t_n) - \overline{a_1}(t_n) \\ \vdots \\ \tilde{a}_m(t_n) - \overline{a_m}(t_n) \end{Bmatrix} \qquad \textbf{(3-2)}$$

where $\tilde{a}_1(t_n)$ is the measured acceleration at 1st measurement location at the nth time step, and

$\overline{a_1}(t_n)$: calculated responses of reference structure at the 1st measurement location at the nth time step.

For each time step, the difference column matrix can be generated and stacked up, just as the sensitivity matrix and if n time steps are available at m measurement locations, the size of the final difference column matrix is nm X 1.

5. With the sensitivity matrix and difference column matrix obtained using Steps 3 and 4, stiffness parameters and damping characteristics are updated, by solving the following system of equations:

$$\begin{bmatrix} \frac{\partial a_1(t_1)}{\partial k_1} & \cdots & \frac{\partial a_1(t_1)}{\partial k_n} & \frac{\partial a_1(t_1)}{\partial c_1} & \cdots & \frac{\partial a_1(t_1)}{\partial c_n} \\ \vdots & \cdots & \vdots & \vdots & \cdots & \vdots \\ \frac{\partial a_m(t_n)}{\partial k_1} & \cdots & \frac{\partial a_m(t_n)}{\partial k_n} & \frac{\partial a_m(t_n)}{\partial c_1} & \cdots & \frac{\partial a_m(t_n)}{\partial c_n} \end{bmatrix} \begin{Bmatrix} \Delta k_1 \\ \vdots \\ \Delta k_M \\ \Delta c_1 \\ \vdots \\ \Delta c_N \end{Bmatrix} = \begin{Bmatrix} \tilde{a}_1(t_1) - \overline{a_1}(t_1) \\ \vdots \\ \tilde{a}_m(t_n) - \overline{a_m}(t_n) \end{Bmatrix} \qquad \textbf{(3-3)}$$

Let

$$\boldsymbol{\alpha} = \begin{Bmatrix} \Delta k_1 \\ \vdots \\ \Delta k_M \\ \Delta c_1 \\ \vdots \\ \Delta c_N \end{Bmatrix} \tag{3-4}$$

then

$$\mathbf{F}\boldsymbol{\alpha} = \mathbf{Z}$$
$$\boldsymbol{\alpha} = (\mathbf{F}^{\mathrm{T}}\mathbf{F})^{-1} ?\ \mathbf{F}^{\mathrm{T}}\mathbf{Z}) \tag{3-5}$$

6. Steps 3 ~ 5 are repeated until $\mathbf{Z} \cong \mathbf{0}$ or $\boldsymbol{\alpha} \cong \mathbf{0}$.

The converged stiffness parameters and damping parameters of the baseline structure are the stiffness parameters and damping parameters of the existing structure, and given the identified parameters, the stiffness-damaged elements and the damping-damaged elements can be located and their associated severities can be estimated. For the energy conservation approach, the displacements, velocities, and accelerations at all nodes are required, but for this methodology, only accelerations at some selected locations are needed. However, the measured accelerations at additional locations will give a better estimation of the stiffness parameters and the damping characteristics.

3.4 OVERALL SOLUTION PROCEDURE

Based on previous process, the overall identification of stiffness and damping scheme can be achieved by completing the four steps described below.

Step 1: Accelerations of the existing structure are measured.

Step 2: A baseline structure is identified based on measured natural frequencies and modal damping values

Step 3: A sensitivity matrix, **F** and a difference column matrix, **Z,** are constructed. Based on these matrices, over-determined linear matrix equation, $\mathbf{F\alpha = Z}$ (Eq.3-5) are constructed

Step 4: The pseudo-inverse technique is used to solve for the adjustment of the stiffness parameters and damping parameters, in $\boldsymbol{\alpha} = (\mathbf{F}^T\mathbf{F})^{-1}\,?\,\mathbf{F}^T\mathbf{Z})$, (Eq.3-5)

Step 5: Step 3 and Step 4 are repeated until $\mathbf{Z} \cong \mathbf{0}$ or $\boldsymbol{\alpha} \cong \mathbf{0}$.

3.5 SUMMARY

In this section, a technique to identify a baseline structure, in which natural frequencies and modal damping values are close to those of the existing structure, has been developed. Next an efficient solution procedure using the sensitivity of the accelerations to the structural parameters has been introduced to identify stiffness parameters and damping parameters of the existing structure. Finally the overall procedure has been summarized.

4 NUMERICAL VERIFICATION OF THE ENERGY CONSERVATION METHOD FOR A SHEAR BUILDING

4.1 INTRODUCTION

The objective of this section is to verify the performance of the proposed method, which uses energy conservation numerically for a shear building with known damage scenarios. Damage scenarios are simulated by reducing spring constants and increasing dash pot constants for a shear building. Displacements and velocities are measured at all horizontal degrees of freedom. The Newmark-β method is used to simulate the displacements and velocities at each measurement location.

4.2 DAMAGE DETECTION IN A SHEAR BUILDING

In this study, a 10-story shear building is introduced for the verification of the proposed methodology. The selected model of a 10-story shear building is depicted in Fig.4-1. The numberings for the DOF, the spring elements, and the dash pots are included in Fig. 4-1. To get the simulated responses such as accelerations, velocities, and displacements in the time domain, a horizontal tensile force of 200 kips was numerically simulated at the 10^{th} story, and the load was instantaneously released thus permitting the structure to vibrate freely. Displacements and velocities were measured with a 1000 Hz sampling rate for 40 seconds. The mass constants, spring constants and dash pot constants of the intact structure are listed in Table 4-1.

Three damage scenarios were introduced to investigate the performance of the developed methodology. In the first damage scenario, only one element had an increased dash pot constant to simulate the early stage of damage at a single location. In the second damage scenario, both stiffness damage and damping damage were simulated at one element with different severities by decreasing spring constant and increasing dash pot constant. In the third damage scenario, two elements were inflicted both stiffness damage and damping damage to check whether the developed methodology works for

multi-damage cases. The locations and the magnitude of the damage of each scenario are listed in Table 4-2.

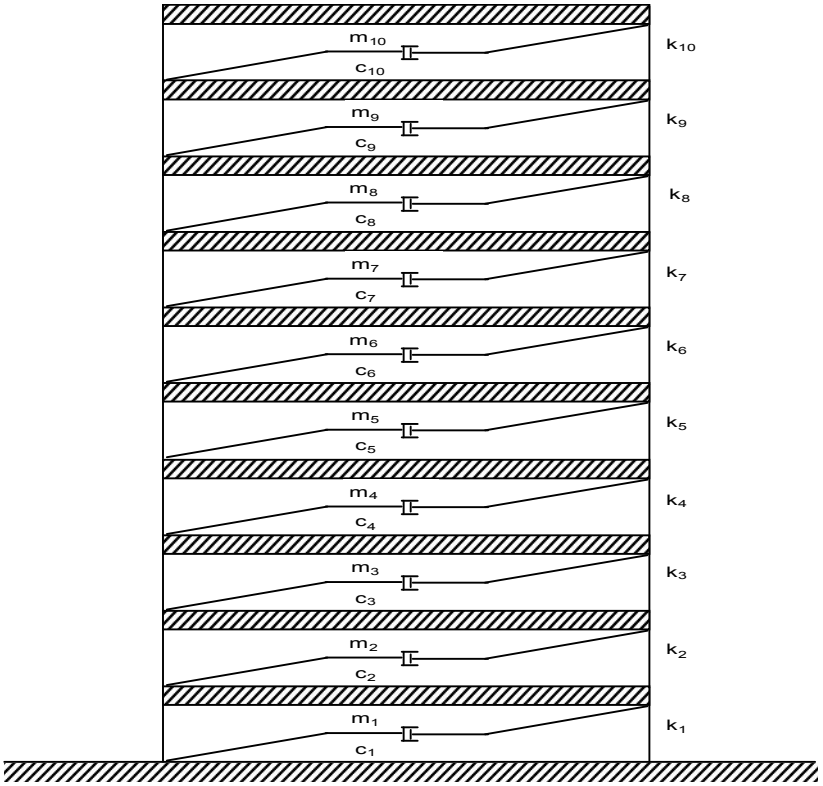

Fig. 4-1 Selected Model of 10-Story Shear Building

Table 4-1. Mass, Spring, and Dash Pot Constants of Undamaged Structure

	Mass	Spring	Dash pot
Element 1	1	1000	5
Element 2	1	1000	5
Element 3	1	1000	5
Element 4	1	1000	5
Element 5	1	1000	5
Element 6	1	1000	5
Element 7	1	1000	5
Element 8	1	1000	5
Element 9	1	1000	5
Element 10	1	1000	5

Table 4-2. Damage Scenarios for a Shear Building

Scenario	Stiffness Damage		Damping Damage	
	Location	Severity (%)	Location	Severity (%)
1			3	+10
2	3	-10	3	+20
3	3	-10	3	+20
	8	-20	8	+40

4.2.1 Case 1

In this damage scenario, only Element 3 has damping damage which is equivalent to 10% increase of the dash pot constant magnitude. To check the conservation of total energy, the total energy, sum of the potential energies of each and every spring element, sum of the kinetic energies of each and every mass element, and sum of the dissipated energy by each and every dash pot element at each time step were calculated with displacements and velocities. These results are shown in Fig. 4-2.

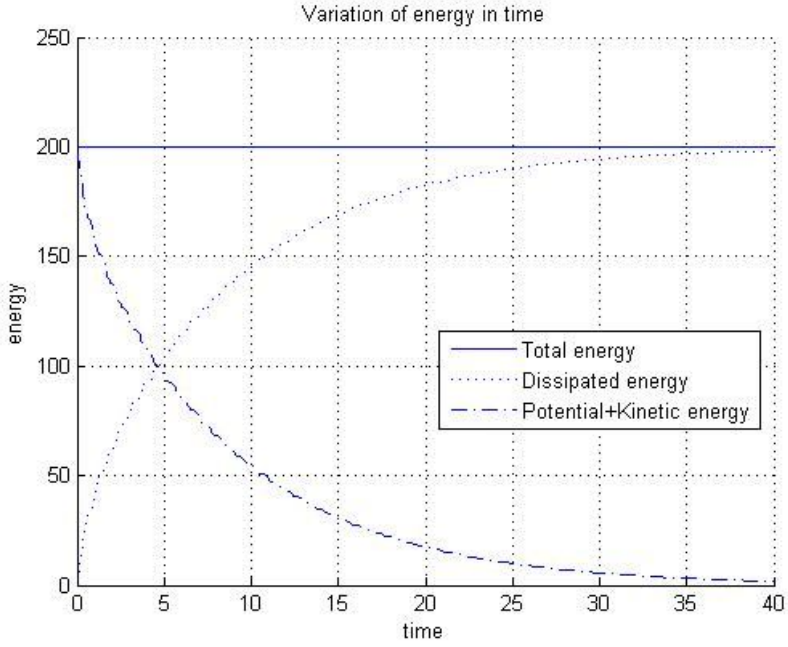

Fig. 4-2 Check of Conservation of Total Energy

In Fig. 4-2, Note that the total energy has a constant value for the observation time as expected and the dissipated energy increases with time and converges to total energy. Note also that the sum of the potential energy and the kinetic energy decreases with time. The measured displacements and velocities at Node 5 and Node 10 are shown in Fig. 4-3 and Fig. 4-4, respectively.

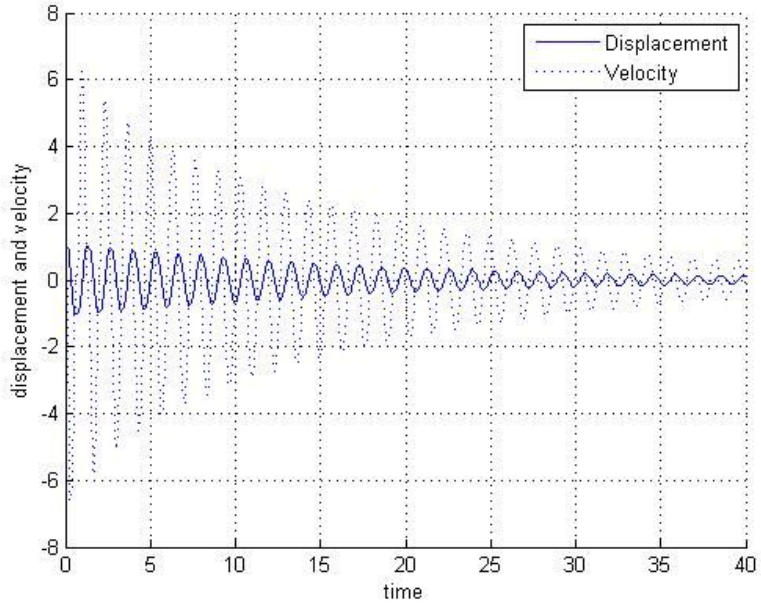

Fig. 4-3 Displacements and Velocities at Node 5 for Case 1

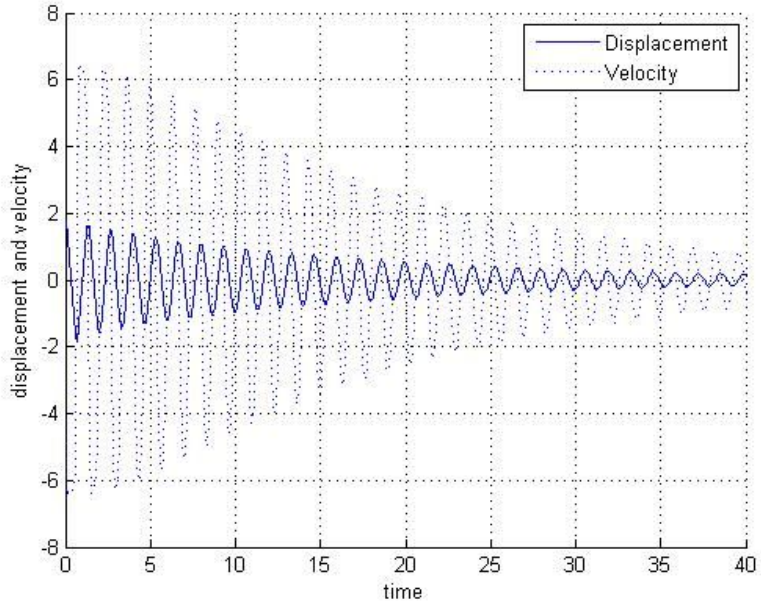

Fig. 4-4 Displacements and Velocities at Node 10 for Case 1

With these assumed measured values for 3 seconds, the spring constant and dash pot constant of each element are identified using the equations proposed in Section 2.3. These identified values are compared with the simulated values in Table 4-3 below.

Table 4-3 Comparison of the Identified and the Simulated Values for Case 1

	Spring		Dash pot	
	Simulated	Identified	Simulated	Identified
Element 1	1000	1000	5.0	5.0
Element 2	1000	1000	5.0	5.0
Element 3	1000	1001	5.5	5.5
Element 4	1000	999	5.0	5.0
Element 5	1000	1001	5.0	5.0
Element 6	1000	999	5.0	5.0
Element 7	1000	1000	5.0	5.0
Element 8	1000	1000	5.0	5.0
Element 9	1000	1000	5.0	5.0
Element 10	1000	1000	5.0	5.0

The simulated values and identified values are compared graphically in Fig. 4-5 and Fig. 4-6.

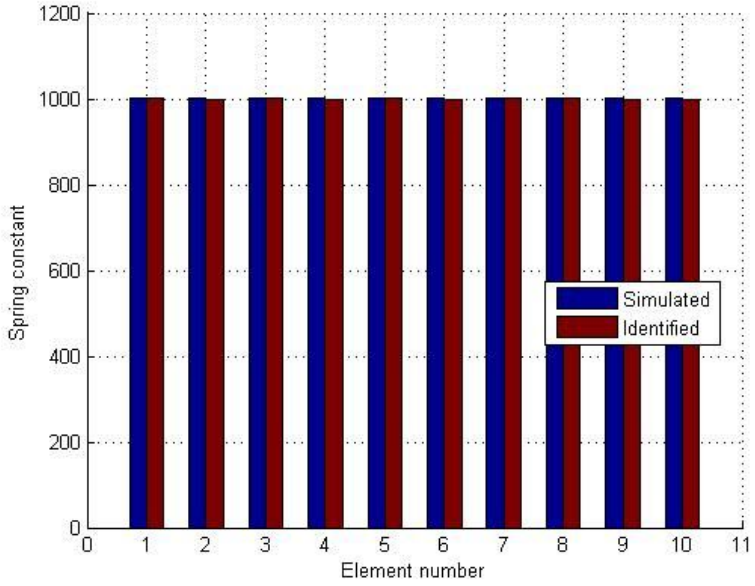

Fig. 4-5 Simulated and Identified Values in Spring for Case 1

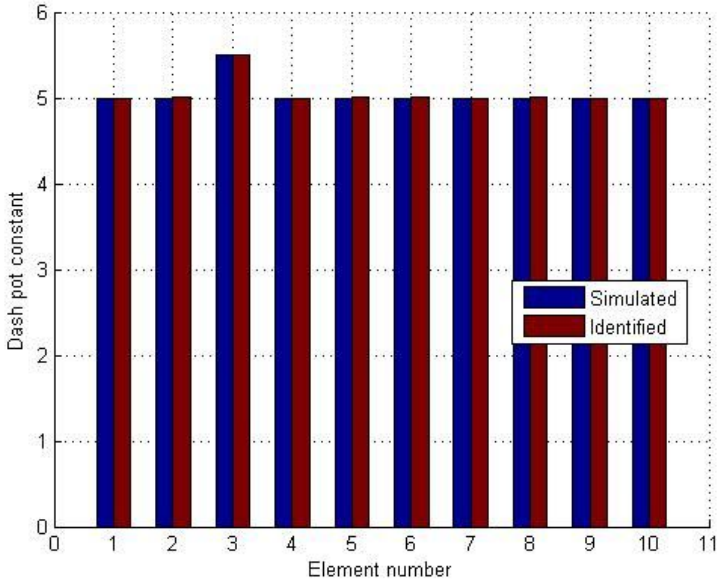

Fig. 4-6 Simulated and Identified Values in Dash Pot for Case 1

Check of influence of observation time on identification

To test the robustness of the method, the observation time for sampling was changed from 3 seconds to 10 seconds by 1 second intervals to investigate its influence on identification accuracy. Sampling rate was fixed at 200 Hz. The identified values with varying observation times for each element are displayed in from Fig. 4-7 to Fig. 4-10.

Identified values are expected to converge to simulated values with increasing observation time. However, it is difficult to find an obvious relationship between observation times and identified values. Only for spring constants for Element 1 to Element 5, identified values appear to converge to the simulated values as observation time increases. Except for those elements, no clear trend is apparent. Increase of the observation time is not effective way to get better identification.

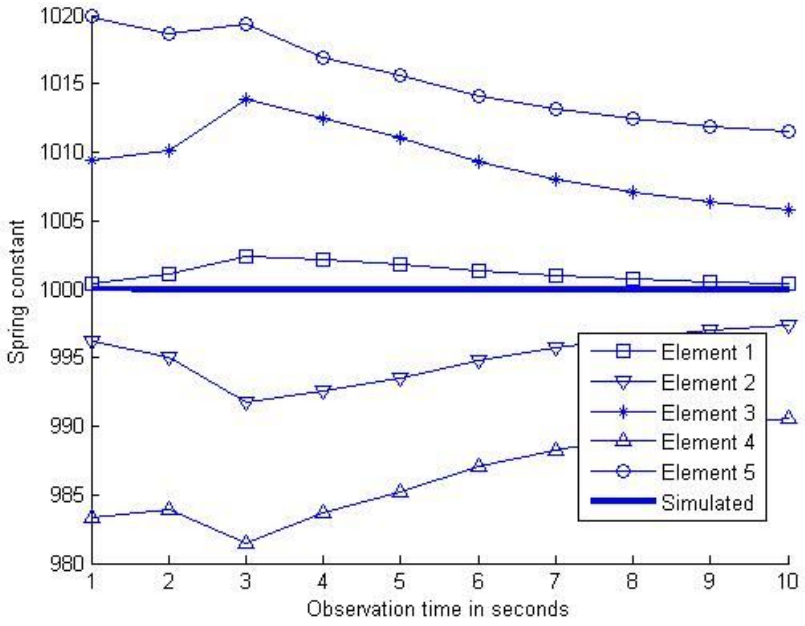

Fig. 4-7 Identified Spring Constants with Observation Time-I

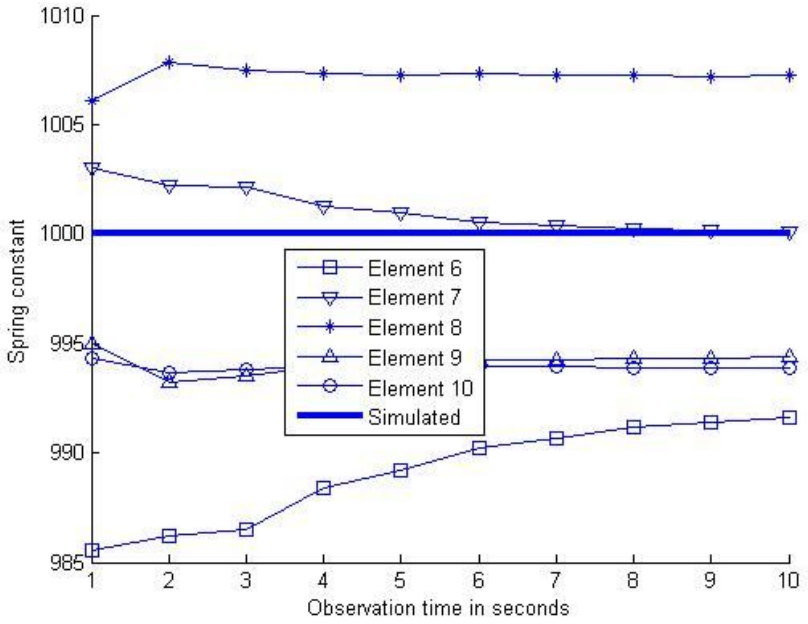

Fig. 4-8 Identified Spring Constants with Observation Time-II

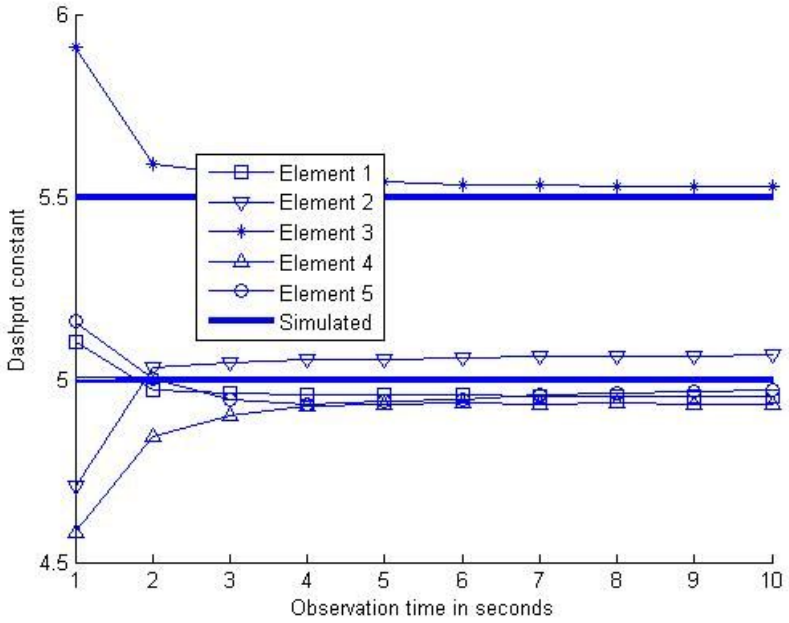

Fig. 4-9 Identified Dash Pot Constants with Observation Time-I

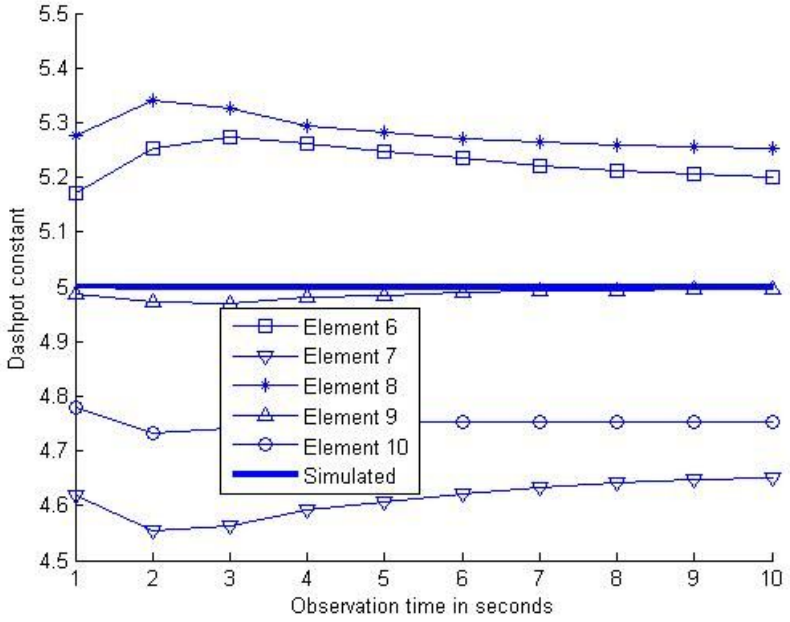

Fig. 4-10. Identified Dash Pot Constants with Observation Time-II

Check of influence of sampling frequency on identification

To check the influence of sampling rate on the identification process, the sampling rate was varied from 100Hz to 1000Hz with a fixed observation time of 3 seconds. Sampling rate was increased by intervals of 100 Hz. The variation of the identified spring constants and dash pot constants with different sampling rate are shown in Fig. 4-11, Fig. 4-12, Fig. 4-13 and Fig. 4-14. From the figures, it is observed that both spring elements and dash pot elements are identified more exactly with higher sampling rates. It can be concluded that identified values converged to the simulated values with increasing sampling rate. This observation holds for both spring and dash pot identification.

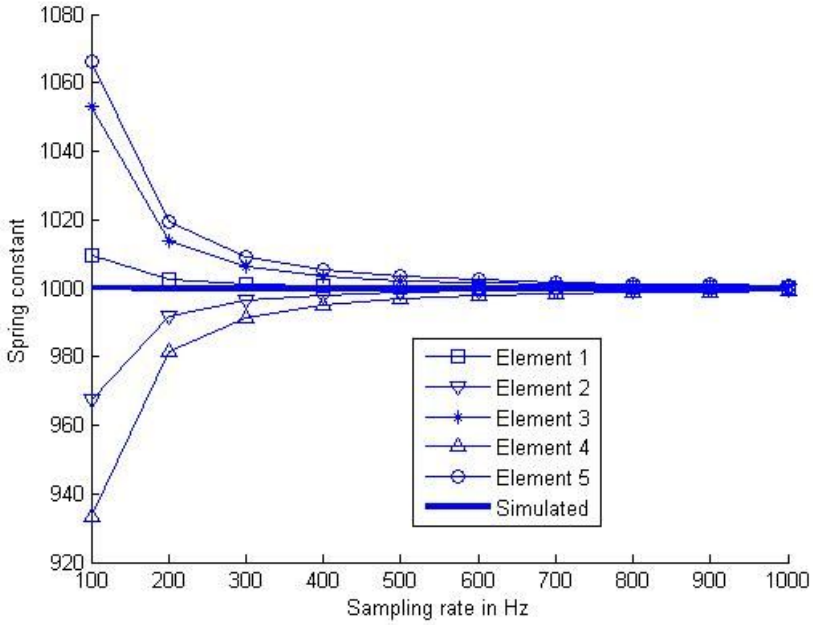

Fig. 4-11 Identified Spring Constants with Sampling Rate-I

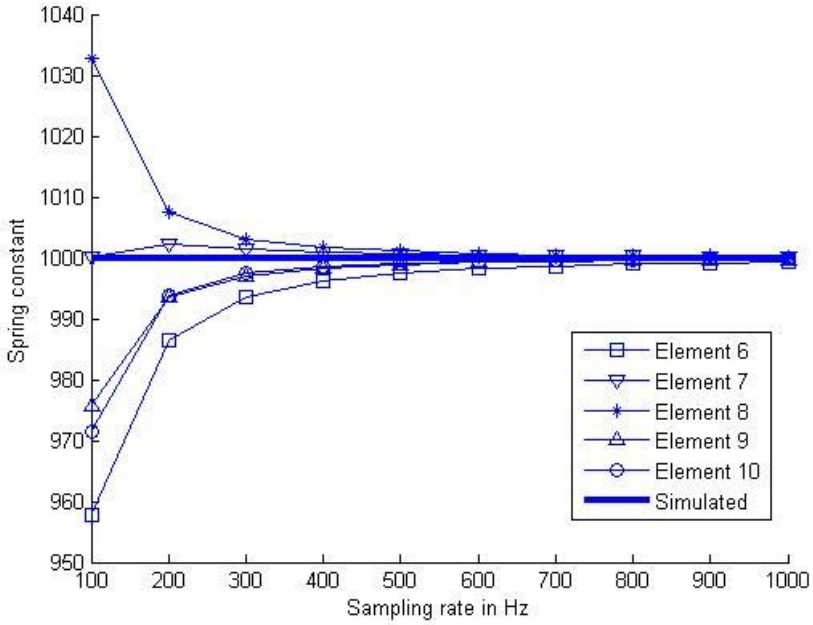

Fig. 4-12 Identified Spring Constants with Sampling Rate-II

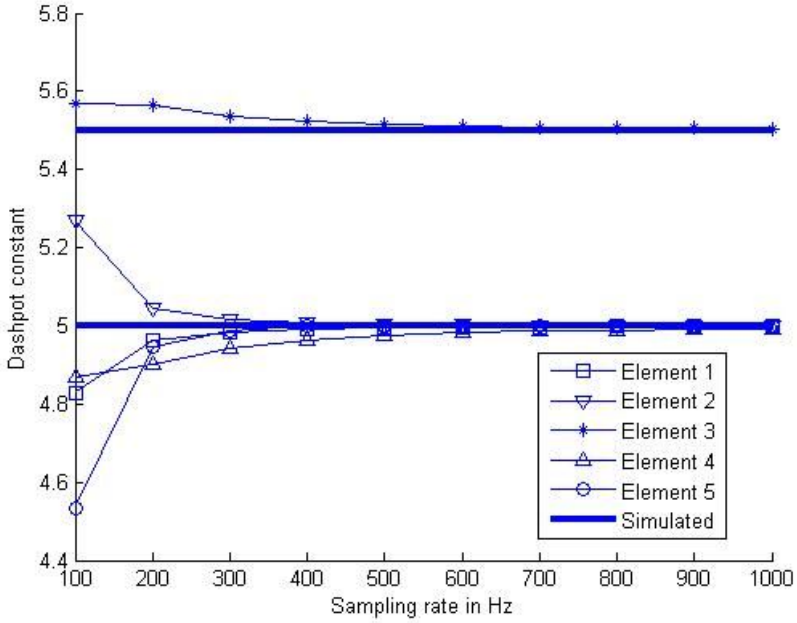

Fig. 4-13 Identified Dash Pot Constants with Sampling Rate-I

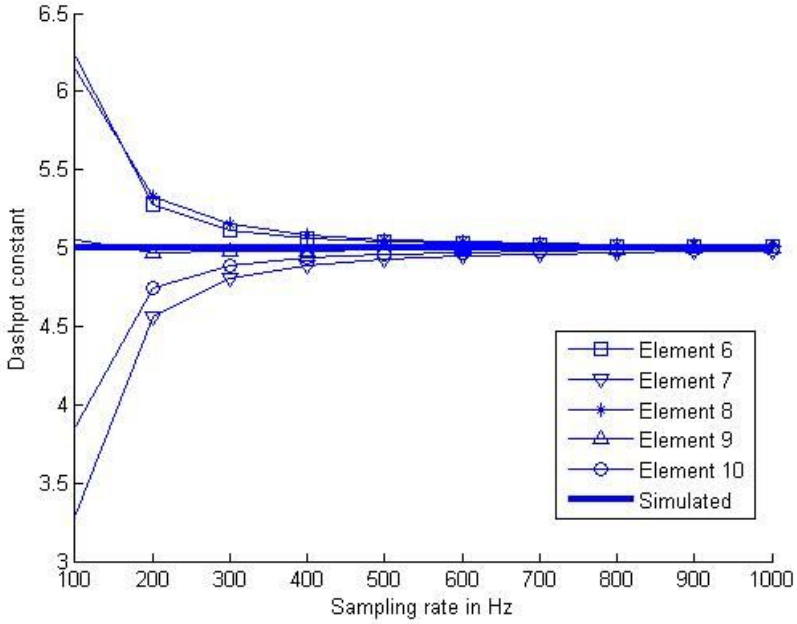

Fig. 4-14 Identified Dash Pot Constants with Sampling Rate-II

4.2.2 Case 2

In this damage scenario, Element 3 has both stiffness damage and damping damage. The spring constant was decreased by 10% and the dash pot constant was increased by 20%. Displacements and velocities are measured with a sampling rate of 1000Hz, at all nodes for 3 seconds. The identified spring constants and dash pot constants are shown in Table 4-4. As seen in Table 4-4, Element 3 is shown to have spring constant of 900, while it is about 1000 for other elements. It can be concluded that Element 3 has 10% stiffness damage. For the dash pot, Element 3 was identified to have a higher dash pot constant than the other elements. Except Element 3, all other elements have dash pot constants of near 5, which is originally simulated value. With this result of identification, we conclude that Element 3 was detected as a damaged element: Note that the element had both damping damage and stiffness damage. The identified results are graphically shown in Fig. 4-15 and Fig. 4-16.

Table 4-4 Identified Spring Constants and Dash Pot Constants by Energy Method for Case 2

	Spring		Dash pot	
	Simulated	Identified	Simulated	Identified
Element 1	1000	1000	5.0	5.0
Element 2	1000	1000	5.0	5.0
Element 3	900	900	6.0	6.0
Element 4	1000	999	5.0	5.0
Element 5	1000	1001	5.0	5.0
Element 6	1000	1000	5.0	5.0
Element 7	1000	1000	5.0	5.0
Element 8	1000	1000	5.0	5.0
Element 9	1000	1000	5.0	5.0
Element 10	1000	1000	5.0	5.0

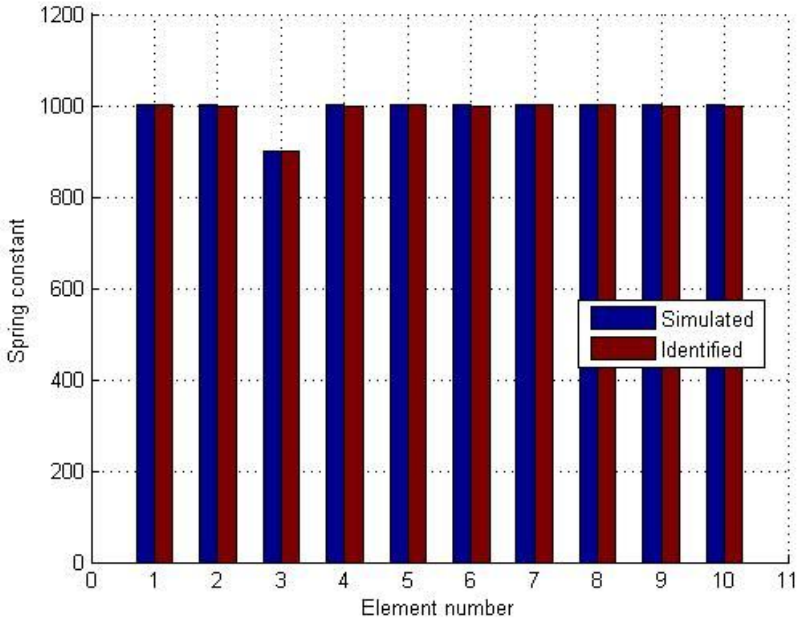

Fig. 4-15 Simulated and Identified Values in Spring for Case 2

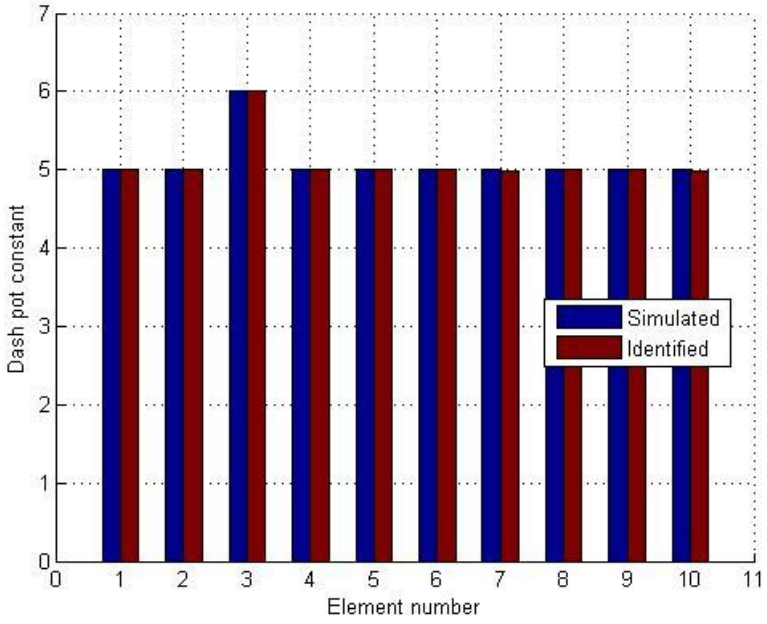

Fig. 4-16 Simulated and Identified Values in Dash Pot for Case 2

4.2.3 Case 3

In this damage scenario, damage at multiple locations is studied by damaging two elements. Element 3 and Element 8 have both stiffness damage and damping damage. For Element 3, the spring constant was decreased by 10% and the dash pot constants was increased by 20%, while for Element 8, spring constant was decreased by 20% and the dash pot constant was increased by 40%. Displacements and velocities are measured with a sampling of 1000Hz, at all nodes for 3 seconds. Identified spring constants and dash pot constants are shown in Table 4-5 and are graphically shown in Fig 4-17 and Fig 4-18. Element 3 and Element 8 were shown to have decreased spring constant of around 900 and 800, respectively, while it is about 1000 for other elements. It is concluded that Element 3 had 10% stiffness damage and Element 8 had 20% stiffness damage. For the dash pots, Element 3 and Element 8 were identified to have higher dash pot constants than other elements. Besides Element 3 and Element 8, all other elements have dash pot constants of near 5, which was the originally simulated value. With these results of identification, we conclude that Element 3 and Element 8 were correctly detected as damaged elements, with both damping damage and stiffness damage.

Table 4-5 Identified Spring Constants and Dash Pot Constants by Energy Method for Case 3

	Spring		Dash pot	
	Damaged	Baseline	Damaged	Baseline
Element 1	1000	1000	5.0	5.0
Element 2	1000	1000	5.0	5.0
Element 3	900	900	6.0	6.0
Element 4	1000	1000	5.0	5.0
Element 5	1000	1000	5.0	5.0
Element 6	1000	1000	5.0	5.0
Element 7	1000	1000	5.0	5.0
Element 8	800	800	7.0	7.0
Element 9	1000	1000	5.0	5.0
Element 10	1000	1000	5.0	5.0

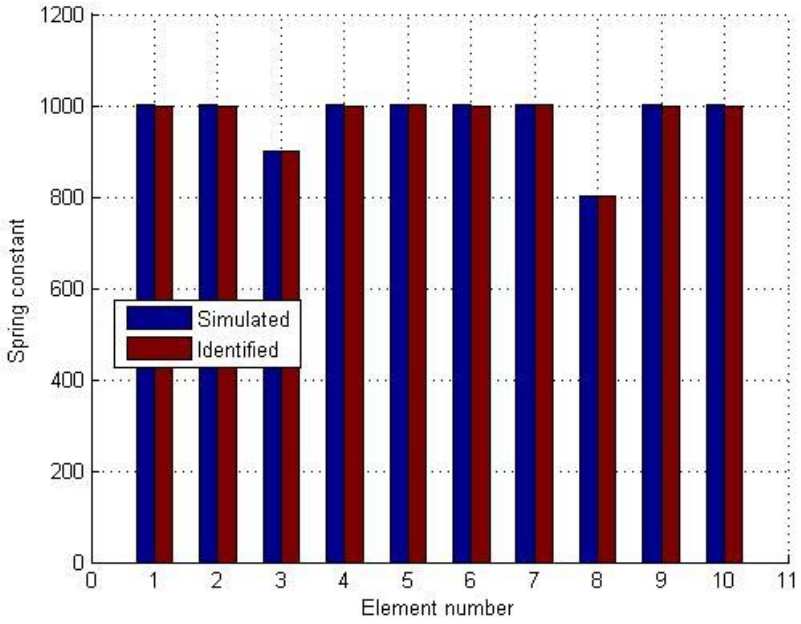

Fig. 4-17 Simulated and Identified Values in Spring for Case 3

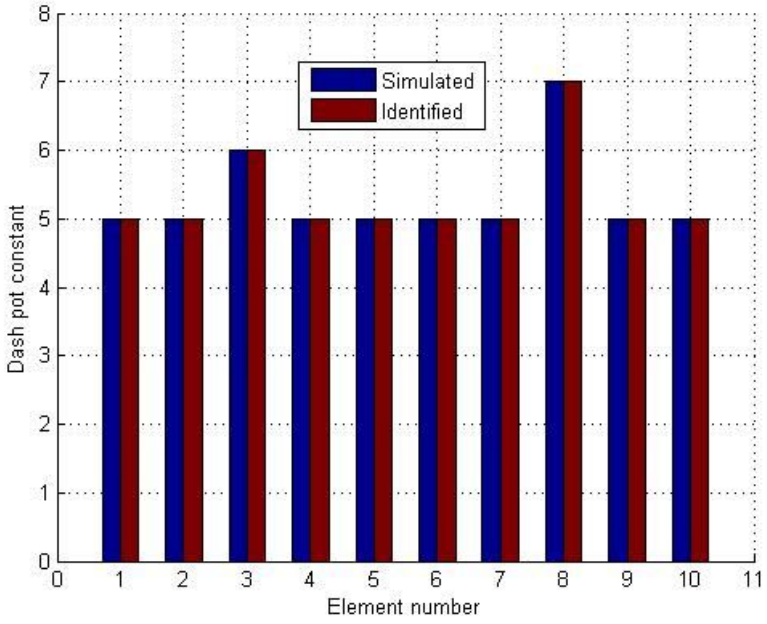

Fig. 4-18 Simulated and Identified Values in Dash Pot for Case 3

4.3 SUMMARY

The proposed damage evaluation method, based on the conservation of total energy, was verified numerically using simultaneous stiffness and damping damage scenarios that were generated from a numerical model of a high-rise building modeled as a shear beam. Three damage scenarios were investigated to simulate the damping damage, combined stiffness damage and damping damage, and multi-damage case. The sampling rate influenced the identified values more than the observation time. The proposed method identified very well both spring constants and dash pot constants for all damage scenarios.

5 NUMERICAL VERIFICATION OF THE SENSITIVITY METHOD FOR A SHEAR BUILDING

5.1 INTRODUCTION

The objective of this section is to verify the performance of the sensitivity method, presented in Section3, which uses acceleration-structural parameter sensitivities for a shear building.

5.2 DAMAGE DETECTION IN A SHEAR BUILDING

The same target structure and same damage scenarios that were used in the last section will be used here. To excite the structure, a horizontal tensile force of 200 kips was applied at the 10^{th} story, and the load was quickly released thus permitting the structure to vibrate freely. The Newmark's-β method was used to calculate the resulting simulated accelerations. While the displacements and velocities at all nodes were needed for the previous method, only accelerations are required for the method proposed here. Accelerations are measured with a sampling rate of 200Hz at all floors for a duration of 3 seconds.

5.2.1 Case 1

In this damage scenario, Element 3 has only damping damage which is equivalent to a 10% increase in the dash pot constant. The first step in this proposed NDE method, which uses the acceleration-structural parameter sensitivities, is to identify a baseline structure, based on the measured natural frequencies and modal damping values. The simulated measured natural frequencies and modal damping values of the damaged structure are shown in Table 5-1.The spring constants, and dash pot constants of a baseline structure were determined to have the natural frequencies and modal damping values close to those of the damaged structure. It was assumed that all elements of the baseline structure had the same spring constants and dash pot constants. Firstly, the initial values were given as 2000 and 10, respectively, for the spring constants and

the dash pot constants. Subsequently, the values of the parameters were adjusted via the iteration process.

Table 5-1 Natural Frequencies and Modal Damping Values of the Existing Structure for Case 1

	Mode 1	Mode 2	Mode 3
Natural frequency (Hz)	0.75	2.24	3.67
Modal damping (%)	1.20	3.53	5.79

The history of the adjustment of the spring constants and the dash pot constants are shown in Fig. 5-1 and Fig. 5-2. The converged values for the spring constants and the dash pot constants were given as initial value and the iteration process was repeated. The converged spring constants and dash pot constants were compared with the simulated damaged structure in Table 5-2. The natural frequencies and modal damping values of the damaged structure and the baseline structure are compared in Table 5-3. The accelerations of the damaged structure at Node 5 and Node 10 are shown in Fig. 5-3 and Fig. 5-4.

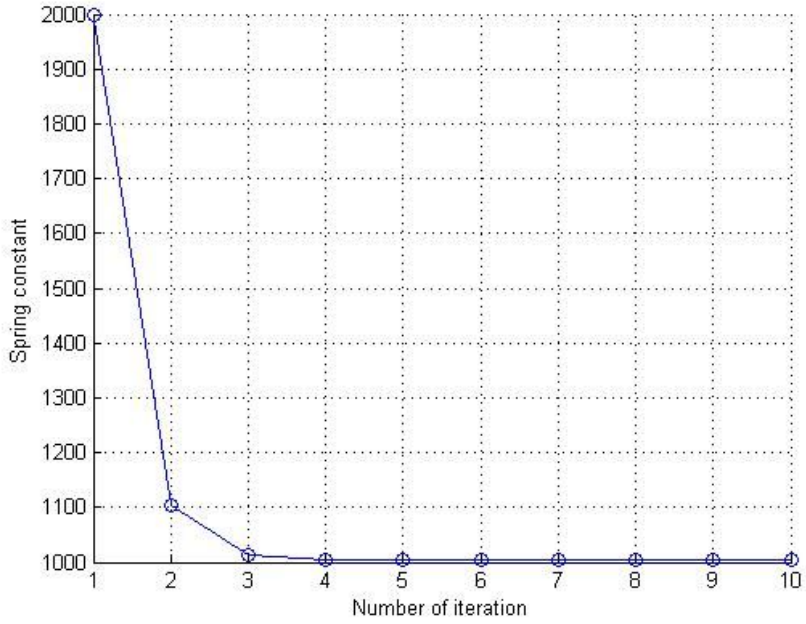

Fig. 5-1 Spring Constant of Baseline Structure

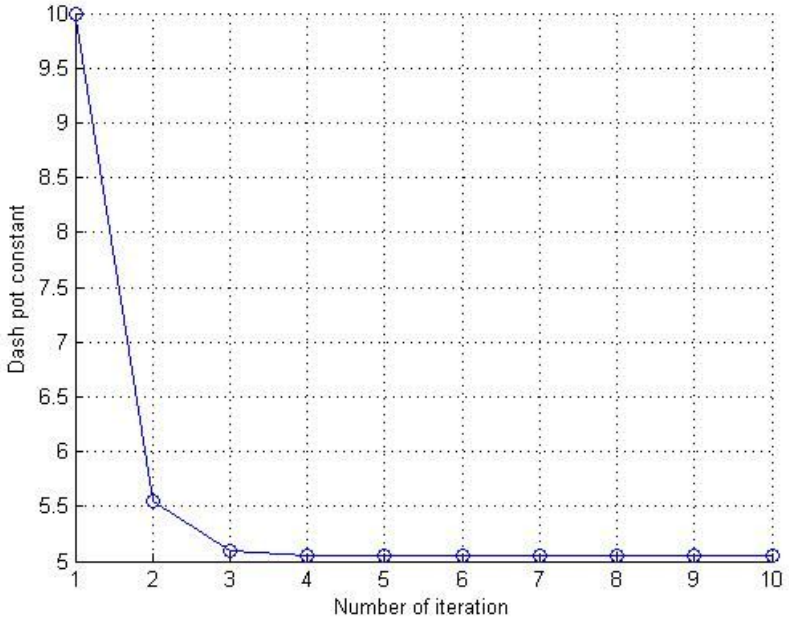

Fig. 5-2 Dash Pot Constant of Baseline Structure

Table 5-2 Comparison of Structural Parameters for Case 1

	Spring		Dash pot	
	Damaged	Baseline	Damaged	Baseline
Element 1	1000	1000.02	5	5.04
Element 2	1000	1000.02	5	5.04
Element 3	1000	1000.02	5.5	5.04
Element 4	1000	1000.02	5	5.04
Element 5	1000	1000.02	5	5.04
Element 6	1000	1000.02	5	5.04
Element 7	1000	1000.02	5	5.04
Element 8	1000	1000.02	5	5.04
Element 9	1000	1000.02	5	5.04
Element 10	1000	1000.02	5	5.04

Table 5-3 Comparison of Natural Frequencies and Modal Damping Values for Case 1

	Natural Frequency (Hz)		Modal damping (%)	
	Damaged	Baseline	Damaged	Baseline
Mode 1	0.75	0.75	1.20	1.19
Mode 2	2.24	2.24	3.53	3.55
Mode 3	3.67	3.67	5.79	5.82

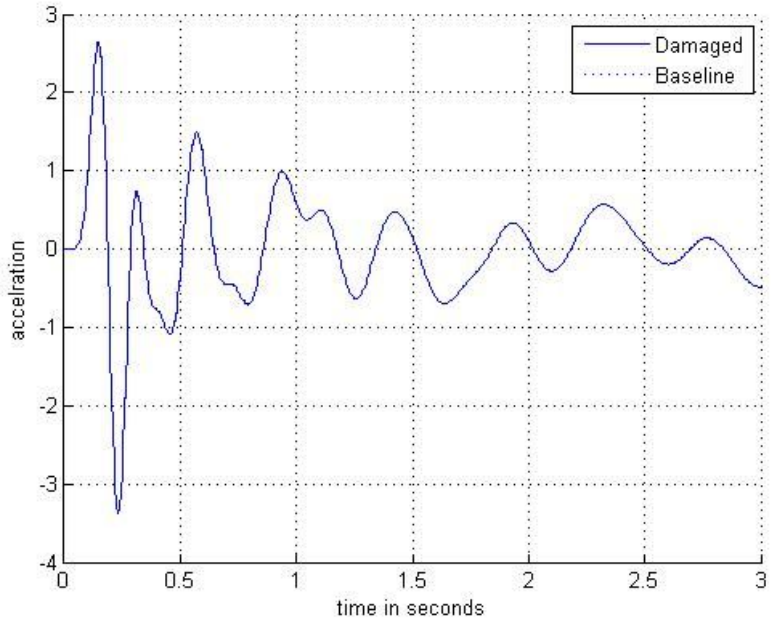

Fig. 5-3 Measured Accelerations at Node 5 for Case 1

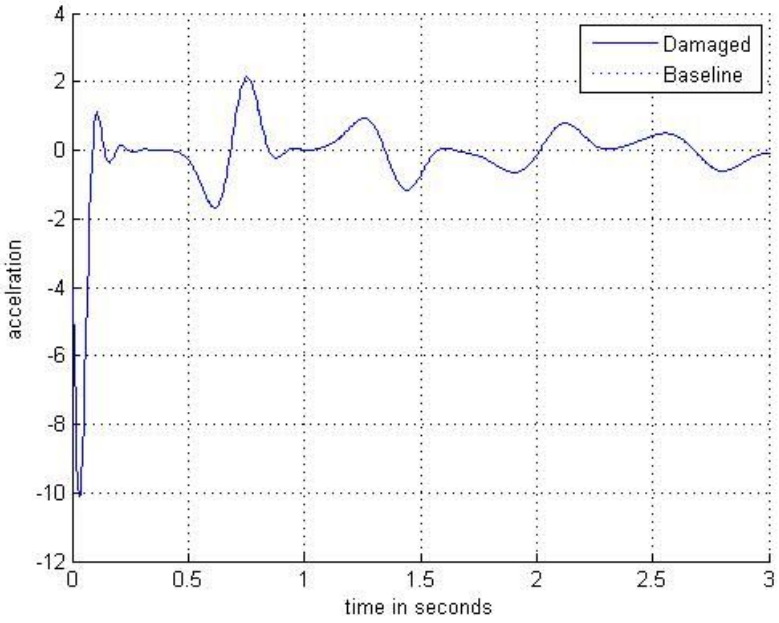

Fig. 5-4 Measured Accelerations at Node 10 for Case 1

The accelerations of the baseline structure were close to the accelerations of the damaged structure. This result follows from the fact that the stiffness parameters of the baseline structure are almost identical to those of the damaged structure, with only damping parameters slightly modified. To identify the spring constants and dash pot constants of the damaged structure, the NDE technique proposed in Section 3 was applied. When the accelerations at all nodes were used, the identified values are shown in Table 5-4.

Table 5-4 Identified Spring Constants and Dash Pot Constants with 10 Measurements for Case 1

	Spring		Dash pot	
	Simulated	Identified	Simulated	Identified
Element 1	1000	1000	5	5
Element 2	1000	1000	5	5
Element 3	1000	1000	5.5	5.5
Element 4	1000	1000	5	5
Element 5	1000	1000	5	5
Element 6	1000	1000	5	5
Element 7	1000	1000	5	5
Element 8	1000	1000	5	5
Element 9	1000	1000	5	5
Element 10	1000	1000	5	5

With the NDE method proposed in Section 3, the spring constants and dash pot constants could be identified exactly, even with the lower sampling rate of 200 Hz.

To investigate the influence of the number of measurement locations on the identified values, it was tried again to identify the structural parameters with the acceleration at Node 5 and 10. The results of the identification are shown in Table 5-5. Even with the accelerations at only 2 measurement locations, the structural parameters were identified exactly.

With the accelerations at only 1 measurement location, it was tried to identify the structural parameters. The measurement location was changed from Node 1 to Node 10. The identified results are listed in Table 5-6 and Table 5-7. Even with the accelerations

at only 1 measurement location, the structural parameters were identified exactly for all cases.

Table 5-5 Identified Spring Constants and Dash Pot Constants with 2 Measurements for Case 1

	Spring		Dash pot	
	Simulated	Identified	Simulated	Identified
Element 1	1000	1000	5	5
Element 2	1000	1000	5	5
Element 3	1000	1000	5.5	5.5
Element 4	1000	1000	5	5
Element 5	1000	1000	5	5
Element 6	1000	1000	5	5
Element 7	1000	1000	5	5
Element 8	1000	1000	5	5
Element 9	1000	1000	5	5
Element 10	1000	1000	5	5

Table 5-6 Identified Spring Constant with 1 Measurement Location for Case 1

	Measurement Location									
	1	2	3	4	5	6	7	8	9	10
Element 1	1000	1000	1000	1000	1000	1000	1000	1000	1000	1000
Element 2	1000	1000	1000	1000	1000	1000	1000	1000	1000	1000
Element 3	1000	1000	1000	1000	1000	1000	1000	1000	1000	1000
Element 4	1000	1000	1000	1000	1000	1000	1000	1000	1000	1000
Element 5	1000	1000	1000	1000	1000	1000	1000	1000	1000	1000
Element 6	1000	1000	1000	1000	1000	1000	1000	1000	1000	1000
Element 7	1000	1000	1000	1000	1000	1000	1000	1000	1000	1000
Element 8	1000	1000	1000	1000	1000	1000	1000	1000	1000	1000
Element 9	1000	1000	1000	1000	1000	1000	1000	1000	1000	1000
Element 10	1000	1000	1000	1000	1000	1000	1000	1000	1000	1000

Table 5-7 Identified Dash Pot Constant with 1 Measurement Location for Case 1

	Measurement Location									
	1	2	3	4	5	6	7	8	9	10
Element 1	5.00	5.00	5.00	5.00	5.00	5.00	5.00	5.00	5.00	5.00
Element 2	5.00	5.00	5.00	5.00	5.00	5.00	5.00	5.00	5.00	5.00
Element 3	5.50	5.50	5.50	5.50	5.50	5.50	5.50	5.50	5.50	5.50
Element 4	5.00	5.00	5.00	5.00	5.00	5.00	5.00	5.00	5.00	5.00
Element 5	5.00	5.00	5.00	5.00	5.00	5.00	5.00	5.00	5.00	5.00
Element 6	5.00	5.00	5.00	5.00	5.00	5.00	5.00	5.00	5.00	5.00
Element 7	5.00	5.00	5.00	5.00	5.00	5.00	5.00	5.00	5.00	5.00
Element 8	5.00	5.00	5.00	5.00	5.00	5.00	5.00	5.00	5.00	5.00
Element 9	5.00	5.00	5.00	5.00	5.00	5.00	5.00	5.00	5.00	5.00
Element 10	5.00	5.00	5.00	5.00	5.00	5.00	5.00	5.00	5.00	5.00

5.2.2 Case 2

In this damage scenario, Element 3 has both stiffness damage and damping damage. The spring constant was decreased by 10% and the dash pot constants was increased by 20%. The natural frequencies and modal damping values of the damaged structure are shown in Table 5-8.

Table 5-8 Natural Frequencies and Modal Damping Values of the Existing Structure for Case 2

	Mode 1	Mode 2	Mode 3
Natural frequency (Hz)	0.75	2.23	3.67
Modal damping (%)	1.24	3.56	5.81

The identified spring constants and dash pot constants of the baseline structure are compared with the simulated damaged structure in Table 5-9. The natural frequencies and modal damping values of the damaged structure and the baseline structure are compared in Table 5-10. The accelerations of the damaged structure and the baseline structure at Node 5 and Node 10 are compared in Fig. 5-5 and Fig .5-6.

Table 5-9 Comparison of Structural Parameters for Case 2

	Spring		Dash pot	
	Damaged	Baseline	Damaged	Baseline
Element 1	1000	992.11	5	5.09
Element 2	1000	992.11	5	5.09
Element 3	900	992.11	6	5.09
Element 4	1000	992.11	5	5.09
Element 5	1000	992.11	5	5.09
Element 6	1000	992.11	5	5.09
Element 7	1000	992.11	5	5.09
Element 8	1000	992.11	5	5.09
Element 9	1000	992.11	5	5.09
Element 10	1000	992.11	5	5.09

Table 5-10 Comparison of Natural Frequencies and Modal Damping Values for Case 2

	Natural Frequency (Hz)		Modal damping (%)	
	Damaged	Baseline	Damaged	Baseline
Mode 1	0.75	0.75	1.24	1.21
Mode 2	2.23	2.23	3.56	3.60
Mode 3	3.67	3.66	5.81	5.91

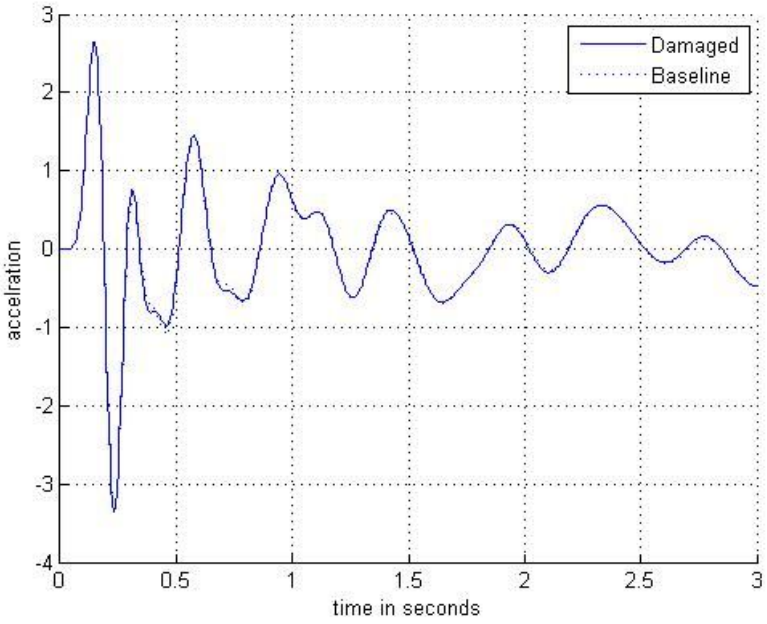

Fig. 5-5 Measured Accelerations at Node 5 for Case 2

The accelerations measured at Node 5 show more deviation than the accelerations at Node 10. It is hypothesized that this is because Node 5 is closer to the damaged element than Node 10. To identify the spring constants and dash pot constants of the damaged structure, the NDE technique proposed in Section 3 was applied. When the accelerations at all nodes were used, the identified values are listed in Table 5-11. It was tried again to identify the structural parameters with the accelerations at Node 5 and Node 10 as in Case 1. The results of the identification are listed in Table 5-12. With the accelerations measured at only 1 location, we tried to identify the structural parameters. The measurement location was changed from Node 1 to Node 10.

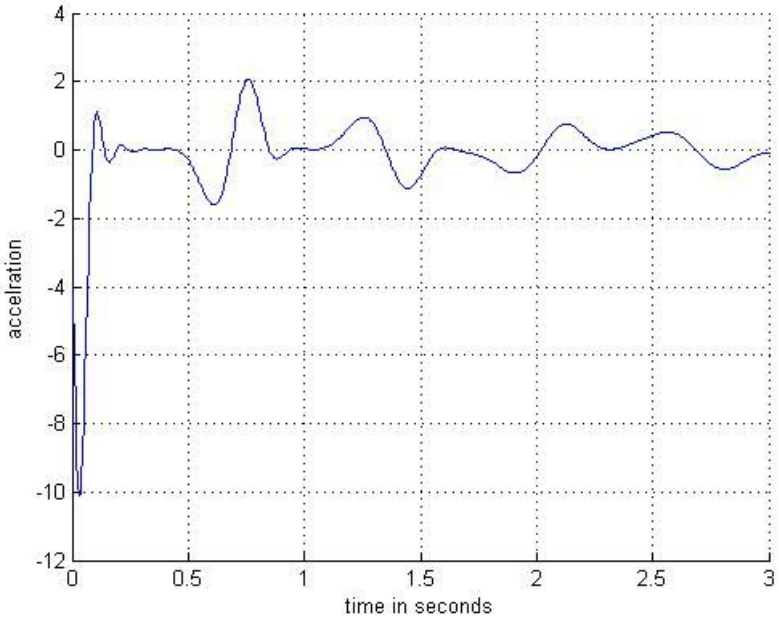

Fig. 5-6 Measured Acceleration at Node 10 for Case 2

Table 5-11 Identified Spring Constants and Dash Pot Constants with 10 Measurements for Case 2

	Spring		Dash pot	
	Simulated	Identified	Simulated	Identified
Element 1	1000	1000	5	5
Element 2	1000	1000	5	5
Element 3	900	900	6	6
Element 4	1000	1000	5	5
Element 5	1000	1000	5	5
Element 6	1000	1000	5	5
Element 7	1000	1000	5	5
Element 8	1000	1000	5	5
Element 9	1000	1000	5	5
Element 10	1000	1000	5	5

Table 5-12 Identified Spring Constants and Dash Pot Constants with 2 Measurements for Case 2

	Spring		Dash pot	
	Simulated	Identified	Simulated	Identified
Element 1	1000	1000	5.00	5.00
Element 2	1000	1000	5.00	5.00
Element 3	900	900	6.00	6.00
Element 4	1000	1000	5.00	5.00
Element 5	1000	1000	5.00	5.00
Element 6	1000	1000	5.00	5.00
Element 7	1000	1000	5.00	5.00
Element 8	1000	1000	5.00	5.00
Element 9	1000	1000	5.00	5.00
Element 10	1000	1000	5.00	5.00

Table 5-13 Identified Spring Constant with 1 Measurement Location for Case 2

	Measurement Location (Node)									
	Simulated	2	3	4	5	6	7	8	9	10
Element 1	1000	993	1003	1000	1000	1000	1000	1000	1000	1000
Element 2	1000	1004	1000	1000	1000	999	1000	1000	1000	1000
Element 3	900	993	897	900	900	899	900	900	900	900
Element 4	1000	1036	998	1000	1000	1000	1000	1000	1000	1000
Element 5	1000	898	1001	1000	1000	1000	1000	1000	1000	1000
Element 6	1000	877	1005	1000	1000	1000	1000	1000	1000	1000
Element 7	1000	978	998	1000	1000	1001	1000	1000	1000	1000
Element 8	1000	1102	997	1000	1000	999	1000	1000	1000	1000
Element 9	1000	1042	997	1000	1000	999	1000	1000	1000	1000
Element 10	1000	988	1003	1000	1000	1000	1000	1000	1000	1000

Table 5-14 Identified Dash Pot Constant with 1 Measurement Location for Case 2

	Measurement Location (Node)									
	Simulated	2	3	4	5	6	7	8	9	10
Element 1	5	5.52	5.03	5.00	5.00	5.01	5.00	5.00	5.00	5.00
Element 2	5	4.59	5.02	5.00	4.99	4.98	5.00	5.00	5.00	5.00
Element 3	6	6.65	5.96	6.00	6.00	6.00	6.00	6.00	6.00	6.00
Element 4	5	6.40	4.98	5.00	5.00	4.99	5.00	5.00	5.00	5.00
Element 5	5	3.65	5.02	5.00	5.00	4.99	5.00	5.00	5.00	5.00
Element 6	5	3.24	4.99	5.00	5.00	5.00	5.00	5.00	5.00	5.00
Element 7	5	4.92	5.00	5.00	5.00	5.00	5.00	5.00	5.00	5.00
Element 8	5	7.25	4.95	5.00	5.00	4.99	5.00	5.00	5.00	5.00
Element 9	5	3.64	4.97	5.00	5.00	5.01	5.00	5.00	5.00	5.00
Element 10	5	5.18	5.03	5.00	5.00	5.00	5.00	5.00	5.00	5.00

As seen in Table 5-13 and Table 5-14, with measured accelerations at Node 1, the spring constants and dash pot constants could not be identified. The identified spring constants diverged at each iteration process. When the measured accelerations at Node 2 were used, the locations of the damaged elements in spring constants were falsely detected. The simulated damaged element was Element 3, but Element 3 was not detected as the damaged element. Instead, Element 5 and Element 6 were identified to have decreased spring constants. With respect to dash pot constants, not only the simulated damaged element, Element 3 was indicated, but Element 4 and Element 8 were falsely detected as the damping damaged elements. However, with the accelerations measured at other nodes, good results for the damage estimation were obtained.

5.2.3 Case 3

In this damage scenario, both Element 3 and Element 8 were inflicted with stiffness damage and damping damage, to simulate a scenario of multiple damages. For Element 3, the spring constant was decreased by 10% and the dash pot constant was increased by 20%, while for Element 8, the spring constant was decreased by 20% and the dash pot constant was increased by 40%. The natural frequencies and modal damping values of the damaged structure are shown in Table 5-15.

Table 5-15 Natural Frequencies and Modal Damping Values of the Existing Structure for Case 3

	Mode 1	Mode 2	Mode 3
Natural frequency (Hz)	0.74	2.18	3.62
Modal damping (%)	1.27	4.06	6.28

The identified spring constants and dash pot constants of the baseline structure are compared with the simulated damaged structure in Table 5-16.

Table 5-16 Comparison of Structural Parameters for Case 3

	Spring		Dash pot	
	Damaged	Baseline	Damaged	Baseline
Element 1	1000	966	5.00	5.44
Element 2	1000	966	5.00	5.44
Element 3	900	966	6.00	5.44
Element 4	1000	966	5.00	5.44
Element 5	1000	966	5.00	5.44
Element 6	1000	966	5.00	5.44
Element 7	1000	966	5.00	5.44
Element 8	800	966	7.00	5.44
Element 9	1000	966	5.00	5.44
Element 10	1000	966	5.00	5.44

The natural frequencies and modal damping values of the damaged structure and the baseline structure are compared in Table 5-17.

Table 5-17 Comparison of Natural Frequencies and Modal Damping Values for Case 3

	Natural Frequency (Hz)		Modal damping (%)	
	Damaged	Baseline	Damaged	Baseline
Mode 1	0.74	0.74	1.27	1.31
Mode 2	2.18	2.20	4.06	3.89
Mode 3	3.62	3.61	6.28	6.40

The accelerations of the damaged structure and the baseline structure at Node 5 and Node 10 are compared in Fig. 5-7 and Fig. 5-8.

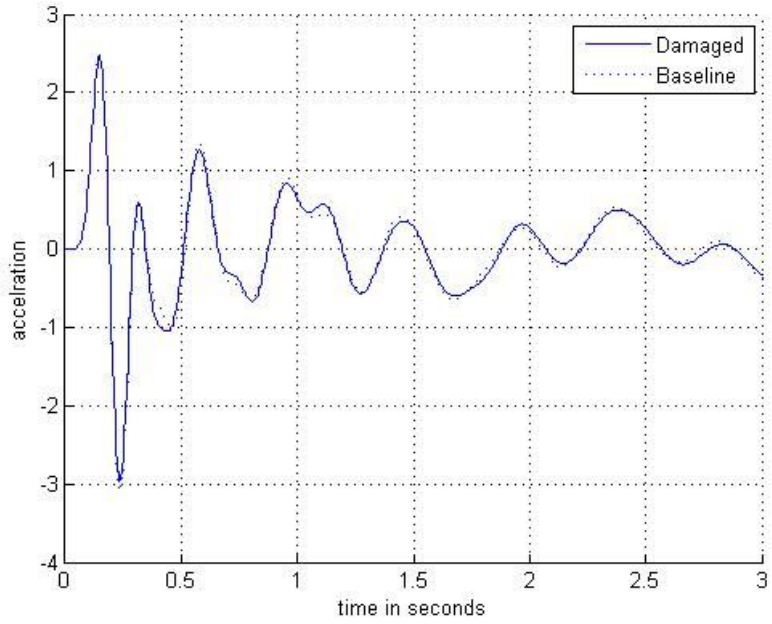

Fig. 5-7 Acceleration at Node 5 for Case 3

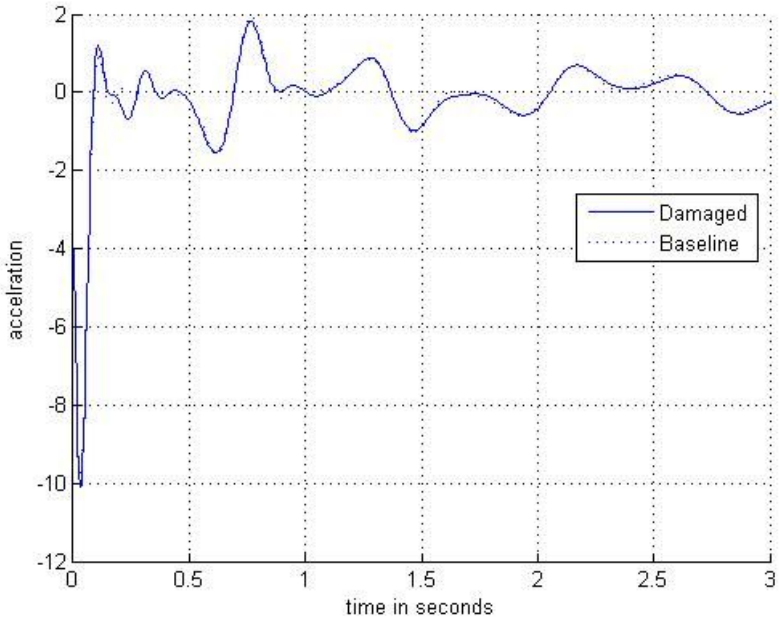

Fig. 5-8 Acceleration at Node 10 for Case 3

Note that from about zero to two seconds, the accelerations measured at Node 5 and Node 10 indicate more deviation; afterwards, the accelerations of the damaged structure and the baseline structure are almost identical. To identify the spring constants and dash pot constants of damaged structure, the NDE technique proposed in Section 3 was applied. When the accelerations measured at all nodes were used, the identified values are listed in Table 5-18.

Table 5-18 Identified Spring Constants and Dash Pot Constants with 10 Measurements for Case 3

	Spring		Dash pot	
	Simulated	Identified	Simulated	Identified
Element 1	1000	1000	5	5
Element 2	1000	1000	5	5
Element 3	900	900	6	6
Element 4	1000	1000	5	5
Element 5	1000	1000	5	5
Element 6	1000	1000	5	5
Element 7	1000	1000	5	5
Element 8	800	800	7	7
Element 9	1000	1000	5	5
Element 10	1000	1000	5	5

We attempted again to identify the structural parameters using the acceleration at Node 5 and Node 10 as in Case 1. The results of identification procedure are listed in Table 5-19.

Table 5-19 Identified Spring Constants and Dash Pot Constants with 3 Measurements for Case 3

	Spring		Dash pot	
	Simulated	Identified	Simulated	Identified
Element 1	1000	1000	5.00	5.00
Element 2	1000	1000	5.00	5.00
Element 3	900	900	6.00	6.00
Element 4	1000	1000	5.00	5.00
Element 5	1000	1000	5.00	5.00
Element 6	1000	1000	5.00	5.00
Element 7	1000	1000	5.00	5.00
Element 8	800	800	7.00	7.00
Element 9	1000	1000	5.00	5.00
Element 10	1000	1000	5.00	5.00

With the accelerations measured at only one location, we attempted to identify the structural parameters. The measurement location was changed from Node 1 to Node 10. Even with the accelerations measured at only one location, the structural parameters were identified exactly for several cases. The identified values are listed in Table 5-20 and Table 5-21.

Table 5-20 Identified Spring Constant with 1 Measurement Location for Case 3

	Measurement Location (Node)							
	Simulated	4	5	6	7	8	9	10
Element 1	1000	1012	1003	1007	998	1000	1000	1000
Element 2	1000	965	1005	1006	998	999	999	999
Element 3	900	913	900	917	903	900	900	900
Element 4	1000	993	992	983	999	1000	1000	1000
Element 5	1000	1015	998	969	1002	1000	1000	1000
Element 6	1000	968	1001	1007	1000	1000	1000	1000
Element 7	1000	1021	995	962	1002	1000	1000	1000
Element 8	800	798	795	796	798	800	800	800
Element 9	1000	1010	1009	1034	1004	1000	1000	1000
Element 10	1000	981	1003	1007	997	1000	1000	1000

Table 5-21 Identified Dash Pot Constant with 1 Measurement Location for Case 3

	Measurement Location (Node)							
	Simulated	4	5	6	7	8	9	10
Element 1	5.00	5.39	4.98	4.57	5.01	5.01	4.99	4.99
Element 2	5.00	6.43	4.93	5.41	5.03	5.00	5.00	5.01
Element 3	6.00	5.63	5.96	6.22	5.99	5.99	6.01	6.00
Element 4	5.00	4.30	5.25	4.37	5.09	4.98	4.99	4.99
Element 5	5.00	4.67	4.98	5.15	4.96	5.02	5.00	5.01
Element 6	5.00	5.35	4.83	5.11	5.01	5.00	5.01	5.00
Element 7	5.00	4.66	5.24	4.41	4.94	5.01	5.00	5.00
Element 8	7.00	6.42	6.96	7.00	6.94	6.99	7.00	7.00
Element 9	5.00	5.21	5.01	5.70	5.04	4.99	5.00	5.00
Element 10	5.00	5.57	4.83	4.76	5.00	5.01	5.00	5.00

With measured accelerations at Node 1, Node 2, and Node 3, the spring constants and dash pot constants could not be identified. The identified spring constants diverged at iterations. For Node 4, the locations of stiffness damaged element were detected, but the damping damaged elements were falsely detected. The dash pot constants were identified satisfactorily with the accelerations measured at Nodes 5, 6, 7, 8, 9, and 10.

5.3 SUMMARY

The proposed method, based on the acceleration-structural parameter sensitivities, was verified numerically using a high-rise building modeled as a shear beam. Three damage scenarios were investigated: 1) damping damage at a single location, 2) both stiffness damage and damping damage at a single location, and 3) several multi-damage cases. The spring constants and dash pot constants of the baseline structure were identified using natural frequencies and modal damping values. The proposed method identified both spring constants and dash pot constants for all damage scenarios. With only one measurement location, the spring constants and dash pot constants were identified exactly.

6 NUMERICAL VERIFICATION OF THE SENSITIVITY METHOD FOR A TWO-SPAN CONTINUOUS BEAM STRUCTURE

6.1 INTRODUCTION

The objective of this section is to verify numerically the performance of the sensitivity method using a two-span continuous beam structure with known damage scenarios. In the shear-beam building model, stiffness damage was simulated by decreasing the spring constant at the damaged element, and damping damage was imposed by increasing the damping coefficient of the appropriate dash pot. For a beam structure, stiffness damage can be simulated by the decreasing bending stiffness of the damaged element in a finite element model. However, how to model the damping of a damaged structure presents another problem.

6.2 MODELING OF DAMPING DAMAGE IN A BEAM STRUCTURE

In this study, it was assumed that the damping of the undamaged structure can be modeled with a proportional damping matrix as follows:

$$\mathbf{C} = a_0\mathbf{M} + a_1\mathbf{K} \tag{6-1}$$

Note that the proportional damping matrix is a linear combination of the mass matrix and the stiffness matrix. With this assumption, damping for the damaged structure is modeled as the combination of proportional damping of the undamaged structure and stiffness proportional damping of the damaged elements as follows:

$$\mathbf{C}^* = \mathbf{C} + \sum_{j=1}^{NDDE} c_j\mathbf{K}_\mathbf{j} = a_0\mathbf{M} + a_1\mathbf{K} + \sum_{j=1}^{NDDE} c_j\mathbf{K}_\mathbf{j} \tag{6-2}$$

Where $\mathbf{C}$ = Damping matrix of the undamaged structure

NDDE= Number of damping damaged element

$\mathbf{M}$ = Mass matrix of the undamaged structure

$\mathbf{K}$ = Stiffness matrix of the undamaged structure

a_0 = Proportional coefficient for the mass matrix

a_1 = Proportional coefficient for the stiffness matrix

$\mathbf{C}^*$ =Damping matrix of the damaged structure

c_j =Proportional coefficient for the jth element

$\mathbf{K_j}$ =Contribution of the jth element to the stiffness matrix

If the damping characteristics of each element can be identified, the damping damaged elements should be able to be detected and estimated. This assumption for the modeling of damping damage in a structure is shown in Fig.6-1. Note that in the damping matrix of the damaged structure, $\mathbf{K}$ and $\mathbf{K_j}$ of the undamaged structure cannot be determined. Thus, the stiffness parameters of the baseline structure are used for $\mathbf{K}$ and $\mathbf{K_j}$.

6.3 DAMAGE DETECTION IN A BEAM STRUCTURE

The structure to be analysed in this study is shown in Fig. 6-2.

(a) Undamaged Structure

Mass : $\mathbf{M}$, Stiffness : $\mathbf{K}$

Damping : $\mathbf{C} = a_0\mathbf{M} + a_1\mathbf{K}$

(b) Damaged Structure

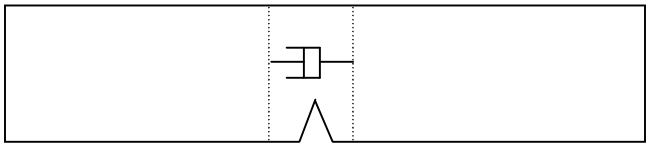

Mass : $\mathbf{M}$, Stiffness : $\mathbf{K}^*$

Damping : $\mathbf{C}^* = \mathbf{C} + \sum_{j=1}^{NDDE} c_j\mathbf{K_j} = a_0\mathbf{M} + a_1\mathbf{K} + \sum_{j=1}^{NDDE} c_j\mathbf{K_j}$

Fig. 6-1 Model of Damping Damaged Structure

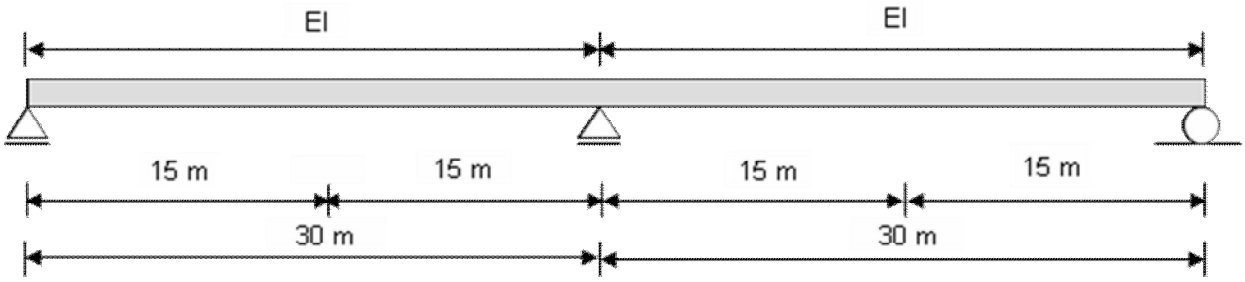

Fig. 6-2 Model of Two-Span Continuous Beam Structure

To obtain the simulated responses of the structure, a finite element model was used. If the model has too many elements, to execute the model may be prohibitive in time and cost. However, if the model doesn't have enough elements, an accurate solution cannot be obtained. To determine an appropriate finite element mesh size for this problem, natural frequencies from finite element model with varying number of finite elements were compared in Fig. 6-3.

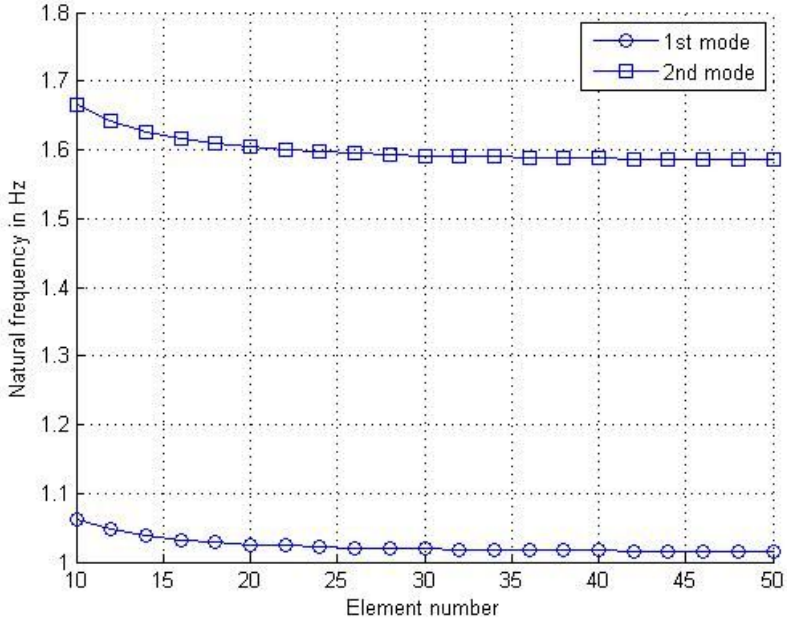

Fig. 6-3 Natural Frequencies with Different Number of Finite Elements

If the natural frequencies obtained with 50 finite elements are considered as the exact solution, the natural frequencies obtained with 20 finite elements have 1.02% and 1.17% errors for first mode and second mode, respectively. These errors were considered as allowable and for the convenience of programming, the beam structure was modeled with 20 finite elements.

To apply the first method, which uses the conservation of energy, the rotations at each node was needed. To get the rotations, differentiation of displacements was required; but differentiation introduces additional errors. Therefore, only the second method, which utilizes accelerations-structural parameters sensitivities, was used for verification purposes.

To get the simulated responses in the time domain (such as accelerations, velocities, and displacements), a vertical force of 20kN was statically applied at the center of left span, and the load was quickly released thus permitting the structure to vibrate freely. Accelerations were measured at a 1000Hz sampling rate. The Newmark-β method was used to evaluate the response.

Three anticipated damage scenarios were introduced to check the performance of the developed methodology. In the first damage scenario, a single element had only damping damage (to simulate the early stage of damage). In the second damage scenario, both stiffness damage and damping damage were simulated in a single element with varying severities. In the third damage scenario, two elements were simulated with stiffness damage and damping damage, in order to check whether or not the developed methodology works for multi-damage case. The anticipated locations and the magnitudes of the damage for each of the scenarios are listed in Table 6-1.

The anticipated sectional properties and material properties for the test structure were as following: Young's modulus E= 0.21×10^{9} kN/m^{2} , sectional area A= 0.459×10^{-2} m^{2}, moment of inertia I= 0.579×10^{-4} m^{4}, and density $\rho = 7850$ kg/m^{3}. For the undamaged element, coefficient c_j had zero value, and for the damaged element, the severity can be estimated with identified a_1 and c_j.

Table 6-1 Damage Scenarios for a Beam Structure

Scenario	Stiffness damage		Damping damaged	
	Location in m	Severity (%)	Location in m	Severity (%)
1			15 ~18	+10
2	15 ~ 18	-10	15 ~ 18	+20
3	15 ~ 18	-10	15 ~ 18	+20
	45 ~ 48	-20	45 ~ 48	+40

6.3.1 Case 1

In this damage scenario, only Element 6 has damping damage which is equivalent to a 10% increase of the damping coefficient. The damping matrix of the undamaged structure was assumed to be a proportional damping matrix with proportional coefficients of 0.01 and 0.005 for the mass matrix and the stiffness matrix, respectively. The damping matrix of the damaged structure was simulated with the combination of the damping matrix of the undamaged structure and the proportional matrix to the stiffness matrix of the damaged element. The relationships between these two matrices are shown in Eq. (6-3).

$$\mathbf{C} = \mathbf{0.01M} + \mathbf{0.005K}$$
$$\mathbf{C}^{*} = \mathbf{0.01M} + \mathbf{0.005K} + \mathbf{0.0005K}_{6} \qquad \textbf{(6-3)}$$

The first step in this proposed NDE method, which uses the acceleration-structural parameters sensitivities, is to identify the baseline structure based on the natural frequencies and modal damping values. The natural frequencies and modal damping values of the damaged structure are shown in Table 6-2.

Table 6-2 Natural Frequencies and Modal Damping Values of the Beam for Case 1

	Mode 1	Mode 2	Mode 3
Natural frequency (Hz)	1.03	1.61	4.25
Modal damping (%)	1.71	2.59	6.72

The bending stiffness and proportional damping coefficients of a baseline structure were determined to have natural frequencies and modal damping values close to those of the damaged structure. Firstly, the initial bending stiffness was given as 0.21×10^5 kN$\bullet$m^2 ; the simulated value is 0.1216×10^5 kN/m^2 . The proportional coefficients were initially assumed to be 0.02 and 0.01 for the mass matrix and the stiffness matrix, respectively. Subsequently, the proportional coefficients were adjusted by the iteration process. The adjustments of bending stiffness and proportional coefficients for damping matrix are shown in Fig. 6-4 and Fig. 6-5.

The converged values for bending stiffness and proportional damping coefficients were taken as the initial values and the iteration process was repeated. The converged identified bending stiffness and proportional damping coefficients were compared with those of the simulated damaged structure in Table 6-3 and Table 6-4. The natural frequencies and modal damping values of the damaged structure and the baseline structure are compared in Table 6-5.

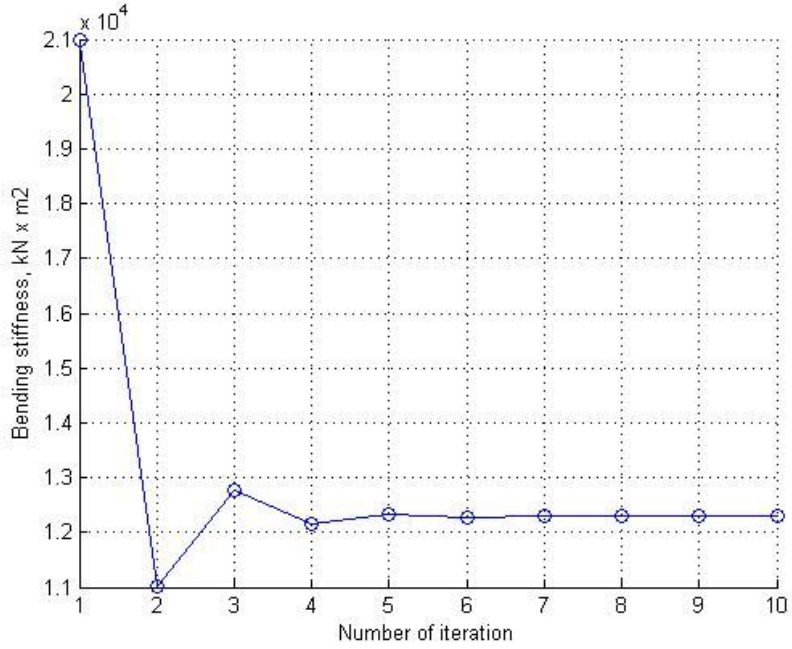

Fig. 6-4 Bending Stiffness of Baseline Structure for Case 1

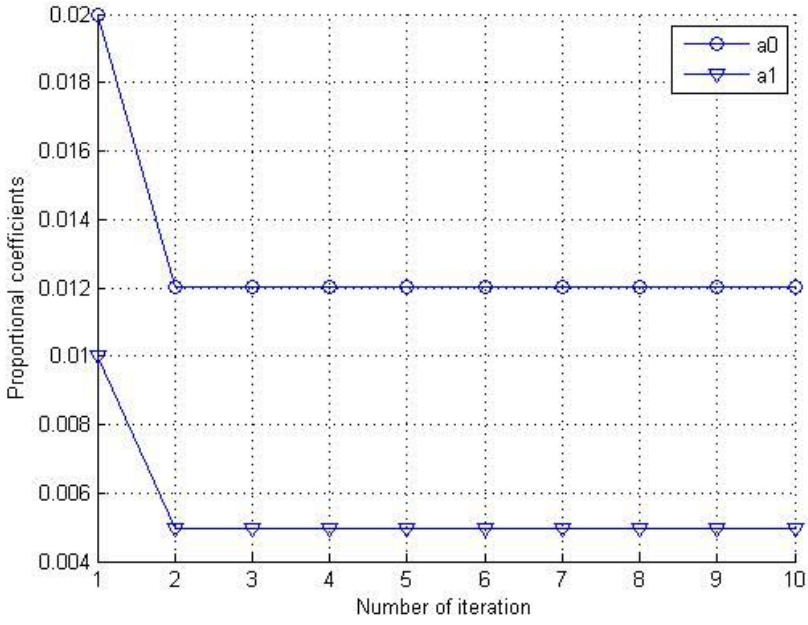

Fig. 6-5 Proportional Coefficients of Baseline Structure for Case 1

Table 6-3 Comparison of Structural Parameters of the Beam for Case 1

	Bending stiffness		Damping cj	
	Damaged	Baseline	Damaged	Baseline
Element 6	12159	12159	0.005	0.000
all other elements	12159	12159	0.000	0.000

Table 6-4 Comparison of Proportional Coefficients of Damping Matrix for Case 1

	Proportional coefficients	
	Damaged	Baseline
a0	0.010	0.012
a1	0.005	0.005

Table 6-5 Comparison of Natural Frequencies and Modal Damping Values of the Beam for Case 1

	Natural Frequency (Hz)		Modal damping (%)	
	Damaged	Baseline	Damaged	Baseline
Mode 1	1.03	1.03	1.71	1.71
Mode 2	1.61	1.61	2.59	2.58
Mode 3	4.25	4.25	6.72	6.71

The accelerations of the damaged structure and the baseline structure at 9m away from left-most support and 9m away from right-most support are compared in Fig. 6-6 and Fig. 6-7. The accelerations of the baseline structure did not show any obvious differences from the acceleration responses of the damaged structure. This observation may be related to the fact that the stiffness parameters of the baseline structure are almost identical to those of the damaged structure, with only the damping parameters differing slightly. To identify the bending stiffness and damping characteristics of the damaged structure, the NDE technique proposed in Section 3 was applied. The accelerations measured at 9m, 21m, 39m and 51m away from left-most support were used. The identified values are shown in Fig. 6-8 and Fig. 6-9.

With the NDE techniques proposed in Section 3, the bending stiffness and damping characteristics constants accurately identified. As shown in Fig. 6-8, there no element indicates stiffness damage. However, in Fig. 6-9, it is obvious that Element 6, which is equivalent to a location 15m ~18m from the left-most support, has damping damage. The damping coefficient of Element 6 was increased about 10% and all other elements had negligible damping change. Therefore, it could be concluded that Element 6 has damping damage, and its severity is 10%.

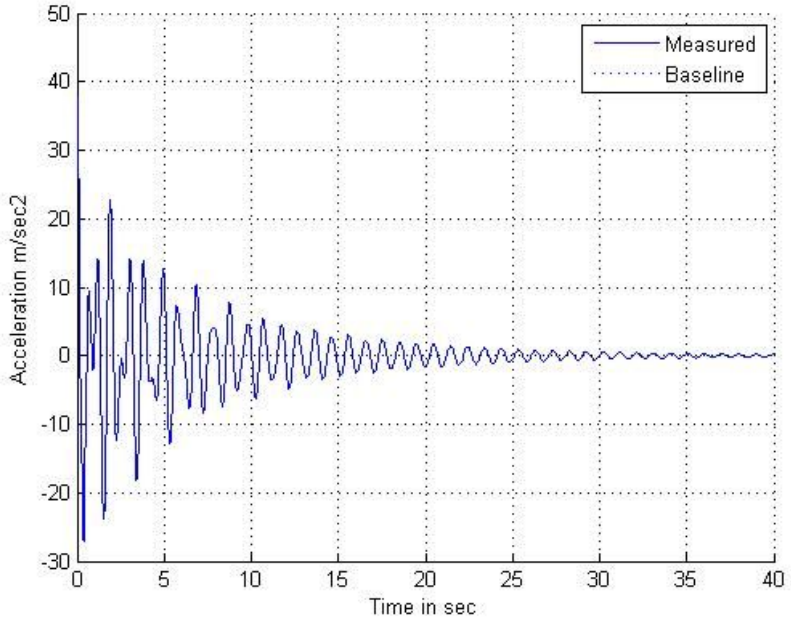

Fig. 6-6 Accelerations at 9m Away from Left-most Support for Case 1

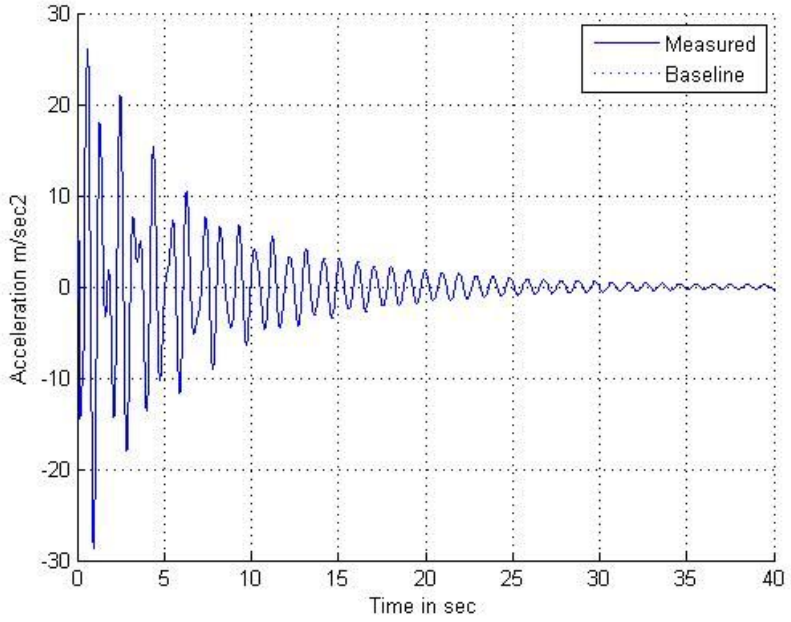

Fig. 6-7 Accelerations at 9m Away from Right-most Support for Case 1

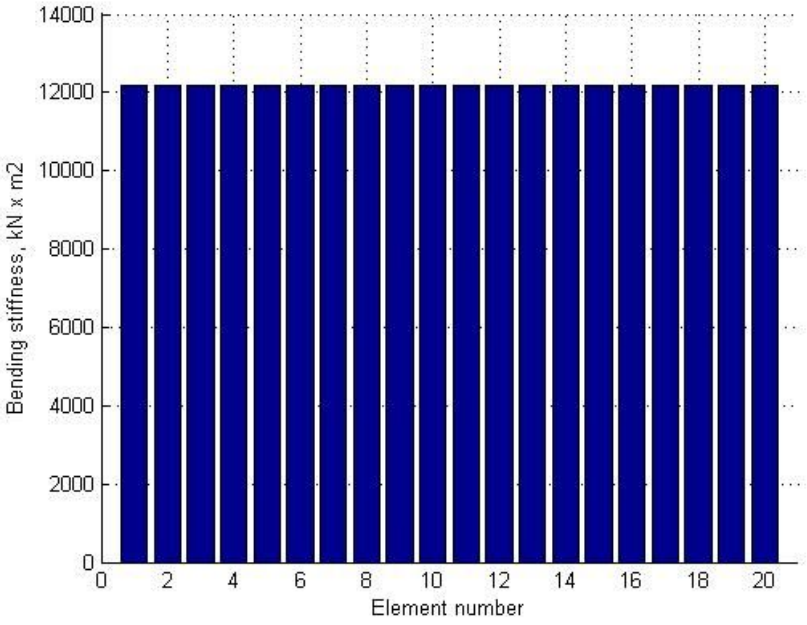

Fig. 6-8 Identified Bending Stiffness for Case 1

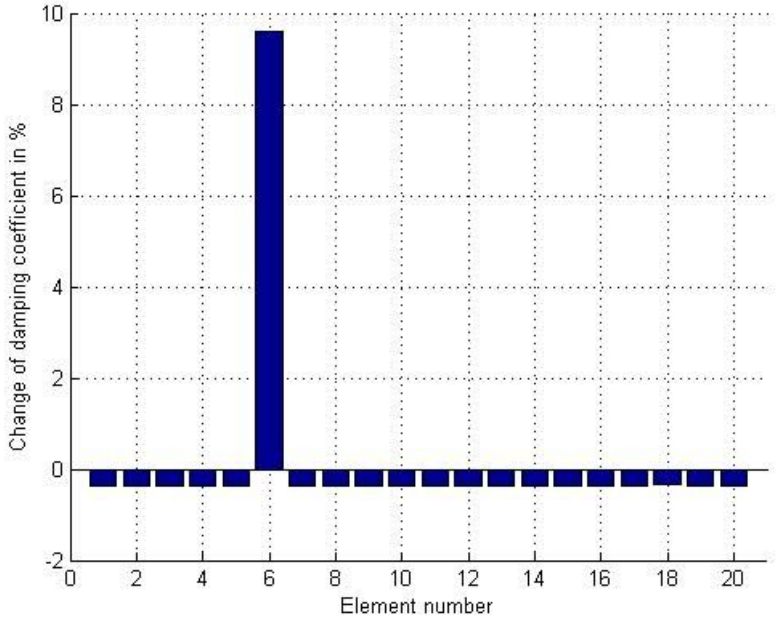

Fig. 6-9 Identified Damping Coefficients for Case 1

6.3.2 Case 2

In this damage scenario, Element 6 has both stiffness damage and damping damage. The severity of stiffness damage is 10% and the severity of damping damage is 20%. The damping matrix of the undamaged structure was assumed to be a proportional damping matrix, in which the proportional coefficients were 0.01 and 0.005 for the mass matrix and the stiffness matrix, respectively, as in Case 1. The damping matrix of the damaged structure was simulated with the combination of the damping matrix of the undamaged structure and a matrix proportional to the stiffness matrix of the damaged element. The relationships between these two matrices are shown in Eq. (6-4).

$$\begin{aligned} \mathbf{C} &= \mathbf{0.01M} + \mathbf{0.005K} \\ \mathbf{C}^{*} &= \mathbf{0.01M} + \mathbf{0.005K} + \mathbf{0.001K}_{6} \end{aligned} \tag{6-4}$$

The natural frequencies and modal damping values of the damaged structure are shown in Table 6-6. The bending stiffness and proportional damping coefficients of a baseline structure were identified by the same process as in Case 1. The adjustment of the

bending stiffness and proportional coefficients for the damping matrix are shown in Fig. 6-10 and Fig. 6-11. The converged identified bending stiffness and proportional damping coefficients were compared with those of the damaged structure in Table 6-7 and Table 6-8.

Table 6-6 Natural Frequencies and Modal Damping Values of the Beam for Case 2

	Mode 1	Mode 2	Mode 3
Natural frequency (Hz)	1.02	1.60	4.24
Modal damping (%)	1.74	2.61	6.73

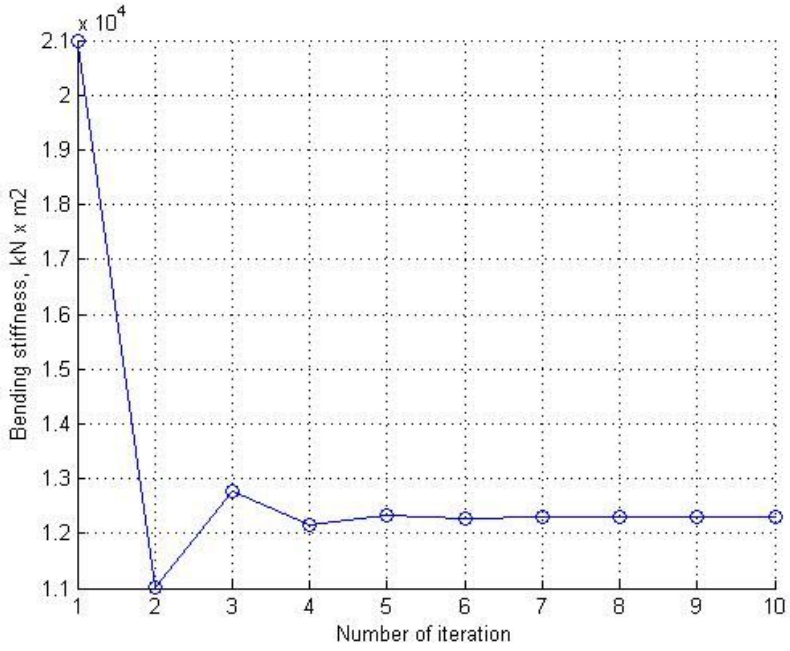

Fig. 6-10 Bending Stiffness of Baseline Structure for Case 2

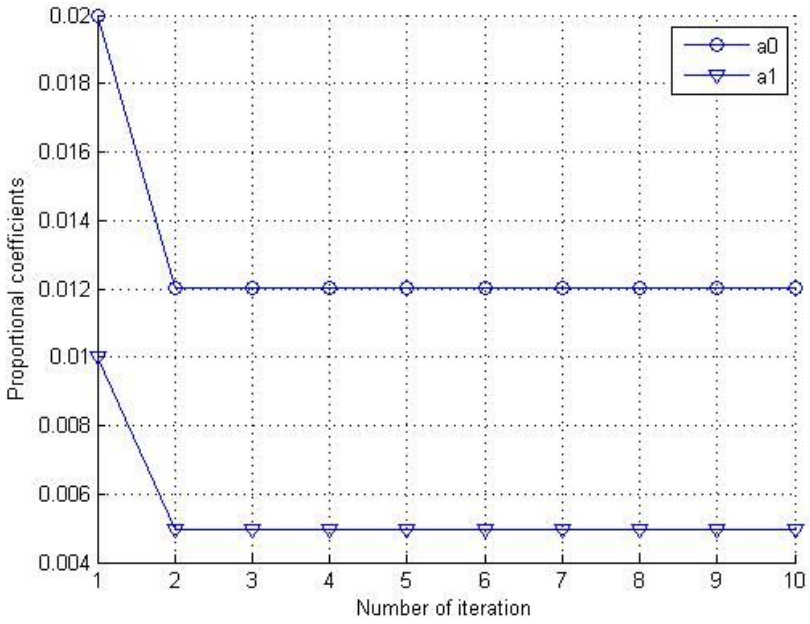

Fig. 6-11 Proportional Coefficients of Baseline Structure for Case 2

Table 6-7 Comparison of Structural Parameters of the Beam for Case 2

	Bending stiffness		Damping cj	
	Damaged	Baseline	Damaged	Baseline
Element 6	12159	12131	0.001	0.0000
all other elements	10943	12131	0.000	0.0000

Table 6-8 Comparison of Proportional Coefficients of Damping Matrix for Case 2

	Proportional coefficients	
	Damaged	Baseline
a0	0.010	0.016
a1	0.005	0.005

The proportional damping coefficient a0 was influenced by the increased damping in the damaged element. However, damping coefficient a1 for the stiffness matrix was not

influenced. The natural frequencies and modal damping values of the damaged structure and the baseline structure are compared in Table 6-9.

Table 6-9 Comparison of Natural Frequencies and Modal Damping Values of the Beam for Case 2

	Natural Frequency (Hz)		Modal damping (%)	
	Damaged	Baseline	Damaged	Baseline
Mode 1	1.02	1.02	1.74	1.74
Mode 2	1.60	1.60	2.61	2.61
Mode 3	4.24	4.24	6.73	6.73

The accelerations of the damaged structure and the baseline structure at 9m away from left-most support and 9m away from right-most support were compared in Fig. 6-12 and Fig. 6-13.

To identify the bending stiffness and damping characteristics of the damaged structure, the NDE technique proposed in Section 3 was applied. The accelerations measured at 9m, 21m, 39m and 51 m away from left-most support were used. The stiffness damage severity and damping damage severity of each element are shown in Fig. 6-14 and Fig. 6-15, respectively.

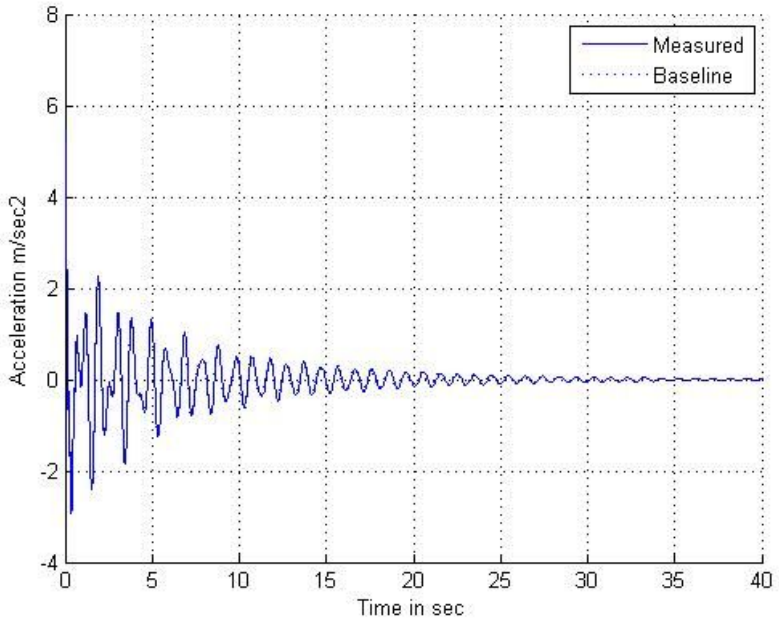

Fig. 6-12 Accelerations at 9m Away from Left-most Support for Case 2

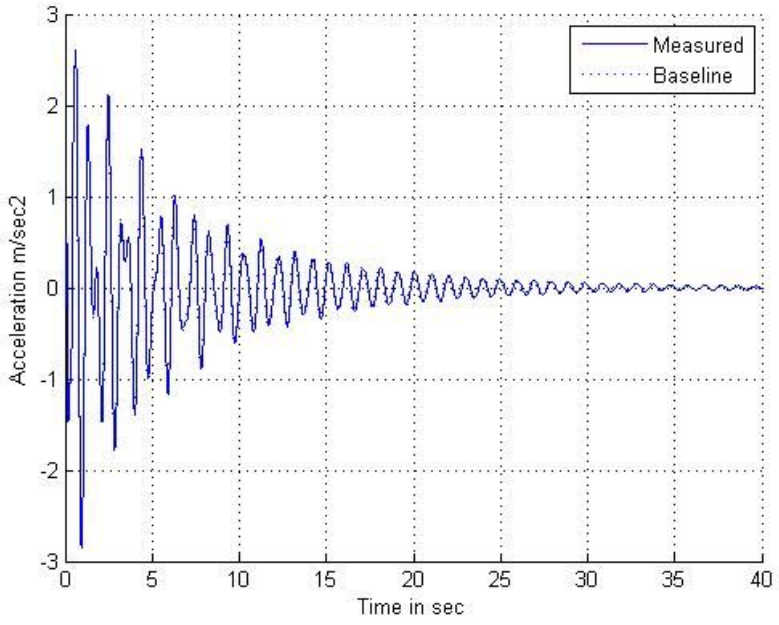

Fig. 6-13 Accelerations at 9m Away from Right-most Support for Case 2

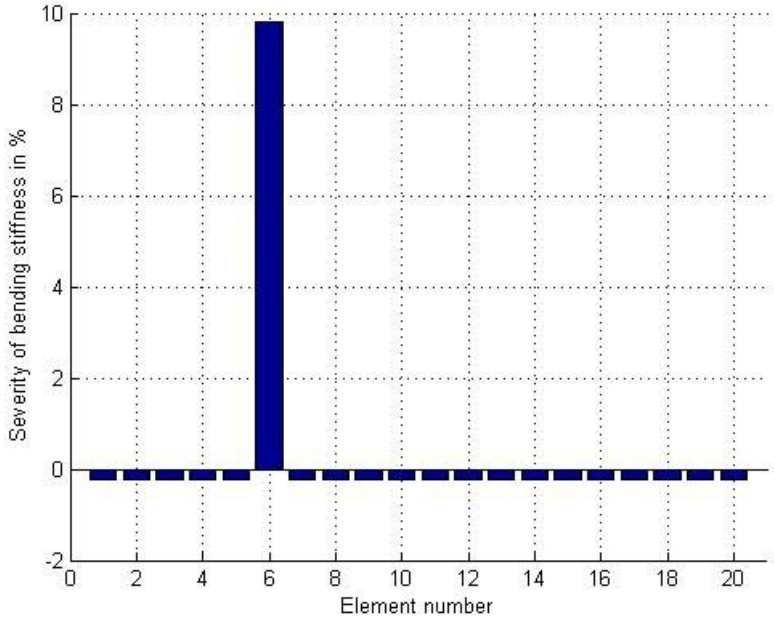

Fig. 6-14 Identified Bending Stiffness for Case 2

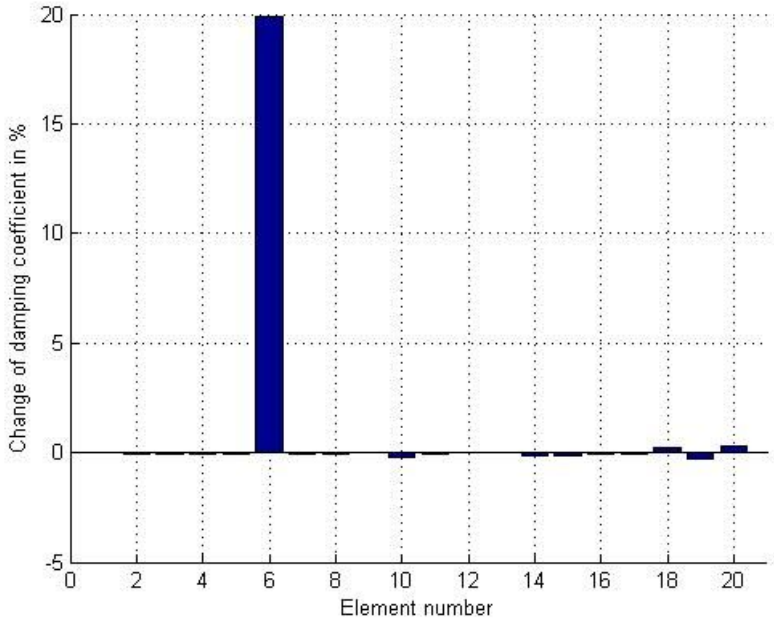

Fig. 6-15 Identified Damping Coefficients for Case 2

As shown in Fig. 6-15, Element 6, which is equivalent to a location 15m ~18m, is suspected to have stiffness damage with a severity of about 10%. In Fig. 6-16, it is observed that Element 6 has damping damage as well as stiffness damage. The damping coefficient of Element 6 increased about 20%. For other elements, increases of the damping coefficients are negligible. Therefore, it is concluded that Element 6 has 10% stiffness damage and 20% damping damage.

6.3.3 Case 3

In this damage scenario, two elements were simulated with stiffness damage and damping damage in order to check whether or not the developed methodology works for multi-damage cases. Damages were inflicted to Element 6 and Element 16. For Element 6, 10% stiffness damage and 20% damping damage were inflicted and 20% stiffness damage and 40% damping damage were inflicted at Element 16. The damping matrix of the undamaged structure was assumed to be a proportional damping matrix, of which proportional coefficients were 0.01 and 0.005 for the mass matrix and the stiffness matrix, respectively, as in Case 1. The damping matrix of the damaged structure was simulated with the combination of the damping matrix of the undamaged structure and the proportional matrix to the stiffness matrix of the damaged element. The relationships between these two matrices are shown in Eq. (6-5).

$$\mathbf{C} = 0.01\mathbf{M} + 0.005\mathbf{K}$$
$$\mathbf{C}^{*} = 0.01\mathbf{M} + 0.005\mathbf{K} + 0.001\mathbf{K}_{6} + 0.002\mathbf{K}_{16} \quad \textbf{(6-5)}$$

The natural frequencies and modal damping values of the damaged structure are shown in Table 6-10.

Table 6-10 Natural Frequencies and Modal Damping Values of the Beam for Case 3

	Mode 1	Mode 2	Mode 3
Natural frequency (Hz)	1.01	1.59	4.24
Modal damping (%)	1.86	2.76	6.79

The bending stiffness and proportional damping coefficients of a baseline structure were identified by the same process in Case 1. The adjustments of the bending stiffness and the proportional coefficients for the damping matrix are shown in Fig. 6-16 and Fig. 6-17. The converged identified bending stiffness and the proportional damping coefficients were compared with those of the damaged structure in Table 6-11 and Table 6-12.

The proportional damping coefficient a0 of the baseline structure was identified to be more than three times a0 of the damaged structure. However damping coefficient a1, which is for the stiffness matrix was identified to be almost the same as that of the damaged structure. The natural frequencies and modal damping values of the damaged structure and the baseline structure are compared in Table 6-13.

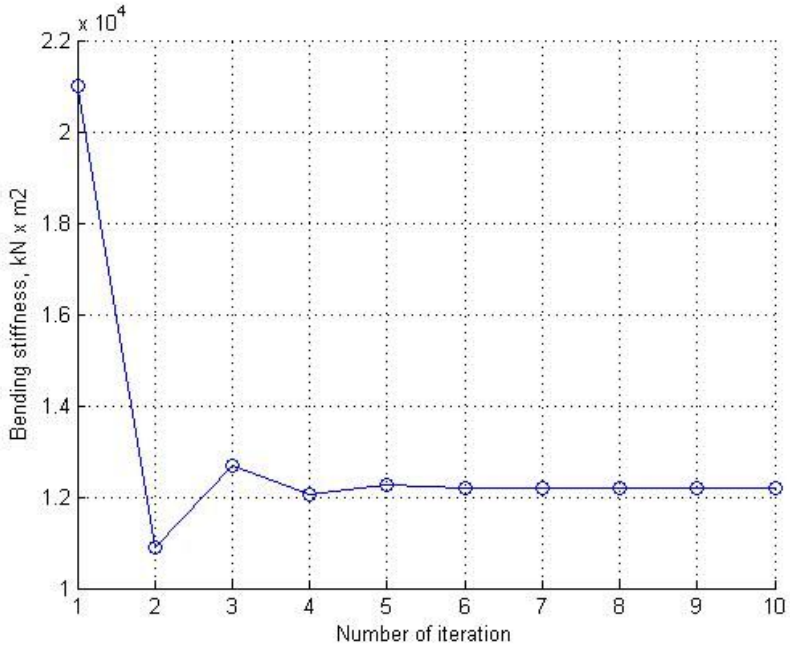

Fig. 6-16 Bending Stiffness of Baseline Structure for Case 3

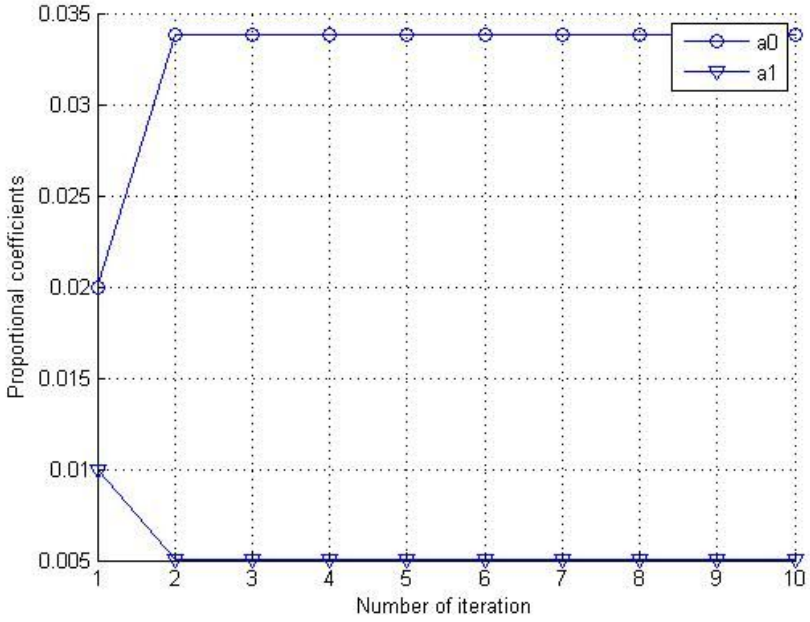

Fig. 6-17 Proportional Coefficients of Baseline Structure for Case 3

Table 6-11 Comparison of Structural Parameters of the Beam for Case 3

	Bending stiffness		Damping cj	
	Damaged	Baseline	Damaged	Baseline
Element 6	10943	12060	0.001	0.000
Element 16	97272	12060	0.002	0.000
all other elements	12159	12060	0.000	0.0000

Table 6-12 Comparison of Proportional Coefficients of Damping Matrix for Case 3

	Proportional coefficients	
	Damaged	Baseline
a0	0.010	0.0336
a1	0.005	0.0051

Table 6-13 Comparison of Natural Frequencies and Modal Damping Values of the Beam for Case 3

	Natural Frequency (Hz)		Modal damping (%)	
	Damaged	Baseline	Damaged	Baseline
Mode 1	1.01	1.02	1.86	1.89
Mode 2	1.59	1.60	2.76	2.71
Mode 3	4.24	4.23	6.79	6.80

The accelerations of the damaged structure and the baseline structure 9m away from the left-most support and 9m away from the right-most support are compared in Fig. 6-18 and Fig. 6-19.

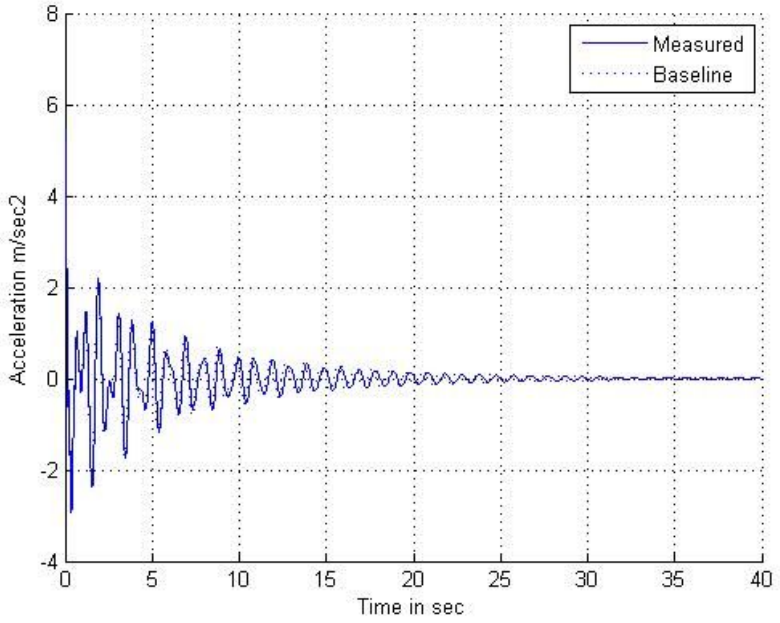

Fig. 6-18 Accelerations at 9m Away from Left-most Support for Case 3

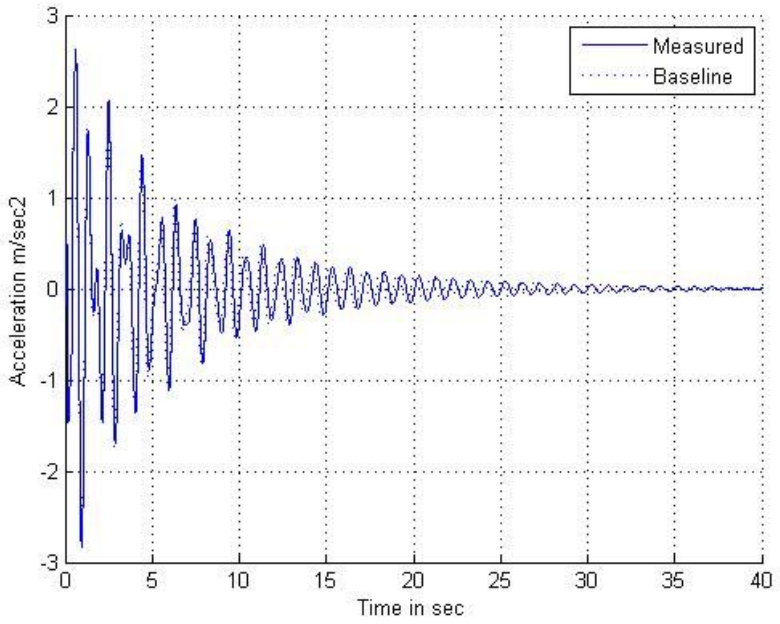

Fig. 6-19 Accelerations at 9m Away from Right-most Support for Case 3

To identify the bending stiffness and damping characteristics of the damaged structure, the NDE technique proposed in Section 3 was applied. The accelerations measured at 9m, 21m, 39m and 51 m away from the left-most support were used. The stiffness damage severity and damping damage severity of each element are shown in Fig. 6-20 and Fig. 6-21, respectively. As shown in Fig. 6-20, Element 6 and Element 16, which are located at 15m~18m and 45m~48m, respectively, are suspected to be damaged in its stiffness and their severities are expected to be about 10% and 20%. In Fig. 6-21, it is observed that Element 6 and Element 16 have damping damage as well as stiffness damage. The damping coefficient of Element 6 was increased by about 20% and the damping coefficient of Element 16 was increased by about 40%. For other elements, the increases of the damping coefficients were negligible. Therefore, it could be concluded that Element 6 had 10% stiffness damage and 20% damping damage and Element 16 had 20% stiffness damage and 40% damping damage.

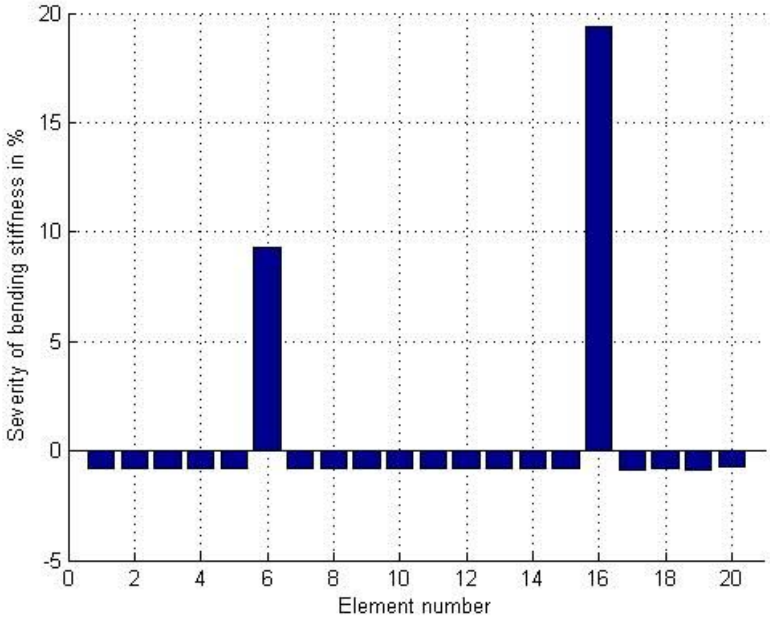

Fig. 6-20 Identified Bending Stiffness for Case 3

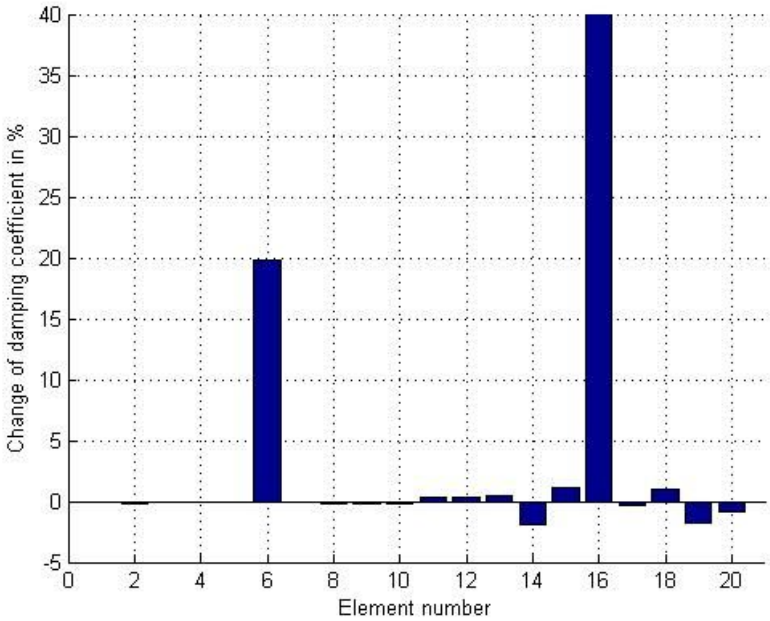

Fig. 6-21 Identified Damping Coefficients for Case 3

6.4 SUMMARY

The proposed method, based on the acceleration-structural parameters sensitivities, was verified numerically using a two-span continuous beam structure. A method to model damping damage in the beam structure was proposed and three damage scenarios were investigated to simulate simultaneously damping damage and stiffness damage for single damage and multi-damage cases. The proportional damping coefficients for the mass matrix and the stiffness matrix were identified using modal damping values and the bending stiffness of the baseline structure was determined using the natural frequencies. The increased damping coefficient of the damping damaged element influenced the proportionality coefficient for the mass matrix. The change in the proportionality coefficient for the stiffness matrix was negligible. The proposed method accurately identified both bending stiffness changes and damping coefficient changes for all damage scenarios investigated here.

7 NUMERICAL VERIFICATION OF THE ENERGY CONSERVATION METHOD FOR A SHEAR BUILDING WITH NOISE-POLLUTED DATA

7.1 INTRODUCTION

The objective of this section is to verify the performance of the proposed method which uses energy conservation numerically for a shear building with known damage scenarios and noise-polluted data.

7.2 DAMAGE DETECTION IN A SHEAR BUILDING

The same target structure and the same damage scenarios considered in Section 4 are used. In this study, to excite the structure, a horizontal tensile force of 200 kips was applied at the 10^{th} story, and the load was quickly removed, thus permitting the structure to vibrate freely as in Section 4. The Newmark-β method was used to obtain the simulated accelerations. Accelerations were measured using a 1000 Hz sampling rate. To simulate noise, random numbers were generated for each time step and each measurement location. The mean value of the parent distribution was set to zero and the standard deviation of the distribution was set to 1. The random numbers were multiplied by the noise level constant and the displacement or velocity at the corresponding time step and measurement location. The scaled random numbers were superposed to the corresponding noise-free displacements and velocities generated by The Newmark-β method. Noise polluted displacements were produced as follows:

$$\overline{u}_{ji} = u_{ji}(1 + s\sigma_{ji}) \qquad \textbf{(7-1)}$$

Where $\overline{u}_{ji}$ = noise-polluted displacement at jth time step for ith node

u_{ji} = noise-free displacement at jth time step for ith node

s = noise level

σ_{ji} = random number produced for the acceleration at jth time step for ith node

In this study, noise levels corresponding to 1%, 3%, and 5% were considered.

7.2.1 Case 1

In this damage scenario, only Element 3 has damping damage equivalent to a 10% increase in the dash pot constant.

1% Noise

The random number scaled by 1% of the displacement and velocity was added to the corresponding noise-free displacement and noise-free velocity. The displacement and velocities at Node 5 and Node 10 are shown in Fig. 7-1 and Fig. 7-2.

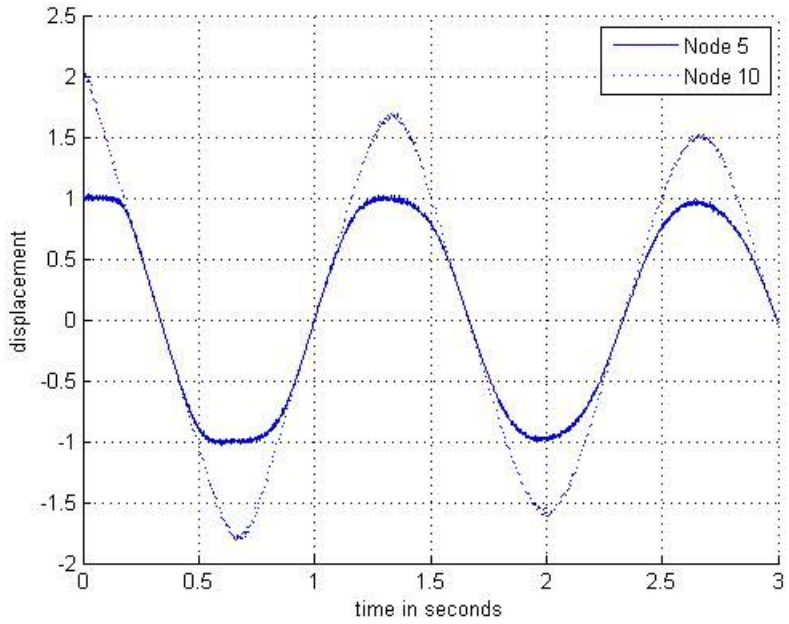

Fig. 7-1 Displacements with 1% Noise for Case 1

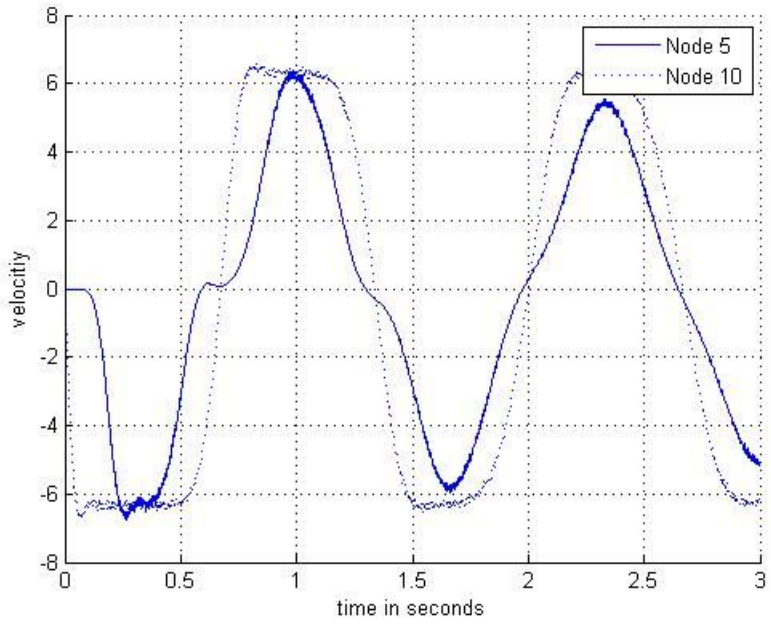

Fig. 7-2. Velocities with 1% Noise for Case 1

To check the conservation of total energy, the sum of the potential energy of each spring element, the sum of the kinetic energy of each mass element, and the sum of the dissipated energy of each dash pot element at each time step was calculated using noise-polluted displacements, velocities. The results of these calculations are shown in Fig. 7-3. Note that in Fig. 7-3 the total energy and the sum of kinetic energy and potential energy vary in time as a result of the noise. Note also that the dissipated energy does not vary as much as the total energy; This is because the influence of the noise is decreased because the dissipated energy is an integrated quantity. Displacements and velocities at each node were measured 10 times and the identified results with 10 sets of the measured displacements and velocities are shown in Fig. 7-4 and Fig. 7-5.

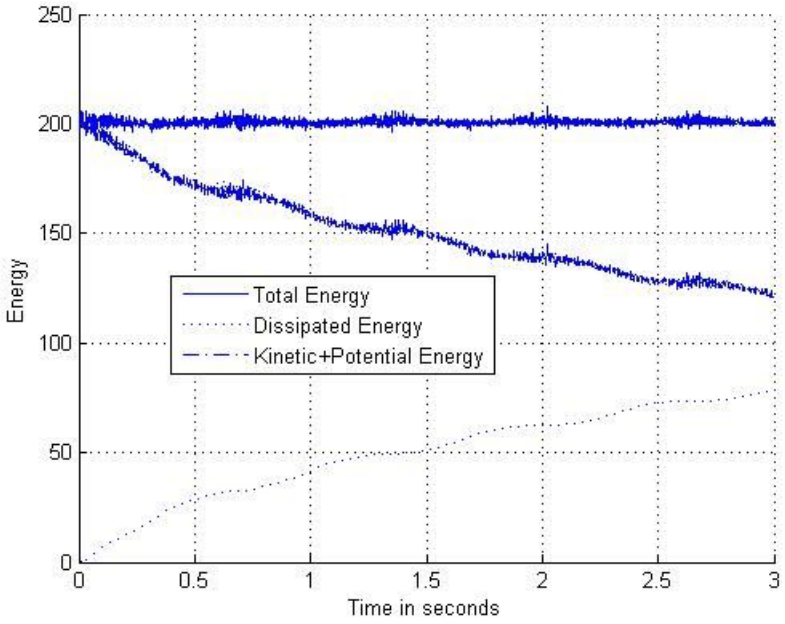

Fig. 7-3 Check of Conservation of Total Energy with Noise Polluted Data

The Damage Index calculated with the identified values are shown in Fig. 7-6 and Fig 7-7. Damage Index for each element is obtained as following:

For spring $$DI_i = \frac{\bar{s} - s_i}{\sigma_s}$$

For dash pot $$DI_i = \frac{d_i - \bar{d}}{\sigma_d} \qquad \textbf{(7-2)}$$

Where $\bar{s}$ = mean value of the identified spring constants.

s_i = identified spring constant of ith element.

σ_s =standard deviation of the identified spring constants.

$\bar{d}$ = mean value of the identified dash pot constants.

d_i = identified dash pot constant of ith element.

σ_d =standard deviation of the identified dash pot constants.

With respect to the spring, Element 9 and Element 10 were falsely detected as damaged elements and with respect to the dash pot, even negative values were identified for some element. On comparing the results presented in Fig. 7-4 and Fig. 7-5, the ranges of identified values for the dash pot constants are very wide compared with those of the identified spring constants. From statistical view point, the identified dash pot constants have larger coefficients of variation than those of the identified spring constants. This observation suggests that the identified values of the dash pot constants are less reliable than the identified values of the spring constants. The average values of the identified values for each set are compared with the simulated values in Table 7-1.

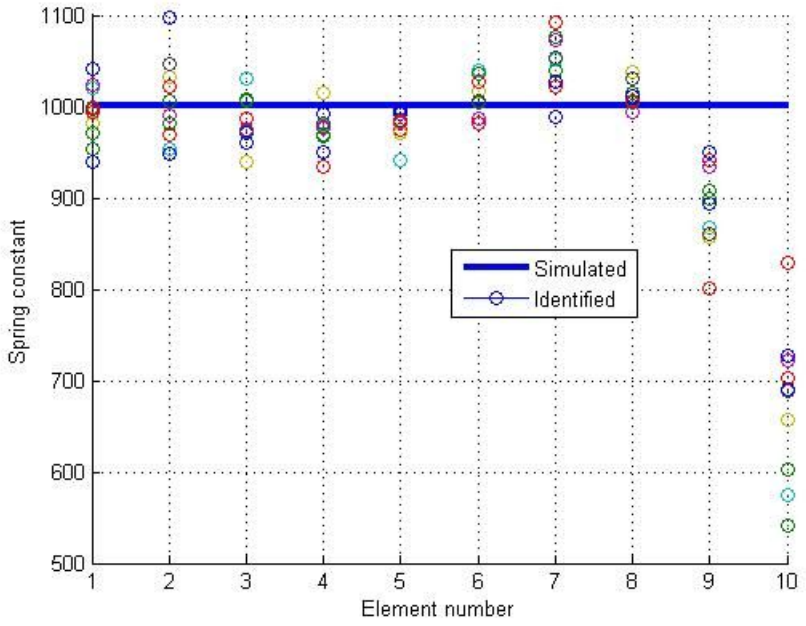

Fig. 7-4 Identified Spring with 1% Noise for Case 1

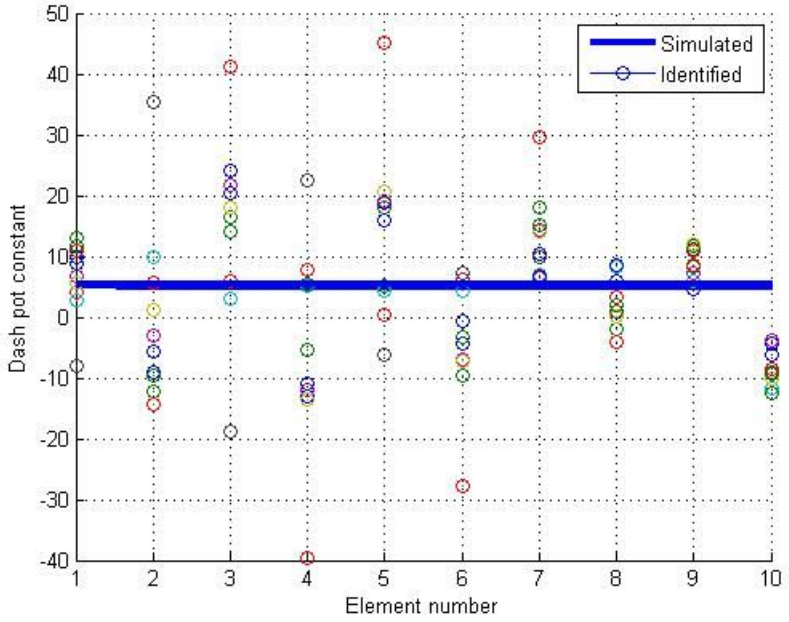

Fig. 7-5 Identified Dash Pot with 1% Noise for Case 1

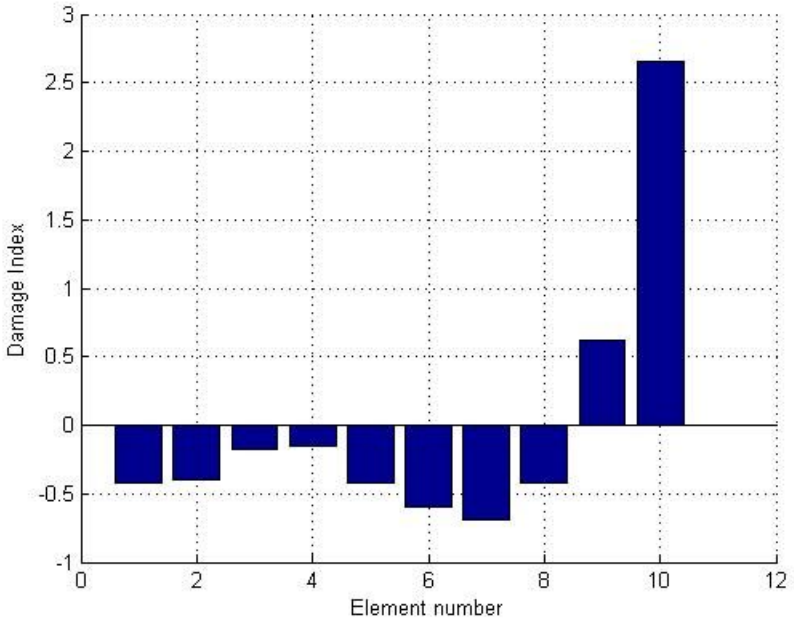

Fig. 7-6 Damage Index for Spring with 1% Noise or Case 1

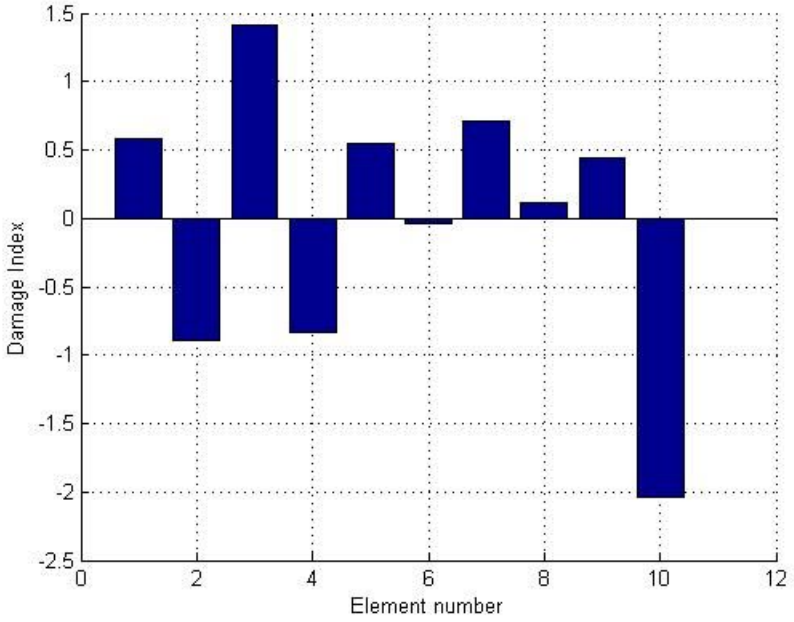

Fig. 7-7 Damage Index for Dash Pot with 1% Noise for Case 1

Table 7-1 Identified Values with 1% Noise for Case 1

	Spring			Dash pot		
	Simulated	Identified	Error (%)	Simulated	Identified	Error (%)
Element 1	1000	1001	0.1	5.0	6.9	38.0
Element 2	1000	992	0.8	5.0	-0.2	104.0
Element 3	1000	987	1.3	5.5	11.0	100.0
Element 4	1000	974	2.6	5.0	1.5	70.0
Element 5	1000	999	0.1	5.0	5.3	6.0
Element 6	1000	1011	1.1	5.0	4.4	12.0
Element 7	1000	1031	3.1	5.0	6.7	34.0
Element 8	1000	1010	1.0	5.0	5.7	14.0
Element 9	1000	888	11.2	5.0	7.0	40.0
Element 10	1000	736	26.4	5.0	-6.4	228.0

For spring constants, the results indicate that the predicted values of the stiffnesses of Element 9 and Element 10 show significant errors. With respect to the dash pot constants, Element 3 was detected as damaged element, but the identified values show 100% error. When the average of the 10 measured displacements and velocities were used, the

identification results listed in Table 7-2 were obtained. On comparing Table 7-1 and Table 7-2, it is observed that no significant improvement is made by averaging the raw data. Thus here, the average of the identified values for each data set will be taken rather than to identify with the average of the measured data.

Table 7-2 Identified Values with Average of Measurements for Case 1

	Spring			Dash pot		
	Simulated	Identified	Error (%)	Simulated	Identified	Error (%)
Element 1	1000	1059	5.9	5.0	5.8	16.0
Element 2	1000	789	21.1	5.0	1.2	76.0
Element 3	1000	1290	29.0	5.5	12.3	123.6
Element 4	1000	854	14.6	5.0	3.5	30.0
Element 5	1000	751	24.9	5.0	-5.8	216.0
Element 6	1000	1683	68.3	5.0	18.5	270.0
Element 7	1000	301	69.9	5.0	4.3	14.0
Element 8	1000	1184	18.4	5.0	-6.8	236.0
Element 9	1000	1190	19.0	5.0	13.0	160.0
Element 10	1000	1035	3.5	5.0	9.5	90.0

3% Noise

The random number scaled by 3% of the displacement and velocity was superposed on the corresponding noise-free displacement and velocity. The displacements and velocities at Node 5 and Node 10 are shown in Fig. 7-8 and Fig. 7-9. Displacements and velocities at each node were measured 10 times and the identified results with 10 sets of the measured displacements and velocities are shown in Fig. 7-10 and Fig. 7-11. It is observed that the variances of the identified dash pot constants increased compared with Fig. 7-5.

Damage indices for each element in spring and dash pot are shown in Fig. 7-12 and Fig. 7-13, respectively. The identified values are listed in Table 7-3. Note that with 1% noise, even if the identified severities were in error, the location of the damping damaged element was detected. However, in with 3% noise, even the location of the damping damaged is not detected.

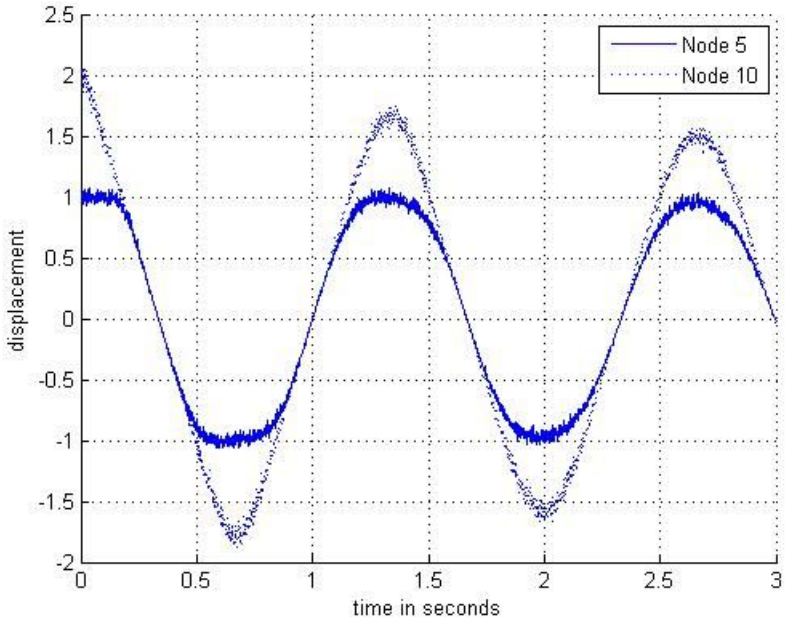

Fig. 7-8 Displacements with 3% Noise for Case 1

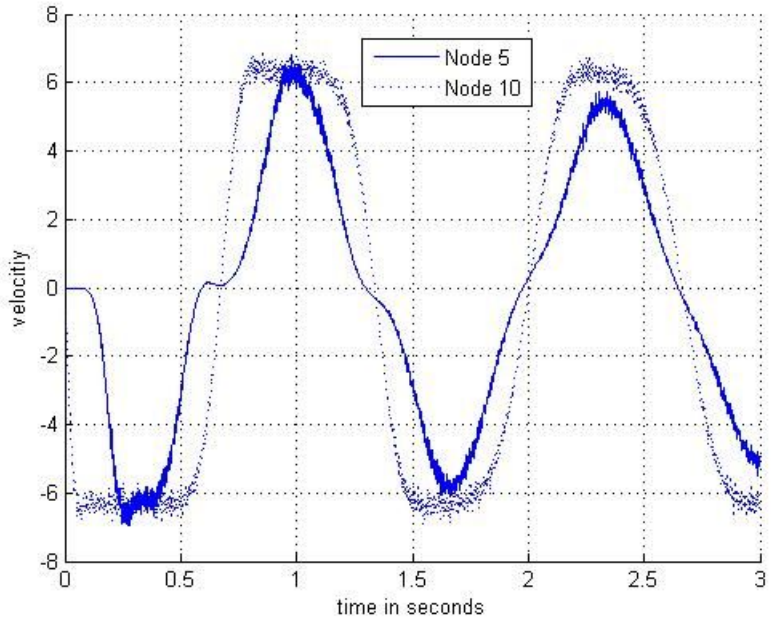

Fig. 7-9 Velocities with 3% Noise for Case 1

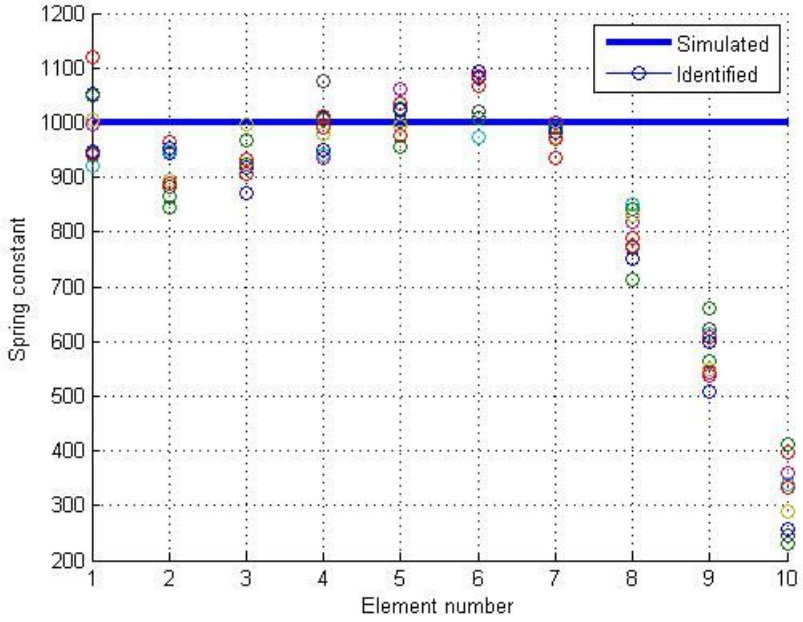

Fig. 7-10 Identified Spring with 3% Noise for Case 1

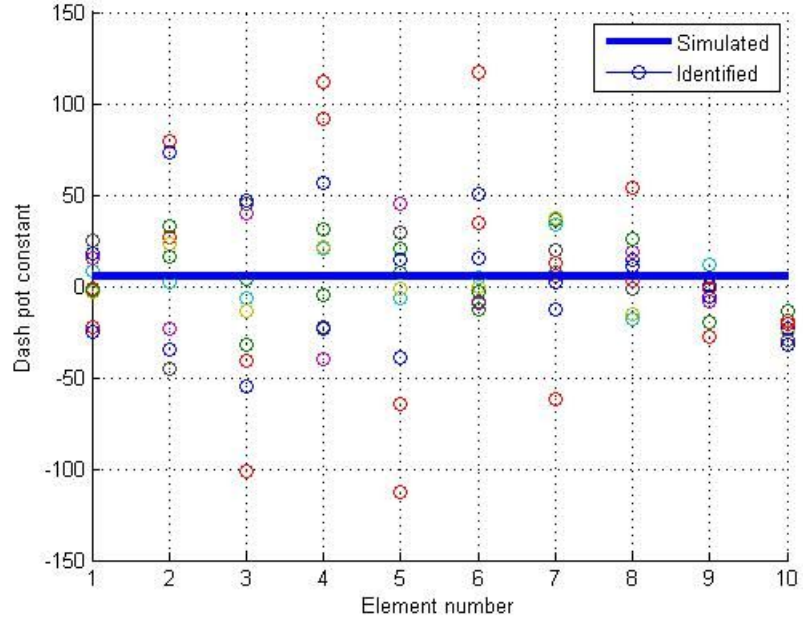

Fig. 7-11 Identified Dash Pot with 3% Noise for Case 1

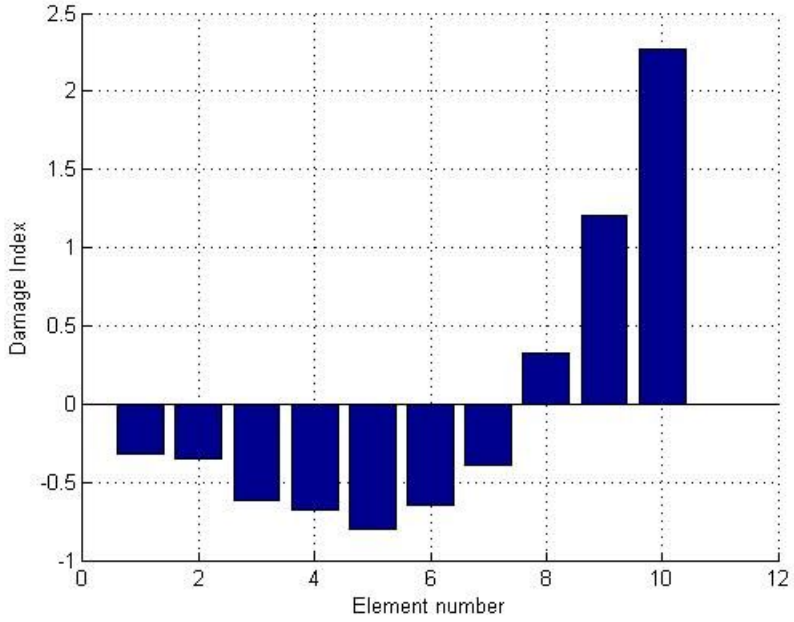

Fig. 7-12 Damage Index for Spring with 3% Noise for Case 1

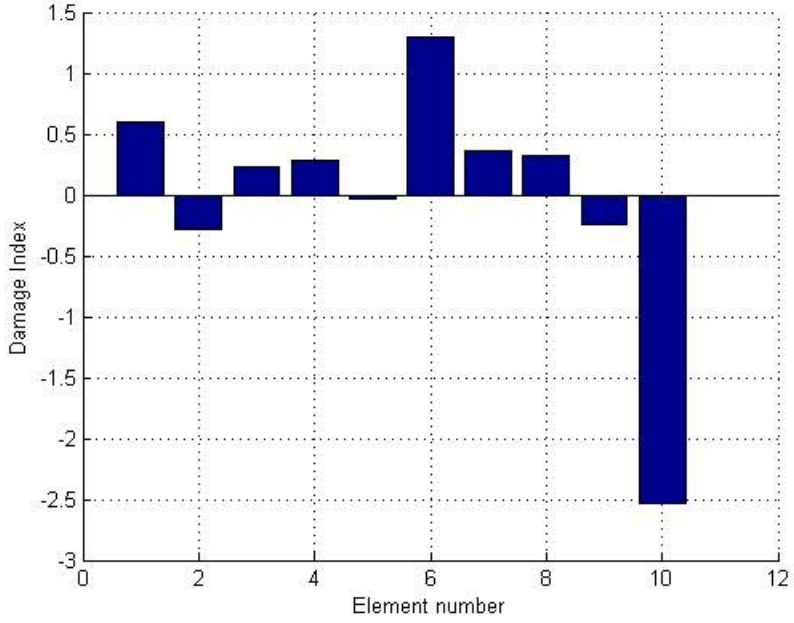

Fig. 7-13 Damage Index for Dash Pot with 3% Noise for Case 1

Table 7-3 Identified Values with 3% Noise for Case 1

	Spring			Dash pot		
	Simulated	Identified	Error (%)	Simulated	Identified	Error (%)
Element 1	1000	922	7.8	5.0	9.4	88.0
Element 2	1000	929	7.1	5.0	-1.7	134.0
Element 3	1000	989	1.1	5.5	4.8	12.7
Element 4	1000	1005	0.5	5.0	5.5	10.0
Element 5	1000	1032	3.2	5.0	1.4	72.0
Element 6	1000	996	0.4	5.0	18.2	264.0
Element 7	1000	937	6.3	5.0	6.5	30.0
Element 8	1000	772	22.8	5.0	6.0	20.0
Element 9	1000	566	43.4	5.0	-1.1	122.0
Element 10	1000	319	68.1	5.0	-29.9	698.0

5% Noise

The randomly generated numbers scaled by 5% of the displacement and velocity were superposed on the corresponding noise-free displacement and velocity. The displacements and velocities at Node 5 and Node 10 are shown in Fig. 7-14 and Fig. 7-15. Displacements and velocities were measured 10 times and the average of the identified parameter values for each data set was taken as the finally identified value. The Damage indices calculated with the average of the identified values for each element in spring and dash pot are shown in Fig. 7-16 and Fig. 7-17, respectively. The identified values are listed in Table 7-4. In the spring constants, Element 8 was falsely detected as a damaged element in addition to Element 9 and Element 10. The increased noise tends to increase the number of false positives. The stiffness of Element 9 and Element 10 were underestimated compared to the case with 3% noise. The coefficients of variation of the identified values of the dash pot constants were increased.

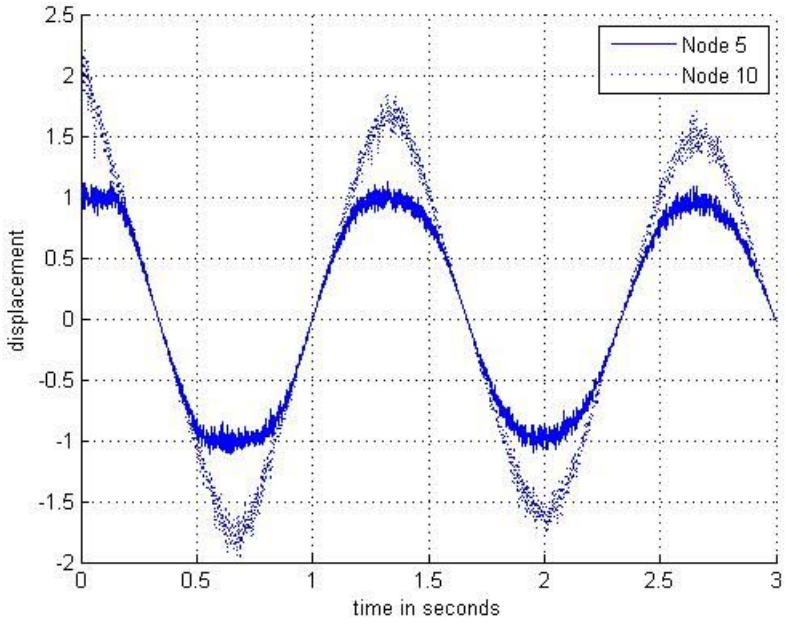

Fig. 7-14 Displacements with 5% Noise for Case 1

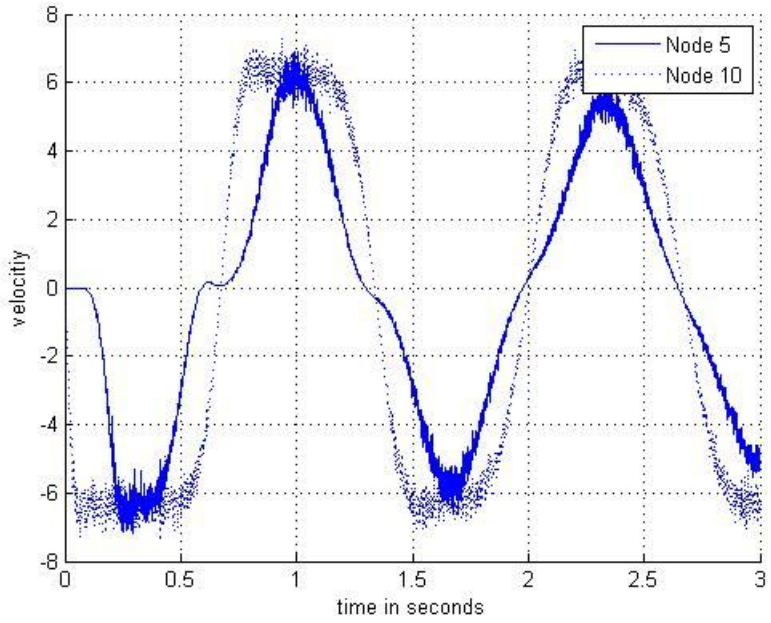

Fig. 7-15 Velocities with 5% Noise for Case 1

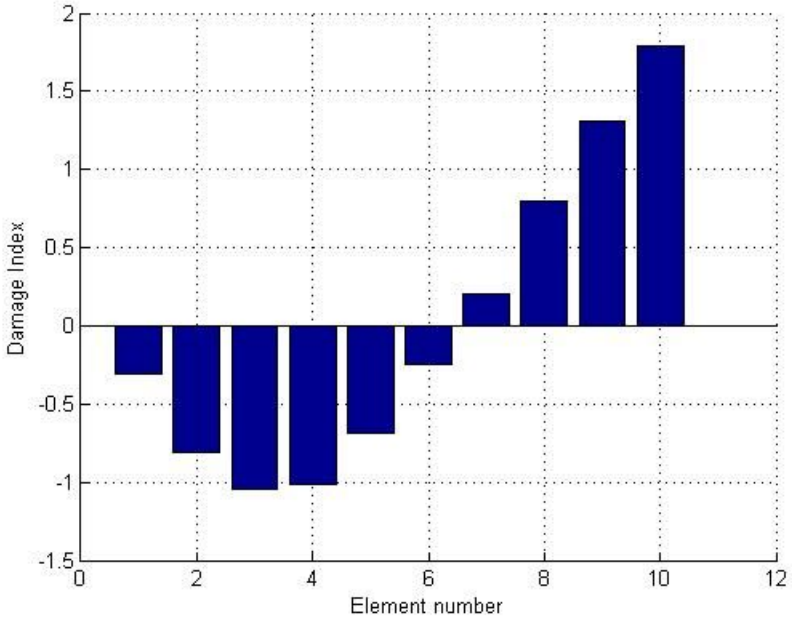

Fig. 7-16 Damage Index for Spring with 3% Noise for Case 1

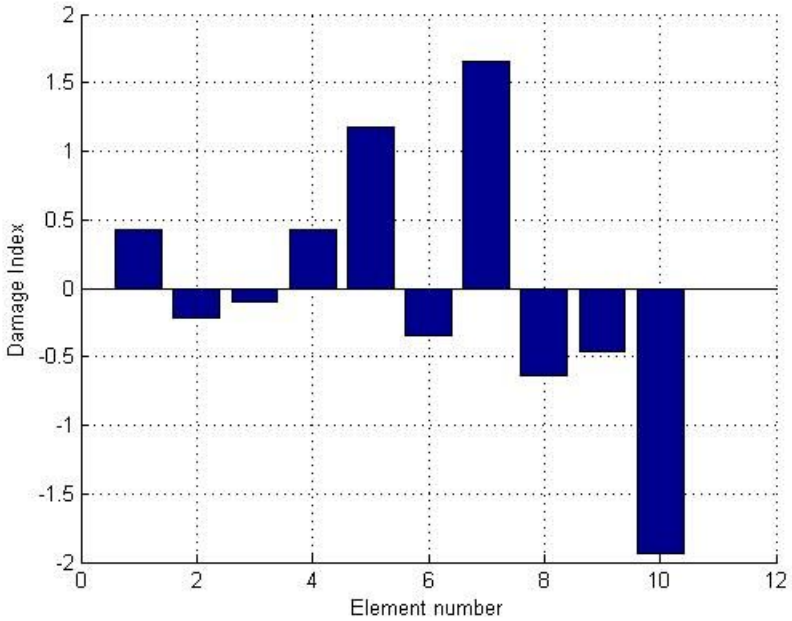

Fig. 7-17 Damage Index for Dash Pot with 3% Noise for Case 1

Table 7-4 Identified Values with 5% Noise for Case 1

	Spring			Dash pot		
	Simulated	Identified	Error (%)	Simulated	Identified	Error (%)
Element 1	1000	835	16.5	5.0	10.4	108.0
Element 2	1000	997	0.3	5.0	-4.3	186.0
Element 3	1000	1075	7.5	5.5	-1.7	130.9
Element 4	1000	1063	6.3	5.0	10.6	112.0
Element 5	1000	957	4.3	5.0	27.8	456.0
Element 6	1000	815	18.5	5.0	-7.2	244.0
Element 7	1000	671	32.9	5.0	38.8	676.0
Element 8	1000	477	52.3	5.0	-14.1	382.0
Element 9	1000	311	68.9	5.0	-9.9	298.0
Element 10	1000	155	84.5	5.0	-43.8	976.0

7.2.2 Case 2

In this damage scenario, Element 3 has both damping damage and stiffness damage. Damping damage was simulated by 20% increase of dash pot constant, and stiffness damage was imposed by 10% decrease of spring constant. The structure was excited in the same way we described in Case 1.

1% Noise

The random number scaled by 1% of the displacement and velocity was superposed on the corresponding noise-free displacement and velocity. Displacements and velocities were measured 10 times, as in Case 1 and the average of the identified values for each data set was taken as the identified values. The Damage indices calculated with the average of the identified values for each element in the springs and the dash pots are shown in Fig. 7-18 and Fig. 7-19, respectively. The identified values are listed in Table 7-5. With respect to spring constant, Element 3 was detected correctly as a damaged element. However, Element 9 and Element 10 were falsely detected as damaged elements. With respect to the dash pot constants, Element 3 and Element 7 were detected as damaged elements; however,. Element7 is a false positive prediction.

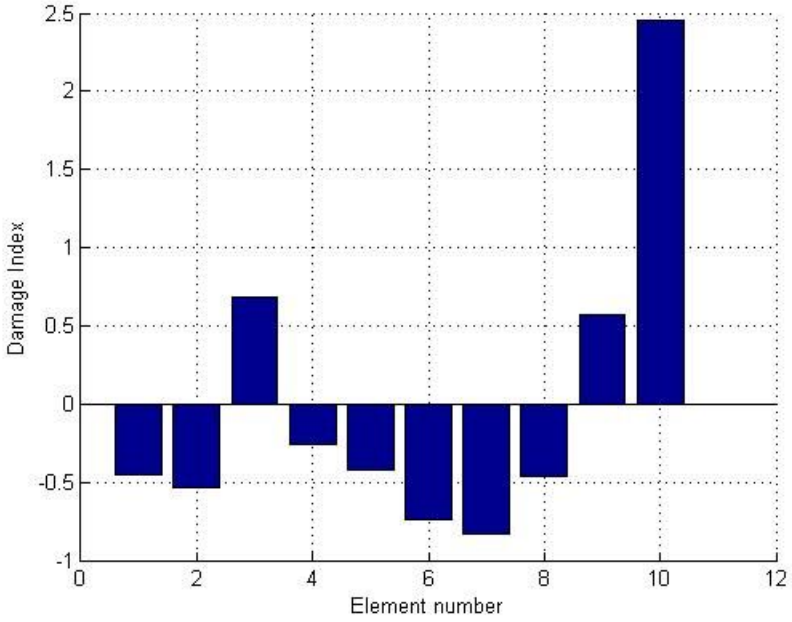

Fig. 7-18 Damage Index for Spring with 1% Noise for Case 2

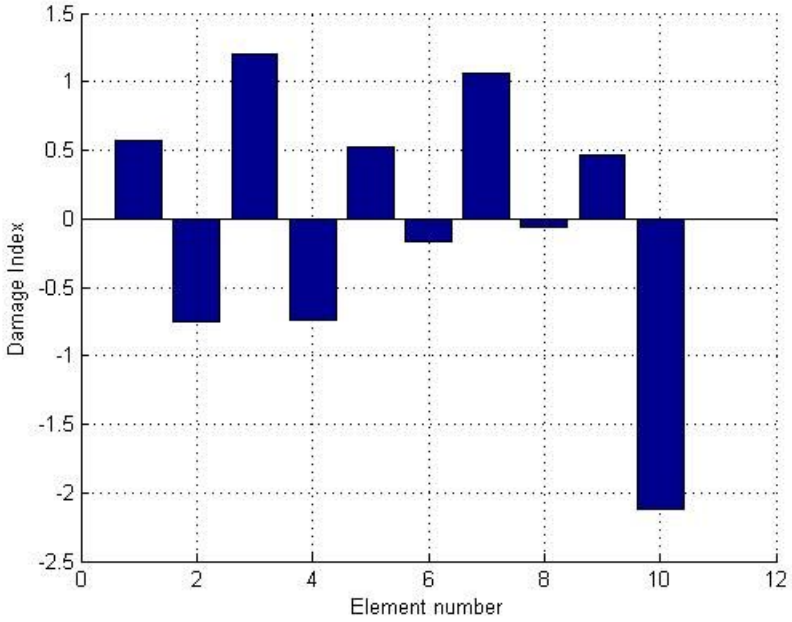

Fig. 7-19 Damage Index for Dash Pot with 1% Noise for Case 2

Table 7-5 Identified Values with 1% Noise for Case 2

	Spring			Dash pot		
	Simulated	Identified	Error (%)	Simulated	Identified	Error (%)
Element 1	1000	995	0.5	5.0	6.9	38.0
Element 2	1000	1003	0.3	5.0	0.5	90.0
Element 3	900	885	1.7	6.0	10.0	66.7
Element 4	1000	976	2.4	5.0	0.5	90.0
Element 5	1000	991	0.9	5.0	6.6	32.0
Element 6	1000	1022	2.2	5.0	3.3	34.0
Element 7	1000	1031	3.1	5.0	9.3	86.0
Element 8	1000	995	0.5	5.0	3.8	24.0
Element 9	1000	895	10.5	5.0	6.4	28.0
Element 10	1000	713	28.7	5.0	-6.2	224.0

3% Noise

The random number scaled by 3% of the displacement and velocity was superposed on the corresponding noise-free displacement and velocity. Displacements and velocities were measured 10 times as in Case 1 and the average of the identified values for each data set was taken to be the identified values. The Damage indices for each element in the springs and dash pots are shown in Fig. 7-20 and Fig. 7-21, respectively. The identified values are listed in Table 7-6. With respect to the spring constant, Element 3 was not detected as a damaged element. Instead, Element 9 and Element 10 were falsely detected as damaged elements. With respect to the dash pot constants, Element 6 and Element 8 were detected as damaged elements. Element 3 was not detected. The 5% noise level analysis was not performed for Case 2, because the damaged element was not detected at the 3% noise level.

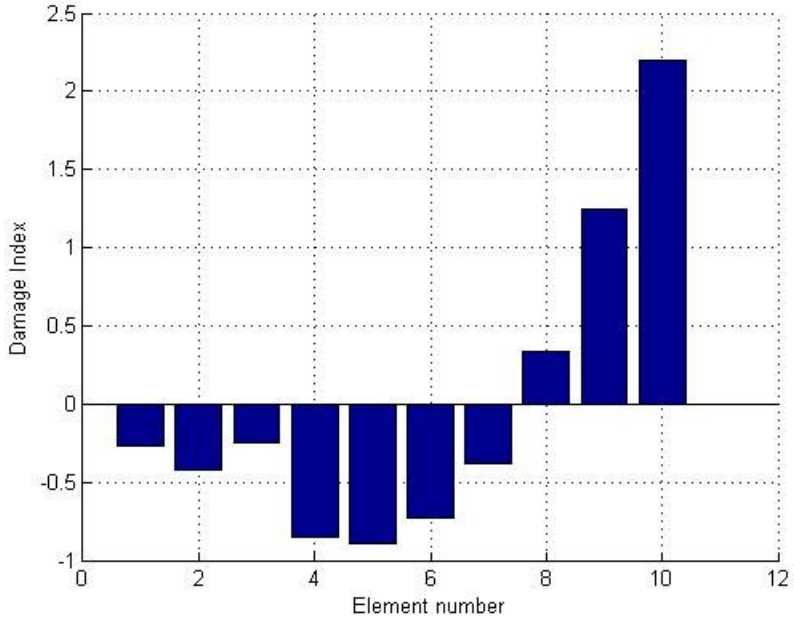

Fig. 7-20 Damage Index for Spring with 3% Noise for Case 2

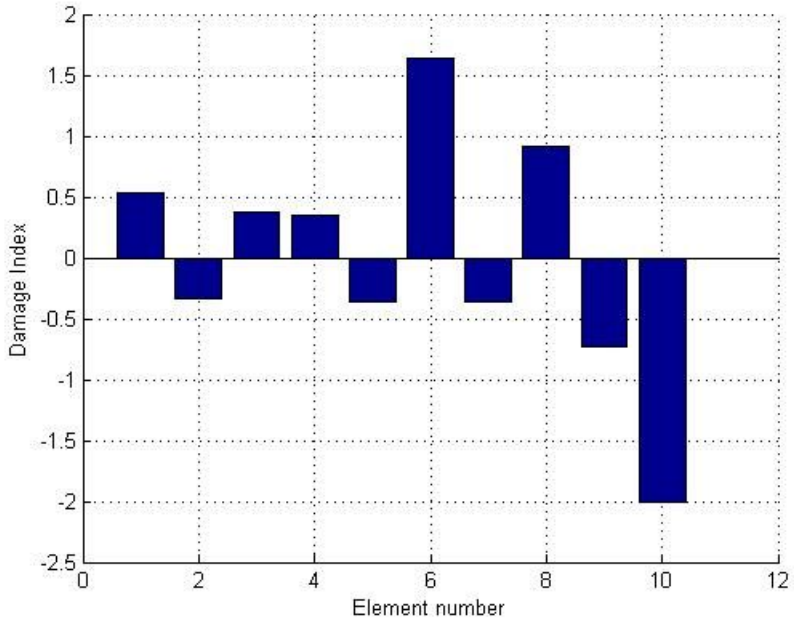

Fig. 7-21 Damage Index for Dash Pot with 3% Noise for Case 2

Table 7-6 Identified Values with 3% Noise for Case 2

	Spring			Dash pot		
	Simulated	Identified	Error (%)	Simulated	Identified	Error (%)
Element 1	1000	893	10.7	5.0	9.6	92.0
Element 2	1000	930	7.0	5.0	-3.1	162.0
Element 3	900	888	1.3	6.0	7.3	21.7
Element 4	1000	1033	3.3	5.0	6.9	38.0
Element 5	1000	1044	4.4	5.0	-3.4	168.0
Element 6	1000	1005	0.5	5.0	25.6	412.0
Element 7	1000	921	7.9	5.0	-3.4	168.0
Element 8	1000	748	25.2	5.0	15.2	204.0
Element 9	1000	530	47.0	5.0	-8.8	276.0
Element 10	1000	299	70.1	5.0	-27.4	648.0

7.2.3 Case 3

In this damage scenario, damages were simulated at multiple elements. Element 3 and Element 6 were assigned both damping damage and stiffness damage. In previous sections, damaged element was Element 8, but in this scenario, it was changed to Element 6. The reason for this decision is that because Element 8 was falsely detected as a damaged element even when it did not have damage. For Element 3, damping damage was simulated as a 20% increase in the dash pot constant, and stiffness damage was simulated as a 10% decrease in the spring constant. The dash pot constant for Element 6 was increased by 40% and the spring constant of Element 6 was decreased by 20%.

1% Noise

The random number scaled by 1% of the displacement and velocity was superposed on the corresponding noise-free displacement and velocity. Displacements and velocities were measured 10 times as in Case 1 and the average of the identified values for each data set was taken as the finally identified values. The Damage indices for each element in the springs and dash pots are shown in Fig. 7-22 and Fig. 7-23, respectively. The identified values are listed in Table 7-7. With respect to the spring constants, Element 3 and Element 6 were detected correctly as damaged elements. However, Element 9 and Element 10 were falsely detected as damaged elements, as in

Case 2. With respect to the dash pot constants, Element 3 and Element 6 were detected correctly as damaged elements and Element 1 and Element 7 were falsely detected .

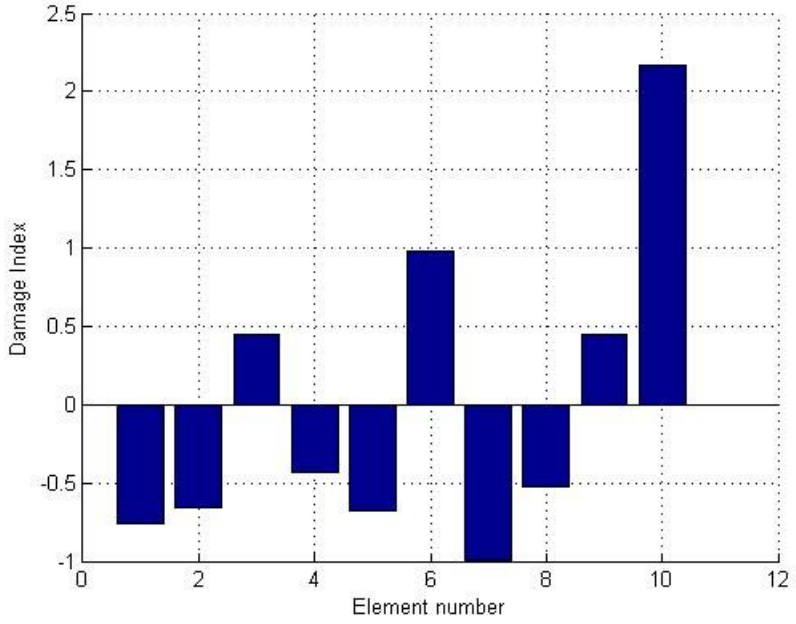

Fig. 7-22 Damage Index for Spring with 1% Noise for Case 3

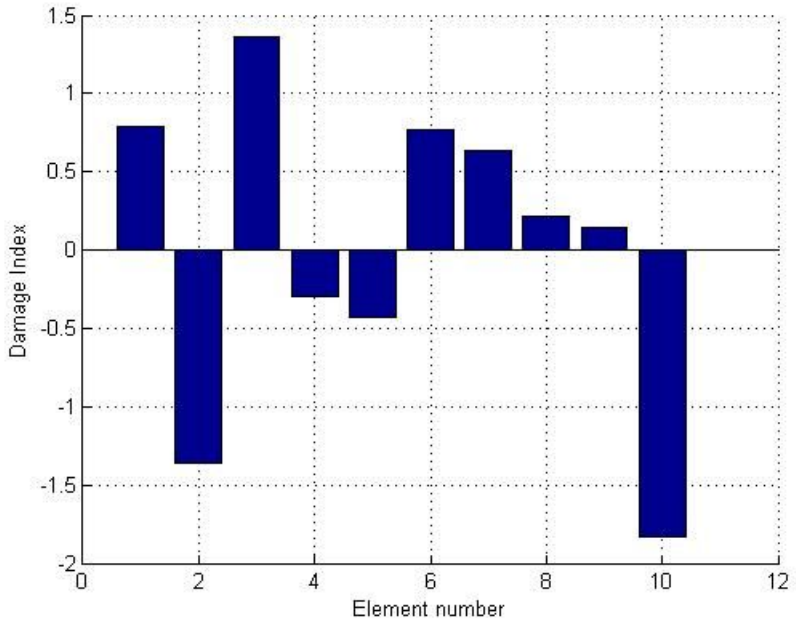

Fig. 7-23 Damage Index for Dash Pot with 1% Noise for Case 3

Table 7-7 Identified Values with 1% Noise for Case 3

	Spring			Dash pot		
	Simulated	Identified	Error (%)	Simulated	Identified	Error (%)
Element 1	1000	1006	0.6	5.0	8.7	74.0
Element 2	1000	996	0.4	5.0	-3.9	178.0
Element 3	900	879	2.3	6.0	12.1	101.7
Element 4	1000	972	2.8	5.0	2.4	52.0
Element 5	1000	997	0.3	5.0	1.6	68.0
Element 6	800	823	2.9	7.0	8.6	22.9
Element 7	1000	1030	3.0	5.0	7.8	56.0
Element 8	1000	982	1.8	5.0	5.4	8.0
Element 9	1000	879	12.1	5.0	4.9	2.0
Element 10	1000	698	30.2	5.0	-6.7	234.0

3% Noise

The random numbers scaled by 3% of the displacement and velocity were superposed on the corresponding noise-free displacement and velocity. Displacements and velocities were measured 10 times as in Case 1 and the average of the identified values for each data set was taken as the finally identified values. The Damage indices for each element are shown in Fig. 7-24 and Fig. 7-25. The identified values are listed in Table 7-6. With respect to spring constant, Element 3 and Element 6 were not detected as damaged element. Instead of the simulated Element 3, Element 9 and Element 10 were falsely detected as damaged elements. In the dash pot constants, Element 6 and Element 8 were detected as damaged elements. Element 3 was not detected. Note that 5% noise level analysis was not performed for Case 2, because the damaged element was not detected at 3% noise level. The 5% noise level analysis is not performed for Case 3, either.

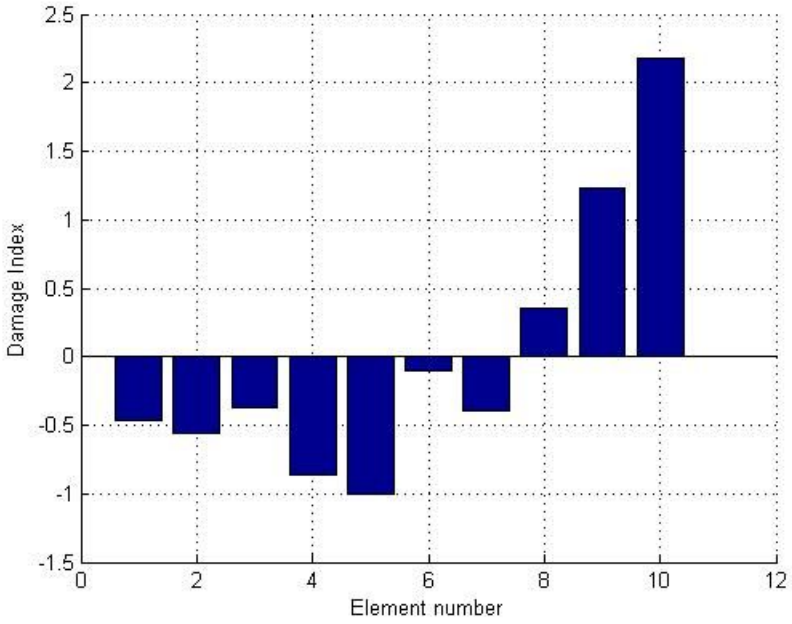

Fig. 7-24 Damage Index for Spring with 3% Noise for Case 3

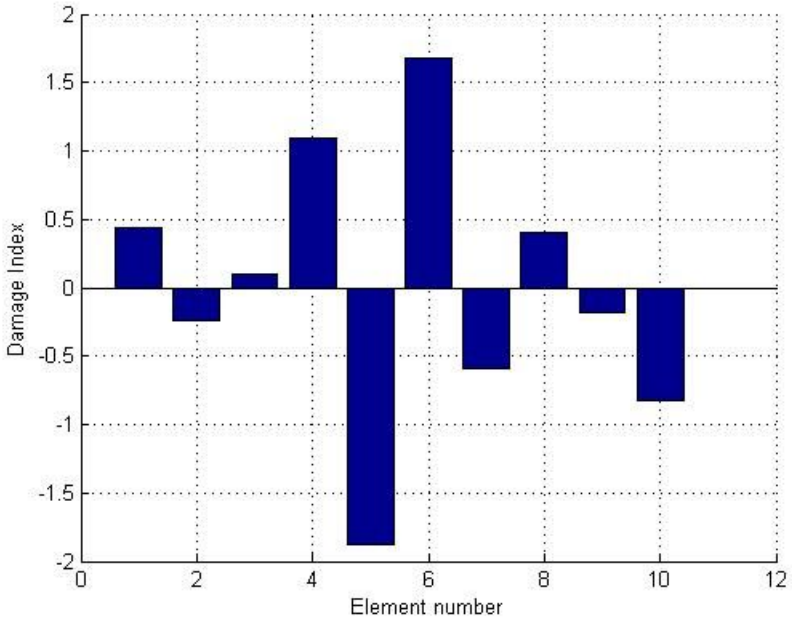

Fig. 7-25 Damage Index for Dash Pot with 3% Noise for Case 3

Table 7-8 Identified Values with 1% Noise for Case 3

	Spring			Dash pot		
	Simulated	Identified	Error (%)	Simulated	Identified	Error (%)
Element 1	1000	916	8.4	5.0	14.6	192.0
Element 2	1000	938	6.2	5.0	-9.4	288.0
Element 3	900	891	1.0	6.0	2.8	53.3
Element 4	1000	1015	1.5	5.0	38.2	664.0
Element 5	1000	1052	5.2	5.0	-68	1460.0
Element 6	800	823	2.9	7.0	59	742.9
Element 7	1000	898	10.2	5.0	-22.2	544.0
Element 8	1000	710	29.0	5.0	13.4	168.0
Element 9	1000	487	51.3	5.0	-7.5	250.0
Element 10	1000	248	75.2	5.0	-30.4	708.0

7.3 SUMMARY

The performance of the proposed damage evaluation method, based on the conservation of total energy with noise-polluted data, was investigated with a high-rise building modeled as a shear beam. Three damage scenarios were investigated: damping damage was simulated at a single location, both stiffness damage and damping damage were simulated at a single location, and multi-damage cases involving both damping and stiffness were simulated. The identified values of the dash pot indicated larger coefficients of variation than the spring constants. The damaged elements were detected correctly, but they were accompanied with false-positive predictions for 1% noise. For 3% noise, the elements simulated to be damaged were not detected as the damaged element. In all cases, Element 10 was falsely detected as a stiffness damaged element and the magnitude of the dash pot constant of Element 10 was identified as negative.

8 NUMERICAL VERIFICATION OF THE SENSITIVITY METHOD FOR A SHEAR BUILDING WITH NOISE-POLLUTED DATA

8.1 INTRODUCTION

The objective of this section is to analyse the performance of the method which uses acceleration-structural parameters sensitivities numerically for a shear building with known damage scenarios and noise-polluted data.

8.2 DAMAGE DETECTION IN A SHEAR BUILDING

The same structure and same damage scenarios discussed in Section 4 are used here. To excite the structure, a horizontal tensile force of 200 kips was applied at the 10^{th} story, and the load was quickly removed thus permitting the structure to vibrate freely as in Section 4. The Newmark-β method was used to get the simulated accelerations. Accelerations were measured at a 1000 Hz sampling rate. The same technique discussed in Section 7 was used to produce the noise-polluted accelerations. Three levels of noise, 1%, 3%, and 5%, were considered.

The accelerations at each node were measured 10 times, and the average values of all measured accelerations were finally used to identify the spring constants and the dash pot constants.

8.2.1 Case 1

In this damage scenario, only Element 3 has damping damage which is equivalent to a 10% increase in the dash pot constant. It was assumed that the modal damping values and natural frequencies are not influenced by noise, so the same baseline structure identified in Section 5 was used as the baseline structure.

1% Noise

The random number scaled by 1% of the acceleration was superposed on the acceleration generated using the The Newmark-β method, to simulate noise-polluted

data. The accelerations of the damaged structure at Node 5 and Node 10 are shown in Fig. 8-1 and Fig. 8-2. With the measured accelerations at five nodes, which are Node 2, 4, 6, 8 and 10, for one second, the identified spring constants and dash pot constants for each measured data set are shown in Fig. 8-3, Fig. 8-4 and the average of the identified values are compared with the simulated values in Table 8-1.

It is observed in Fig. 8-3 that all of the identified spring constant values are near the simulated value,1000.

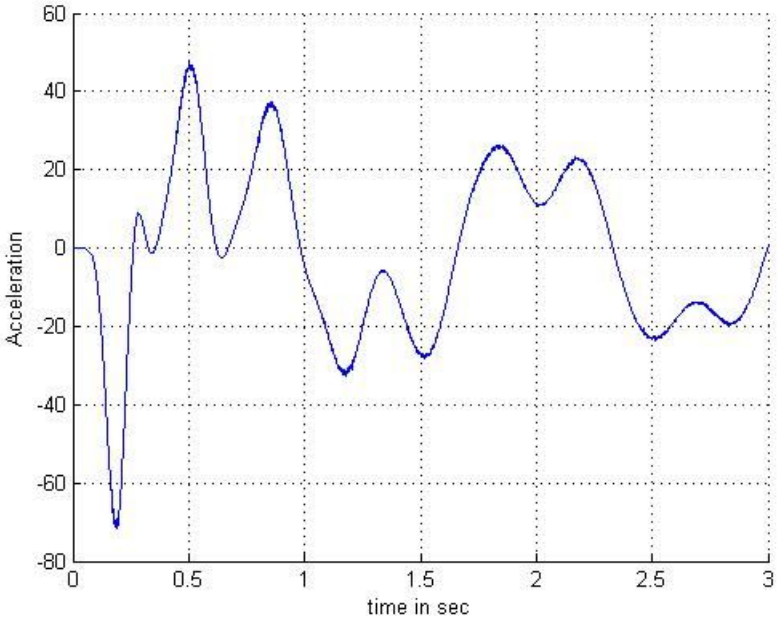

Fig. 8-1 Accelerations at Node 5 with 1% Noise for Case 1

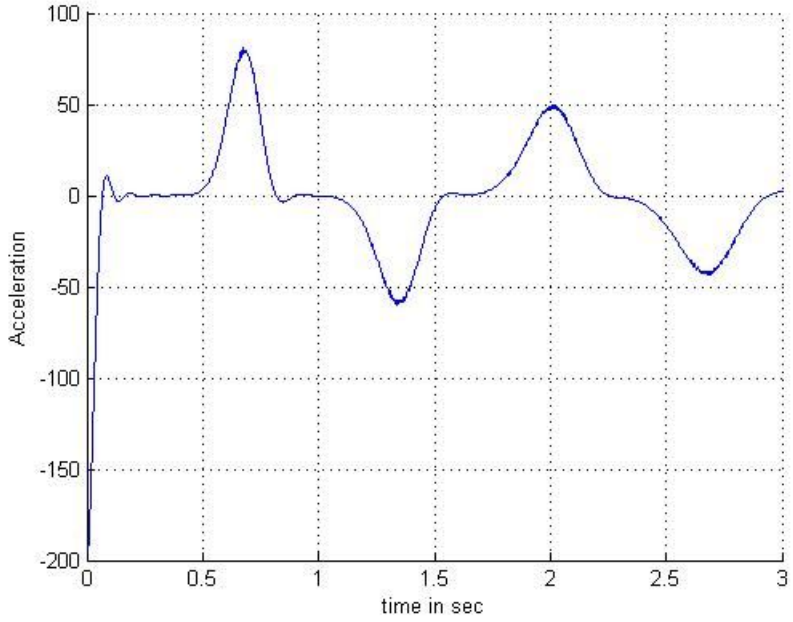

Fig. 8-2 Accelerations at Node 10 with 1% Noise for Case 1

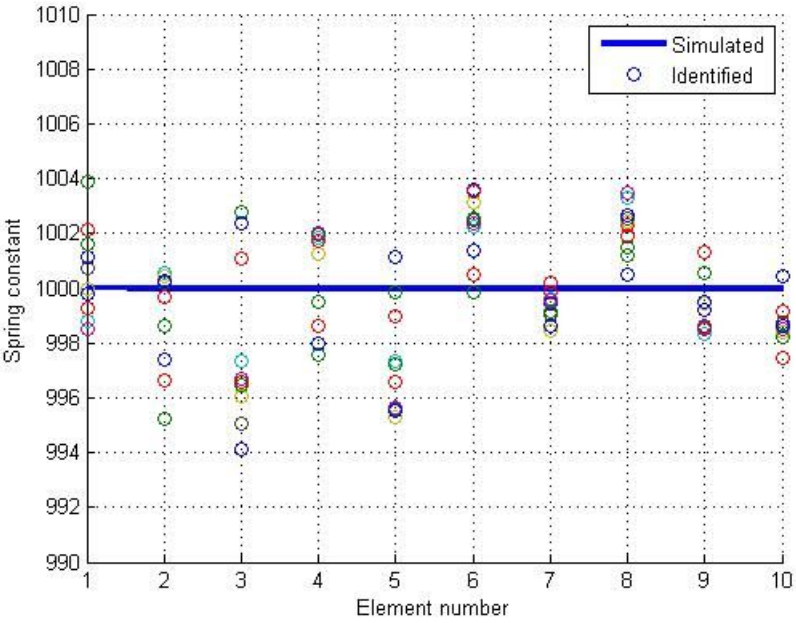

Fig. 8-3 Identified Spring with 5 Measurements and 1% Noise for Case 1

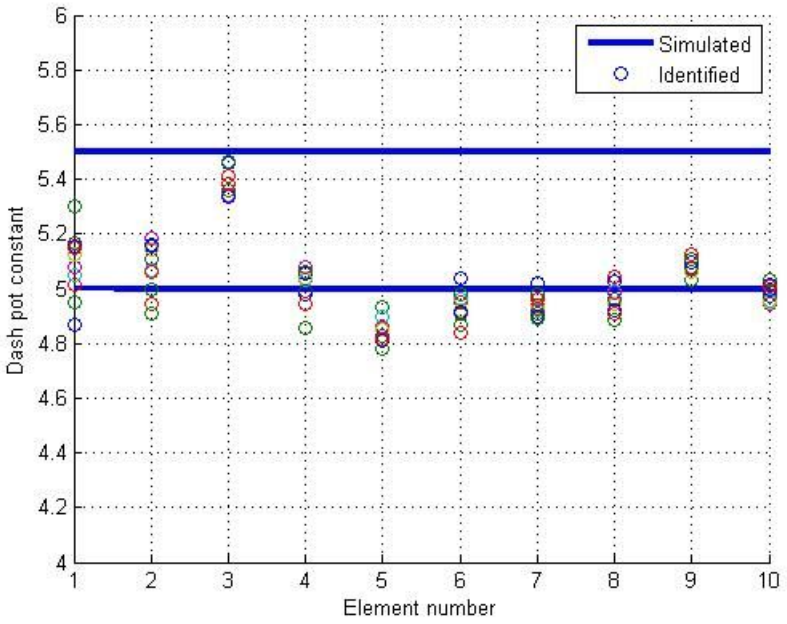

Fig. 8-4 Identified Dash Pot with 5 Measurements and 1% Noise for Case 1

Table 8-1. Identified Values with 5 Measurements and 1% Noise for Case 1

	Spring			Dash pot		
	Simulated	Identified	Error (%)	Simulated	Identified	Error (%)
Element 1	1000	1001	0.1	5.0	5.1	1.7
Element 2	1000	999	0.1	5.0	5.1	1.5
Element 3	1000	998	0.2	5.5	5.4	2.0
Element 4	1000	1000	0.0	5.0	5.0	0.2
Element 5	1000	997	0.3	5.0	4.9	2.9
Element 6	1000	1002	0.2	5.0	4.9	1.4
Element 7	1000	999	0.1	5.0	4.9	1.2
Element 8	1000	1002	0.2	5.0	5.0	0.6
Element 9	1000	999	0.1	5.0	5.1	1.5
Element 10	1000	999	0.1	5.0	5.0	0.4

There is no element which shows any obvious difference from the simulated values in the spring constant or in the dash pot constant. Element 3 was identified to have the largest dash pot constant. Therefore, it can be concluded that Element 3 was damaged in damping without stiffness damage.

It was attempted again to identify the structural parameters with accelerations at Nodes 5 and 10. With the accelerations at these two nodes for 1 second, the identified spring constants and dash pot constants for each measured data set are shown in Fig. 8-5 and Fig. 8-6. The average values are compared with the simulated values in Table 8-2. When the comparing Fig. 8-5 with Fig. 8-3, it is observed that the variation of the identified values were increased with the decreased measurement locations. The same fact is applied to Fig. 8-4 and Fig. 8-6. In dash pot constant, Element 3 was correctly detected as the most severely damping damaged element. The damping damaged element was detected correctly with 2 measurement locations.

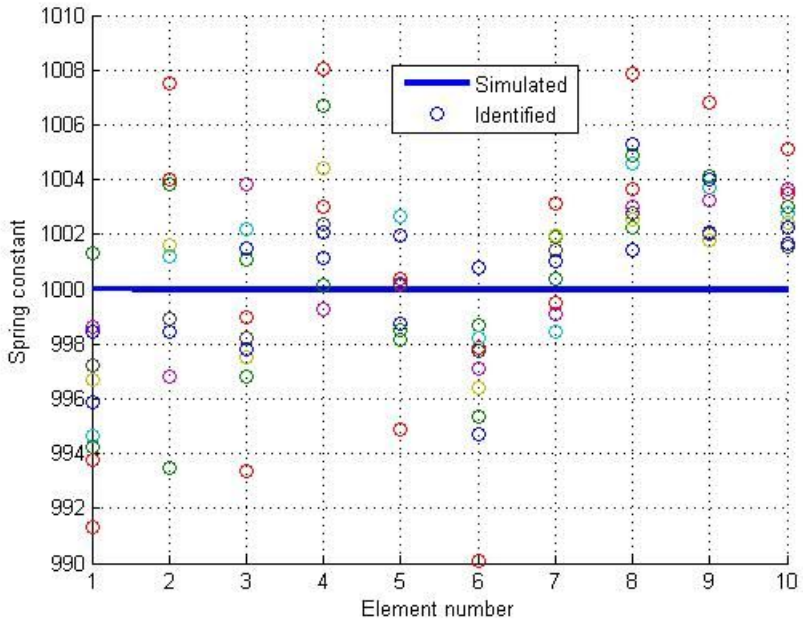

Fig. 8-5 Identified Spring with 1% Noise for Case 1

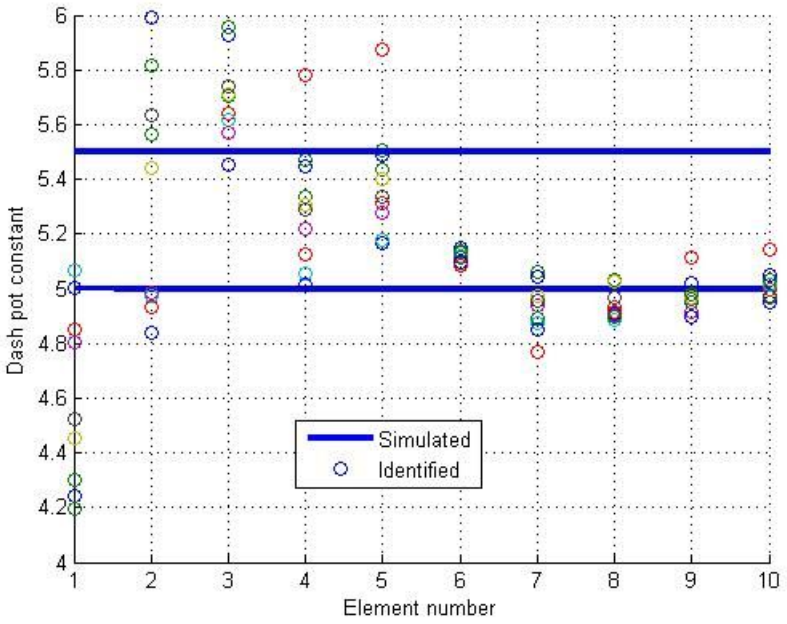

Fig. 8-6 Identified Dash Pot with 1% Noise for Case 1

Table 8-2 Identified Values with 2 Measurements and 1% Noise for Case 1

	Spring			Dash pot		
	Simulated	Identified	Error (%)	Simulated	Identified	Error (%)
Element 1	1000	998	0.2	5.00	4.98	0.4
Element 2	1000	1002	0.2	5.00	5.22	4.4
Element 3	1000	995	0.5	5.50	5.50	0.1
Element 4	1000	1003	0.3	5.00	4.97	0.5
Element 5	1000	998	0.2	5.00	4.98	0.4
Element 6	1000	999	0.1	5.00	4.90	2.0
Element 7	1000	1002	0.2	5.00	4.90	2.0
Element 8	1000	1001	0.1	5.00	5.00	0.1
Element 9	1000	1001	0.1	5.00	5.07	1.3
Element 10	1000	1001	0.1	5.00	5.07	1.5

We attempted again to identify the structural parameters with the average of the measured accelerations. The identified values obtained by the average accelerations at Node 5 and Node 10 are listed in Table 8-3.

Table 8-3 Identified Values with Average Accelerations for Case 1

	Spring			Dash pot		
	Simulated	Identified	Error (%)	Simulated	Identified	Error (%)
Element 1	1000	1001	0.1	5.00	5.05	0.9
Element 2	1000	999	0.1	5.00	5.00	0.0
Element 3	1000	1000	0.0	5.50	5.52	0.3
Element 4	1000	999	0.1	5.00	4.99	0.3
Element 5	1000	1001	0.1	5.00	4.93	1.4
Element 6	1000	1001	0.1	5.00	4.95	1.0
Element 7	1000	1000	0.0	5.00	4.97	0.6
Element 8	1000	1000	0.0	5.00	5.01	0.3
Element 9	1000	999	0.1	5.00	5.03	0.7
Element 10	1000	1000	0.0	5.00	5.07	1.5

On comparing Table 8-2 and Table 8-3, better identification results were obtained when the average of the measured accelerations were used than when taking the average of the identified values. Thus, for the next cases, the structure parameters are identified using the average of the measured accelerations.

3% Noise

As before, the random number scaled by 3% of acceleration was superposed on the produced accelerations generated by the Newmark-β method to simulate noise-polluted data. The accelerations of the damaged structure at Node 5 and Node 10 are shown in Fig. 8-7 and Fig. 8-8.

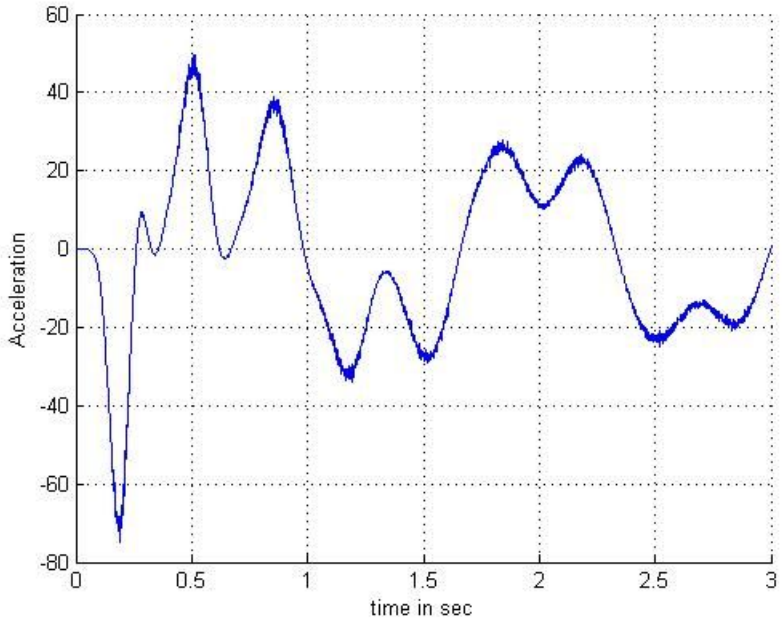

Fig. 8-7 Accelerations at Node 5 with 3% Noise for Case 1

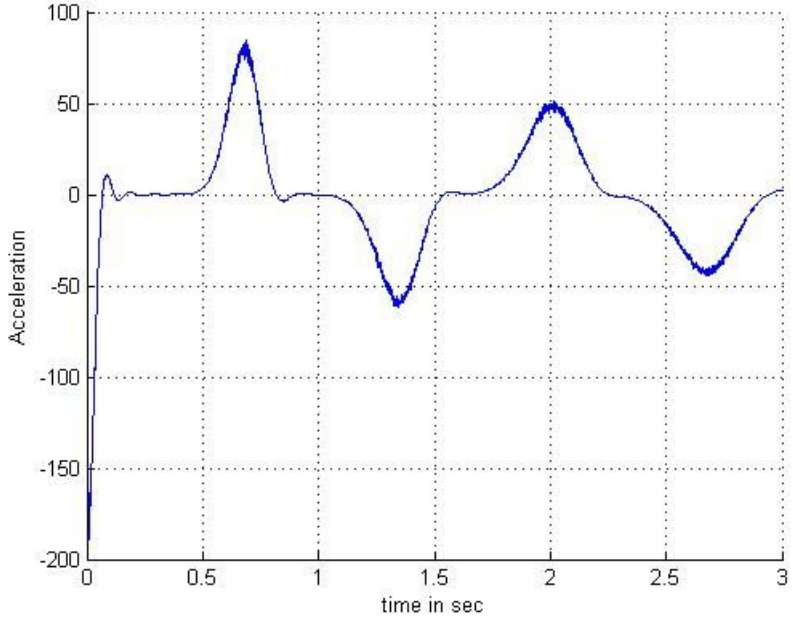

Fig. 8-8 Accelerations at Node 10 with 3% Noise for Case 1

When the accelerations at Nodes 2, 4, 6, 8 and 10 were used, the identified results generated using the same process as in the 1% noise, are listed in Table 8-4. For the dash pot constants, Element 3 was correctly detected as the damaged element.

Table 8-4 Identified Values with 5 Measurements and 3% Noise for Case 1

	Spring			Dash pot		
	Simulated	Identified	Error (%)	Simulated	Identified	Error (%)
Element 1	1000	998	0.2	5.00	5.04	0.7
Element 2	1000	1001	0.1	5.00	5.01	0.1
Element 3	1000	1000	0.0	5.50	5.47	0.6
Element 4	1000	1001	0.1	5.00	5.01	0.1
Element 5	1000	1000	0.0	5.00	5.01	0.1
Element 6	1000	1000	0.0	5.00	5.05	1.1
Element 7	1000	999	0.1	5.00	5.00	0.0
Element 8	1000	1000	0.0	5.00	4.98	0.4
Element 9	1000	1000	0.0	5.00	4.98	0.4
Element 10	1000	1000	0.0	5.00	5.00	0.0

When the accelerations at only two nodes, Node 5 and Node 10, for 1 second were used, a singular stiffness matrix was obtained because the spring constants were identified as negative; thus the spring constants and dash pot constants were not identified. When the observation time was extended to 2 seconds, the identified results with 2 measurements are listed in Table 8-5. Element 3 was identified as the damping damaged element correctly and Element 2 was false-positive. The Element 1 had the largest error, 16% in its estimated dash pot constant.

Table 8-5 Identified Values with 2 Measurements and 3% Noise for Case 1

	Spring			Dash pot		
	Simulated	Identified	Error (%)	Simulated	Identified	Error (%)
Element 1	1000	999	0.1	5.00	4.20	16.0
Element 2	1000	997	0.3	5.00	5.45	8.9
Element 3	1000	997	0.3	5.50	5.70	3.6
Element 4	1000	1007	0.7	5.00	5.21	4.1
Element 5	1000	998	0.2	5.00	5.41	8.2
Element 6	1000	1000	0.0	5.00	4.99	0.2
Element 7	1000	1010	1.0	5.00	5.31	6.2
Element 8	1000	997	0.3	5.00	5.28	5.7
Element 9	1000	997	0.3	5.00	4.96	0.9
Element 10	1000	1000	0.0	5.00	4.89	2.2

5% Noise

The random number scaled by 5% of the acceleration was superposed on the produced acceleration generated by The Newmark-β method to simulate noise-polluted data. The accelerations of the damaged structure at Node 5 and Node 10 are shown in Fig. 8-9 and Fig. 8-10. When the accelerations at five nodes, Nodes 2, 4, 6, 8, and 10, were used, the identification results are listed in Table 8-6. Element 3 was detected correctly as the damping damaged element. Element 2 was falsely detected as in 3% noise.

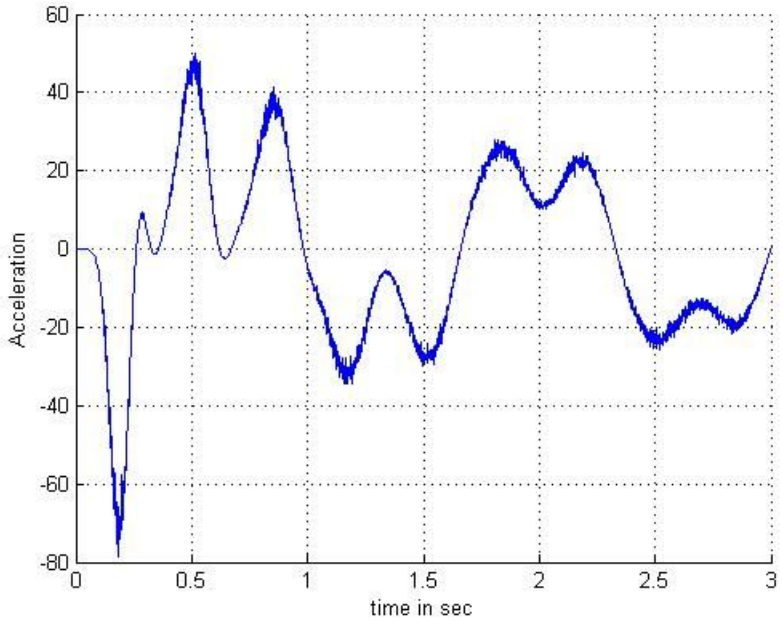

Fig. 8-9 Accelerations at Node 5 with 5% Noise for Case 1

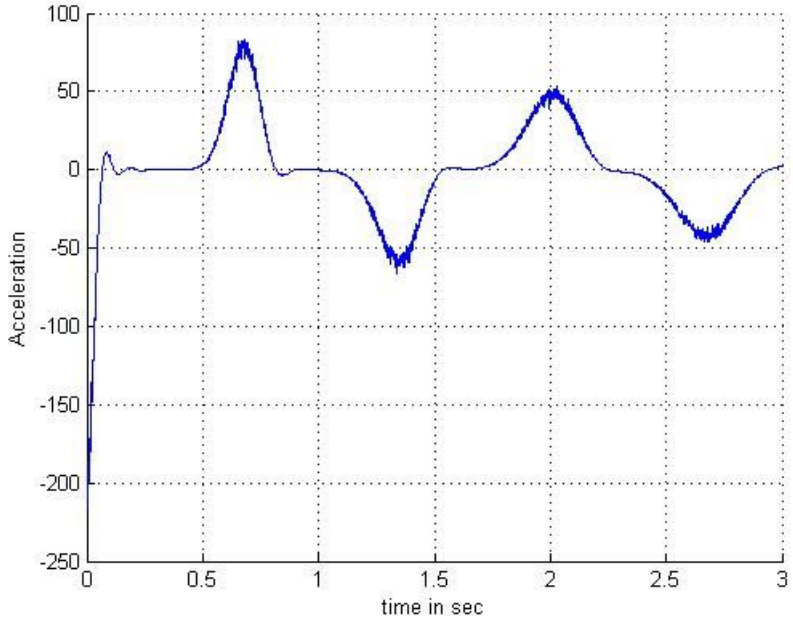

Fig. 8-10 Accelerations at Node 10 with 5% Noise for Case 1

Table 8-6 Identified Values with 5 Measurements and 5% Noise for Case 1

	Spring			Dash pot		
	Simulated	Identified	Error (%)	Simulated	Identified	Error (%)
Element 1	1000	1004	0.4	5.00	4.61	7.8
Element 2	1000	994	0.6	5.00	5.34	6.9
Element 3	1000	1002	0.2	5.50	5.56	1.2
Element 4	1000	999	0.1	5.00	5.13	2.6
Element 5	1000	997	0.3	5.00	4.97	0.6
Element 6	1000	1004	0.4	5.00	5.04	0.8
Element 7	1000	997	0.3	5.00	5.11	2.2
Element 8	1000	999	0.1	5.00	4.99	0.2
Element 9	1000	1000	0.0	5.00	5.03	0.7
Element 10	1000	1001	0.1	5.00	5.07	1.4

When the accelerations at only two nodes, Node 5 and Node 10, for a 2-second time period were used, the identified results are listed in Table 8-7. Element 3 was identified as the damping damaged element, but Element 10 indicated the existence of the possible damage. The errors increased compared when the accelerations at 5 locations were used.

Table 8-7 Identified Values with 2 Measurements and 5% Noise for Case 1

	Spring			Dash pot		
	Simulated	Identified	Error (%)	Simulated	Identified	Error (%)
Element 1	1000	989	1.1	5.00	5.22	4.5
Element 2	1000	1016	1.6	5.00	5.14	2.8
Element 3	1000	991	0.9	5.50	5.97	8.6
Element 4	1000	1000	0.0	5.00	4.47	10.7
Element 5	1000	1005	0.5	5.00	5.07	1.4
Element 6	1000	991	0.9	5.00	4.57	8.6
Element 7	1000	1005	0.5	5.00	4.68	6.5
Element 8	1000	1000	0.0	5.00	4.93	1.3
Element 9	1000	1003	0.3	5.00	5.18	3.7
Element 10	1000	1007	0.7	5.00	5.32	6.4

8.2.2 Case 2

In this damage scenario, Element 3 has both damping damage and stiffness damage. Damping damage was simulated by 20% increase of the undamaged dash pot

constant, and stiffness damage imposed was a 10% decrease in the spring constant. The structure was excited by the same condition as in Case 1.

It was assumed that the modal damping values and natural frequencies are not influenced much by noise, so the same baseline structure identified in Section 5 was used as the baseline structure. Note that in Case 1, the structural parameters were identified well with 5% noise level. Therefore, 1% noise and 3% noise were not considered in Case 2. Only 5% noise case was treated in Case 2.

When the accelerations at all nodes for a time period of 1 second were used, the Damage indices for spring constants and dash pot constants are shown in Fig. 8-11 and Fig. 8-12, respectively. As seen in Fig. 8-11 and Fig. 8-12, Element 3 was detected correctly as the damaged element both in spring and dash pot. The identification results are listed in Table 8-8.

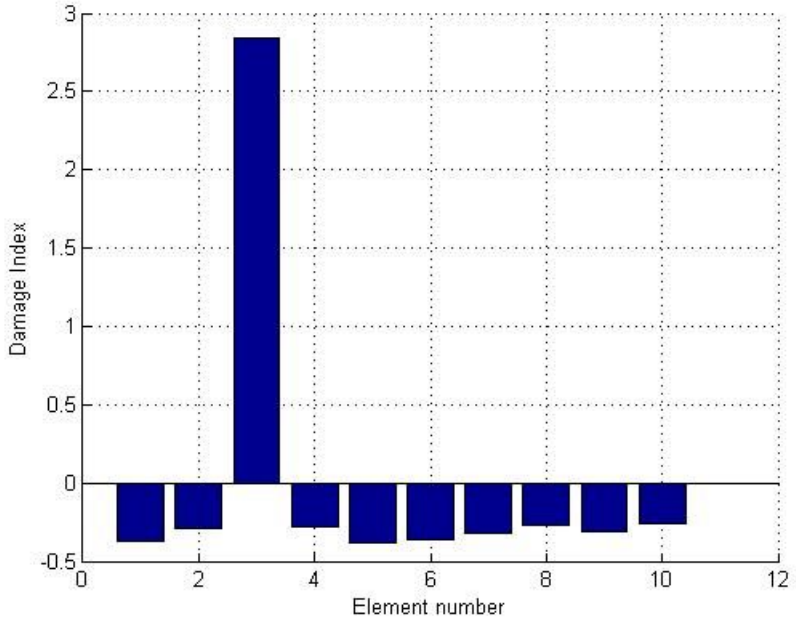

Fig. 8-11 Damage Index for Spring with 10 Measurements for Case 2

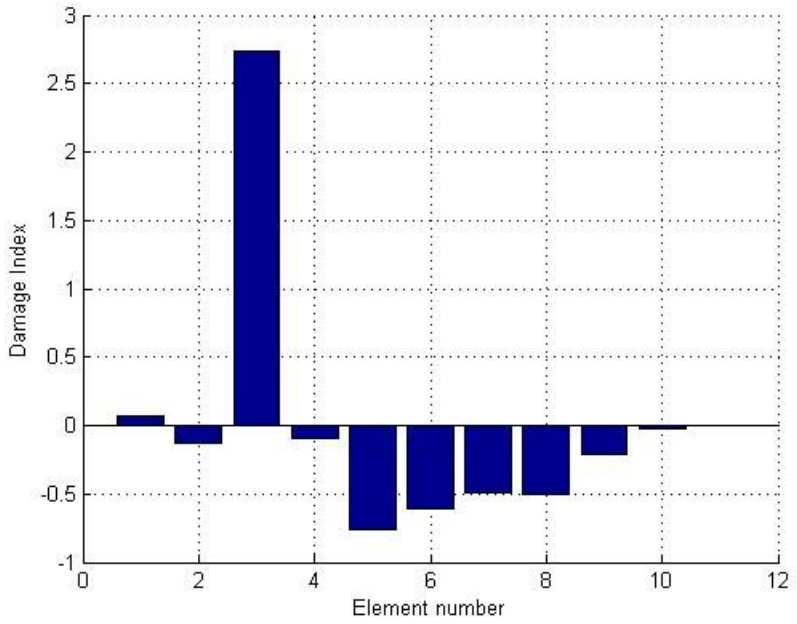

Fig. 8-12 Damage Index for Dash Pot with 10 Measurements for Case 2

Table 8-8 Identified Values with 10 Measurements and 5% Noise for Case 2

	Spring			Dash pot		
	Simulated	Identified	Error (%)	Simulated	Identified	Error (%)
Element 1	1000	1002	0.2	5.00	5.12	2.4
Element 2	1000	999	0.1	5.00	5.06	1.2
Element 3	900	899	0.1	6.00	5.97	0.5
Element 4	1000	999	0.1	5.00	5.07	1.4
Element 5	1000	1002	0.2	5.00	4.86	2.9
Element 6	1000	1001	0.1	5.00	4.90	1.9
Element 7	1000	1000	0.0	5.00	4.94	1.2
Element 8	1000	999	0.1	5.00	4.94	1.2
Element 9	1000	1000	0.0	5.00	5.03	0.6
Element 10	1000	1007	0.7	5.00	5.09	1.8

It was tried again to identify structural parameters with the measured accelerations at five nodes, Node 2, Node 4, Node 6, Node 8, and Node 10, for a time interval 2 seconds; the identification results are shown in Fig. 8-13 and Fig. 8-14.

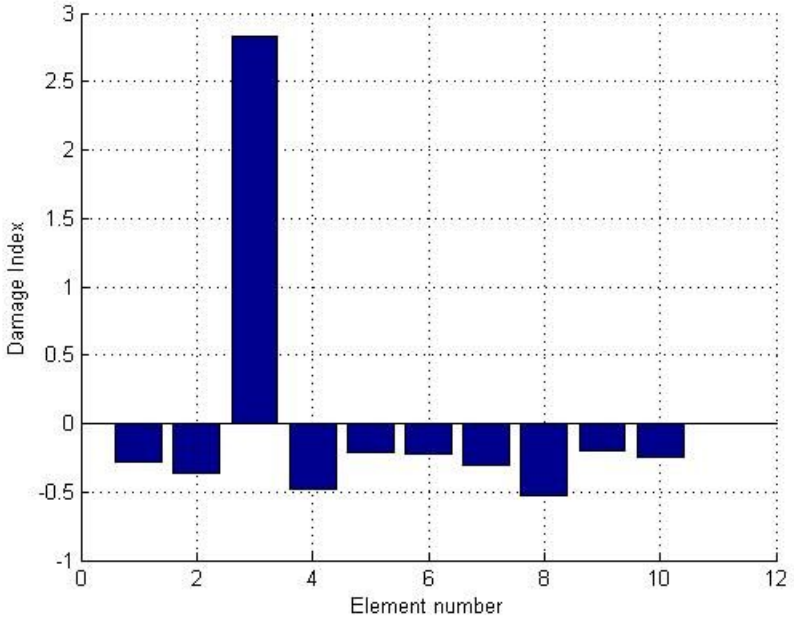

Fig. 8-13 Damage Index for Spring with 5 Measurements for Case 2

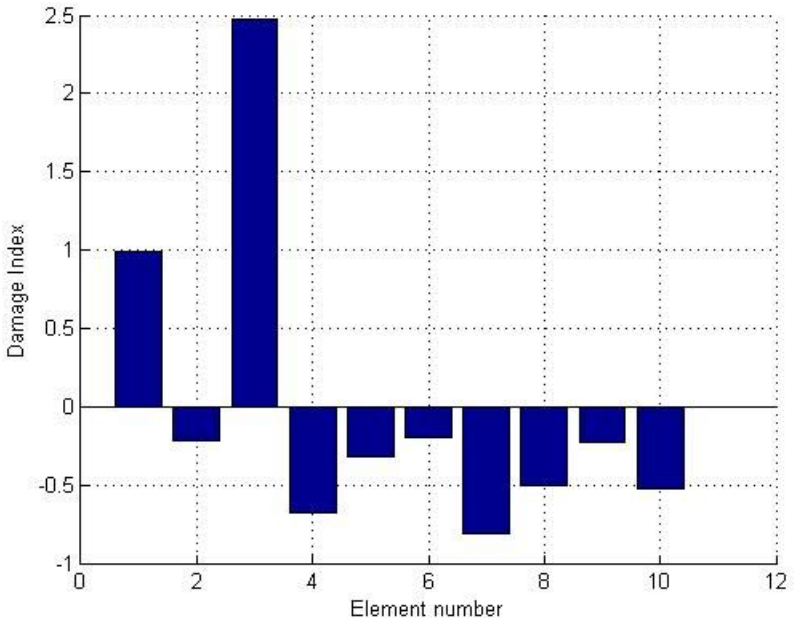

Fig. 8-14 Damage Index for Dash Pot with 5 Measurements for Case 2

For spring constants, Element 3 was detected as stiffness damaged element correctly, but for dash pot constants, not only Element 3, which was originally simulated as the damping damaged element, but also Element 1 indicated some possible damage. The identification results are listed in Table 8-9.

Table 8-9 Identified Values with 5 Measurements and 5% Noise for Case 2

	Spring			Dash pot		
	Simulated	Identified	Error (%)	Simulated	Identified	Error (%)
Element 1	1000	998	0.2	5.00	5.43	8.7
Element 2	1000	1001	0.1	5.00	5.03	0.6
Element 3	900	898	0.2	6.00	5.93	1.1
Element 4	1000	1005	0.5	5.00	4.87	2.6
Element 5	1000	996	0.4	5.00	4.99	0.1
Element 6	1000	997	0.3	5.00	5.04	0.7
Element 7	1000	999	0.1	5.00	4.83	3.4
Element 8	1000	1006	0.6	5.00	4.93	1.3
Element 9	1000	996	0.4	5.00	5.02	0.5
Element 10	1000	997	0.3	5.00	4.92	1.5

It was tried again to identify structural parameters with the measured accelerations at Node 5 and 10 for a time interval of 2 seconds, and the identification results are shown in Fig. 8-15 and Fig. 8-16. With only 2 measurement locations, the damaged element was correctly detected in spring, but the Elements 4, 5, 6, and 7 were falsely detected in dash pot. The identified values are listed in Table 8-10.

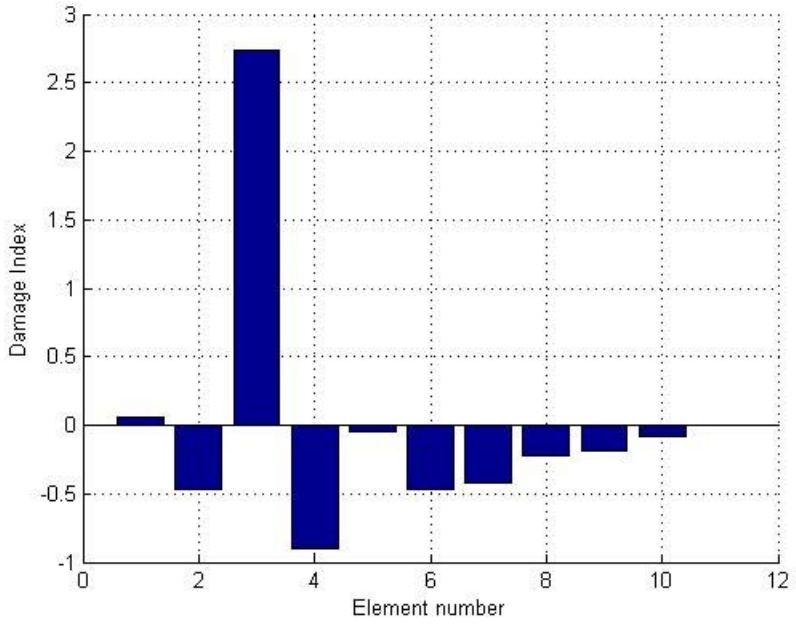

Fig. 8-15 Damage Index for Spring with 2 Measurements for Case 2

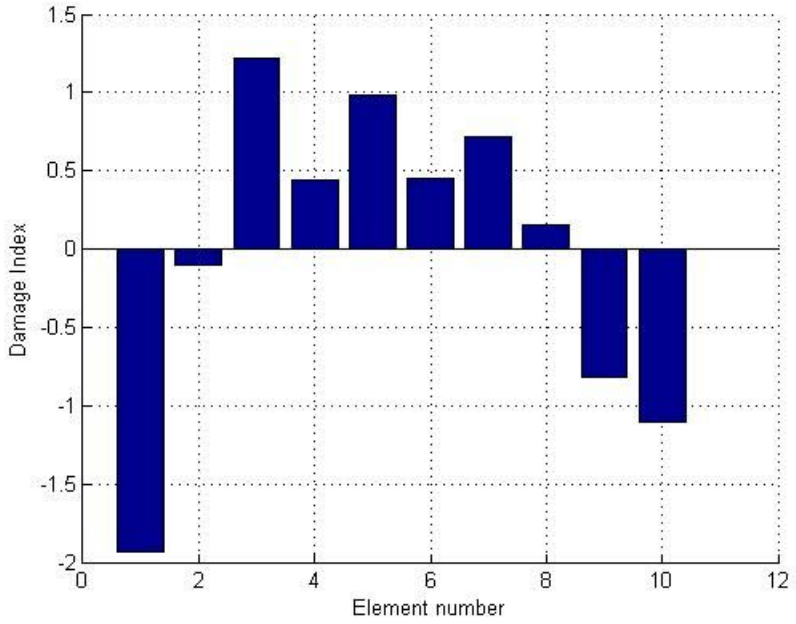

Fig. 8-16 Damage Index for Dash Pot with 2 Measurements for Case 2

Table 8-10 Identified Values with 2 Measurements and 5% Noise for Case 2

	Spring			Dash pot		
	Simulated	Identified	Error (%)	Simulated	Identified	Error (%)
Element 1	1000	988	1.2	5.00	4.03	19.5
Element 2	1000	1008	0.8	5.00	5.16	3.1
Element 3	900	890	1.1	6.00	5.97	0.4
Element 4	1000	1023	2.3	5.00	5.49	9.8
Element 5	1000	992	0.8	5.00	5.83	16.5
Element 6	1000	1007	0.7	5.00	5.50	9.9
Element 7	1000	1006	0.6	5.00	5.66	13.3
Element 8	1000	999	0.1	5.00	5.31	6.3
Element 9	1000	997	0.3	5.00	4.71	5.7
Element 10	1000	994	0.6	5.00	4.54	9.3

8.2.3 Case 3

In this damage scenario, damage was simulated to multiple elements. Element 3 Element 6 had both damping damage and stiffness damage. For Element 3, damping damage was simulated by 20% increase of dash pot constant, and stiffness damage was imposed by 10% decrease of spring constant. The dash pot constant of Element 8 was increased by 40% and the spring constant of Element 8 was decreased by 20%. It was assumed that the modal damping values and natural frequencies are not influenced much by noise, so the same baseline structure identified at Section 5 was used as the baseline structure. 1% noise and 3% noise were not considered in Case 3. Only 5% noise case was treated in Case 3.

When the accelerations at all nodes for 1 second were used, the Damage Indices for spring constants and dash pot constants are shown in Fig. 8-17 and Fig. 8-18, respectively. As seen in Fig. 8-17 and Fig. 8-18, Element 3 and Element 8 were correctly detected as the damaged elements both in spring constants and dash pot constants. The identification results are listed in Table 8-11.

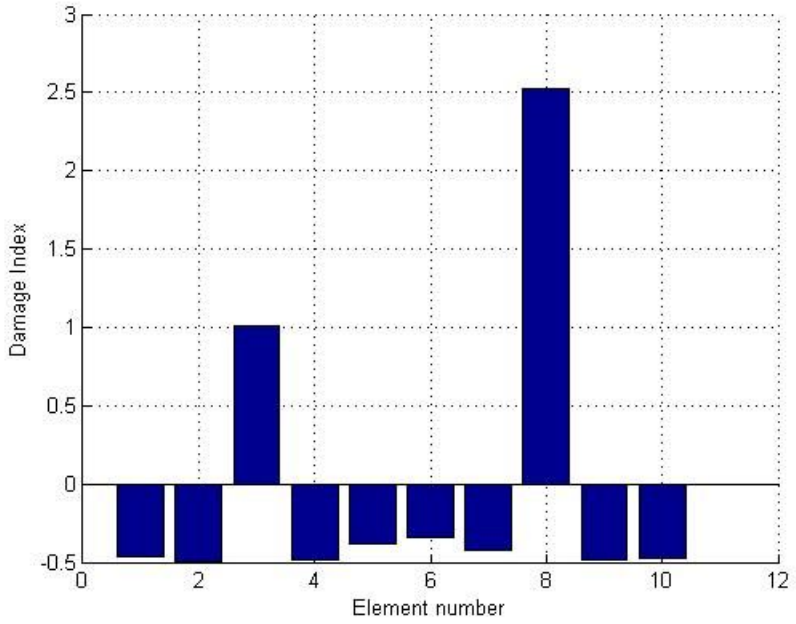

Fig. 8-17 Damage Index for Spring with 10 Measurements for Case 3

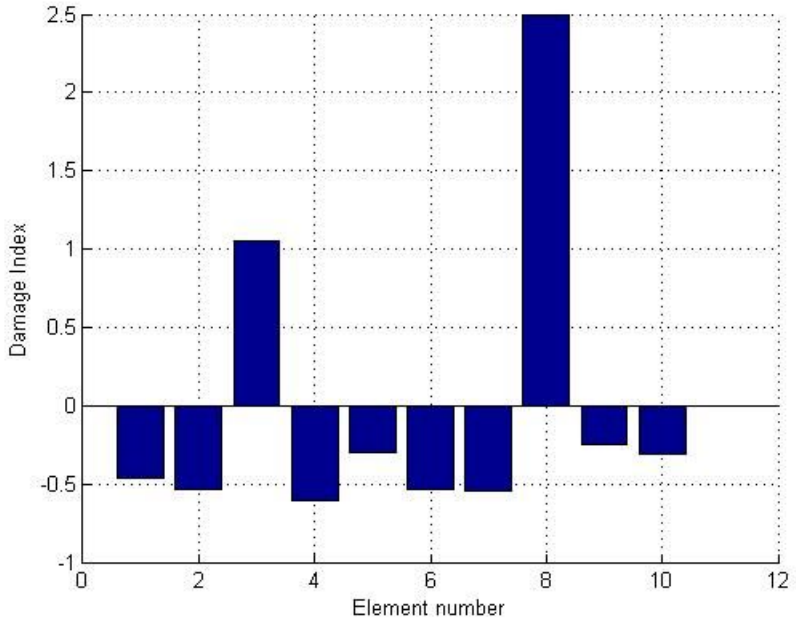

Fig. 8-18 Damage Index for Dash Pot with 10 Measurements for Case 3

Table 8-11 Identified Values with 10 Measurements and 5% Noise for Case 3

	Spring			Dash pot		
	Simulated	Identified	Error (%)	Simulated	Identified	Error (%)
Element 1	1000	1001	0.1	5.00	4.96	0.8
Element 2	1000	1003	0.3	5.00	4.91	1.9
Element 3	900	902	0.2	6.00	6.01	0.2
Element 4	1000	1003	0.3	5.00	4.86	2.8
Element 5	1000	996	0.4	5.00	5.07	1.4
Element 6	1000	993	0.7	5.00	4.91	1.8
Element 7	1000	999	0.1	5.00	4.90	1.9
Element 8	800	800	0.0	7.00	7.01	0.1
Element 9	1000	1002	0.2	5.00	5.10	2.1
Element 10	1000	1002	0.2	5.00	5.07	1.3

When the accelerations at Node 2, Node 4, Node 6, Node 8, and Node 10 for a duration of 1 second were used, the Damage Indices for spring constants and dash pot constants are shown in Fig. 8-19 and Fig. 8-20, respectively. The identification results are listed in Table 8-12.

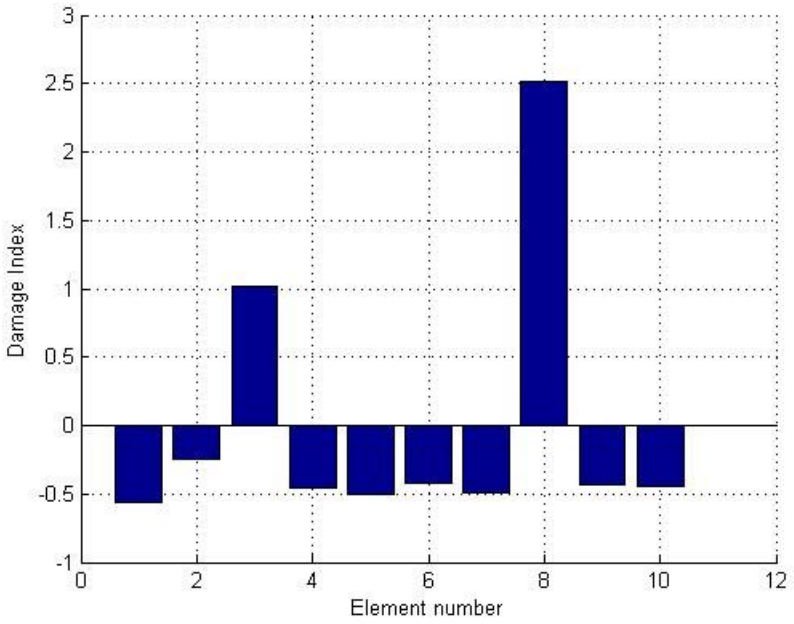

Fig. 8-19 Damage Index for Spring with 5 Measurements for Case 3

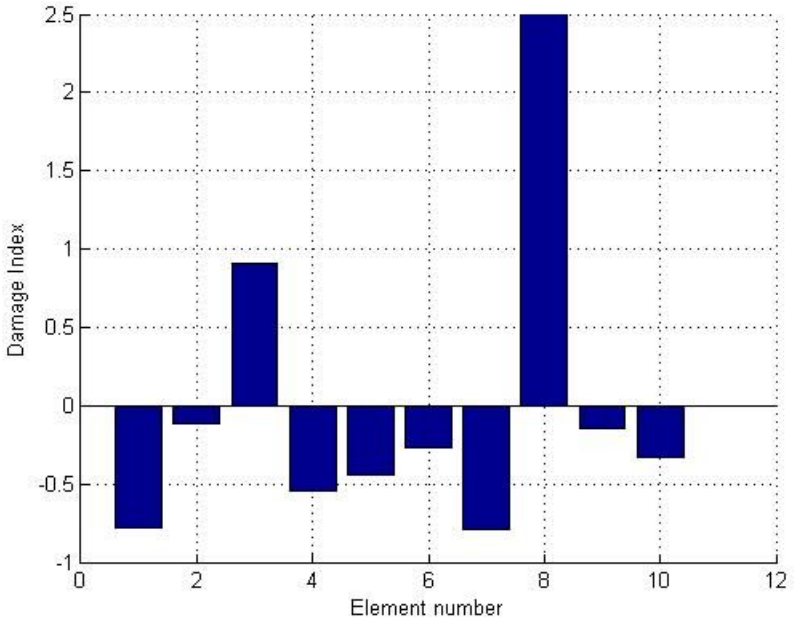

Fig. 8-20 Damage Index for Dash Pot with 5 Measurements for Case 3

With respect to both spring constants and dash pot constants, Element 3 and Element 8 were correctly detected as the damaged elements. The errors in the predicted values of the dash pot constants are larger than those of the spring constants.

Table 8-12 Identified Values with 5 Measurements and 5% Noise for Case 2

	Spring			Dash pot		
	Simulated	Identified	Error (%)	Simulated	Identified	Error (%)
Element 1	1000	1007	0.7	5.00	4.78	4.3
Element 2	1000	986	1.4	5.00	5.25	4.9
Element 3	900	902	0.2	6.00	5.96	0.7
Element 4	1000	1000	0.0	5.00	4.95	1.0
Element 5	1000	1003	0.3	5.00	5.02	0.4
Element 6	1000	998	0.2	5.00	5.14	2.8
Element 7	1000	1002	0.2	5.00	4.78	4.4
Element 8	800	802	0.2	7.00	7.06	0.8
Element 9	1000	999	0.1	5.00	5.23	4.6
Element 10	1000	1000	0.0	5.00	5.10	2.0

We attempted again to identify the structural parameters with the measured accelerations at Node 5 and 10 for a duration of 2 seconds; the identification results are shown in Fig. 8-21 and Fig. 8-22. Element 3 and Element 8 were correctly detected as the damaged elements both in spring constants and in dash pot constants. However, the identified value for the dash pot constant of Element 3 included 9% error.

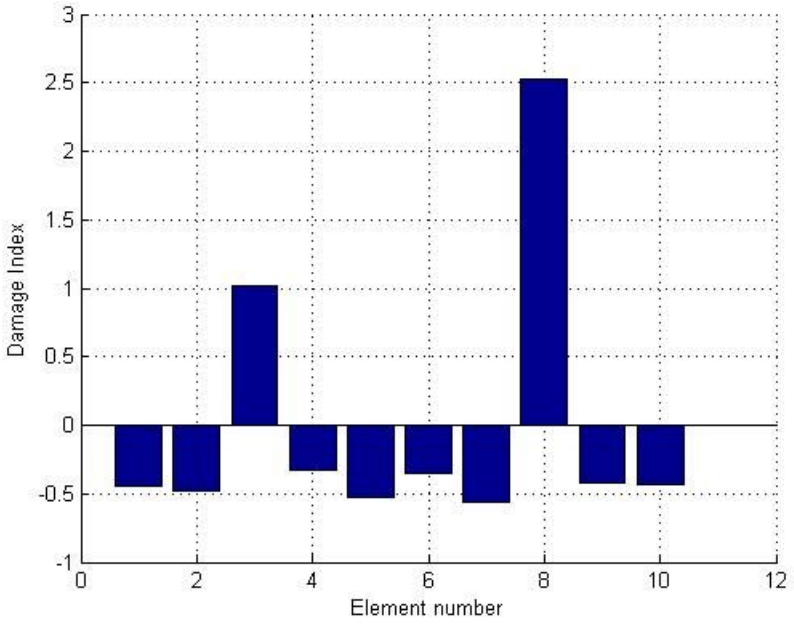

Fig. 8-21 Damage Index for Spring with 2 Measurements for Case 3

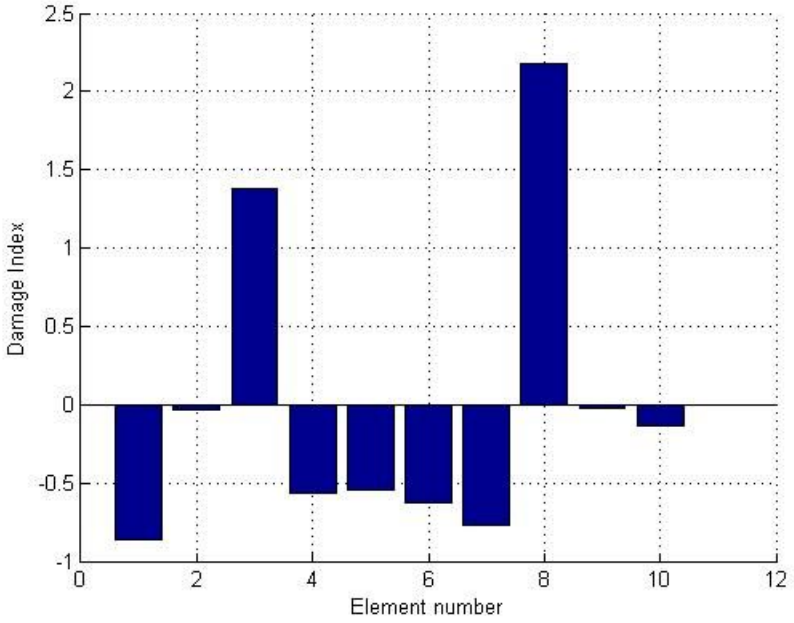

Fig. 8-22 Damage Index for Dash Pot with 2 Measurements for Case 3

Table 8-13 Identified Values with 2 Measurements and 5% Noise for Case 3

	Spring			Dash pot		
	Simulated	Identified	Error (%)	Simulated	Identified	Error (%)
Element 1	1000	1000	0.0	5.00	4.57	8.6
Element 2	1000	1002	0.2	5.00	5.30	6.0
Element 3	900	902	0.2	6.00	6.54	9.0
Element 4	1000	992	0.8	5.00	4.83	3.4
Element 5	1000	1005	0.5	5.00	4.85	3.1
Element 6	1000	993	0.7	5.00	4.78	4.5
Element 7	1000	1008	0.8	5.00	4.65	7.0
Element 8	800	801	0.1	7.00	7.24	3.5
Element 9	1000	999	0.1	5.00	5.31	6.2
Element 10	1000	999	0.1	5.00	5.20	4.1

8.3 SUMMARY

The proposed method, based on the acceleration-structural parameters sensitivities, was verified numerically using a high-rise building modeled as a shear beam. Three levels of noise (1%, 3%, and 5%) were introduced to investigate the robustness of the proposed method to predict damping and stiffness damage in a noise environment. Three damage scenarios were investigated: (1) damping damage in a single location, (2) both stiffness damage and damping damage in a single location and (3) multi-damage cases. Better identification results to identify the structural parameters were produced with the averages of the measured accelerations compared with those obtained by taking the average of the identified values. By increasing the number of measurement locations, false-positive predictions were avoided and more accurate results were obtained.

9 EXPERIMENTAL VERIFICATION OF THE SENSITIVITY METHOD

9.1 INTRODUCTION

In this section, the performance of the sensitivity method is verified using experimental data for a three-story R/C frame building. The proposed method is applied to experimental data generated in a laboratory to identify structural parameters. The experimental data were provided by Bracci(1992).

9.2 DESCRIPTION OF THE RC FRAME BUILDING

The test structure is a three-story R/C fame building with 3 bays. This type of structure is considered to be representative of low-rise buildings typically constructed in the Eastern and Central United States. The general layout of the tested structure is shown in Fig. 9-1 and Fig. 9-2.

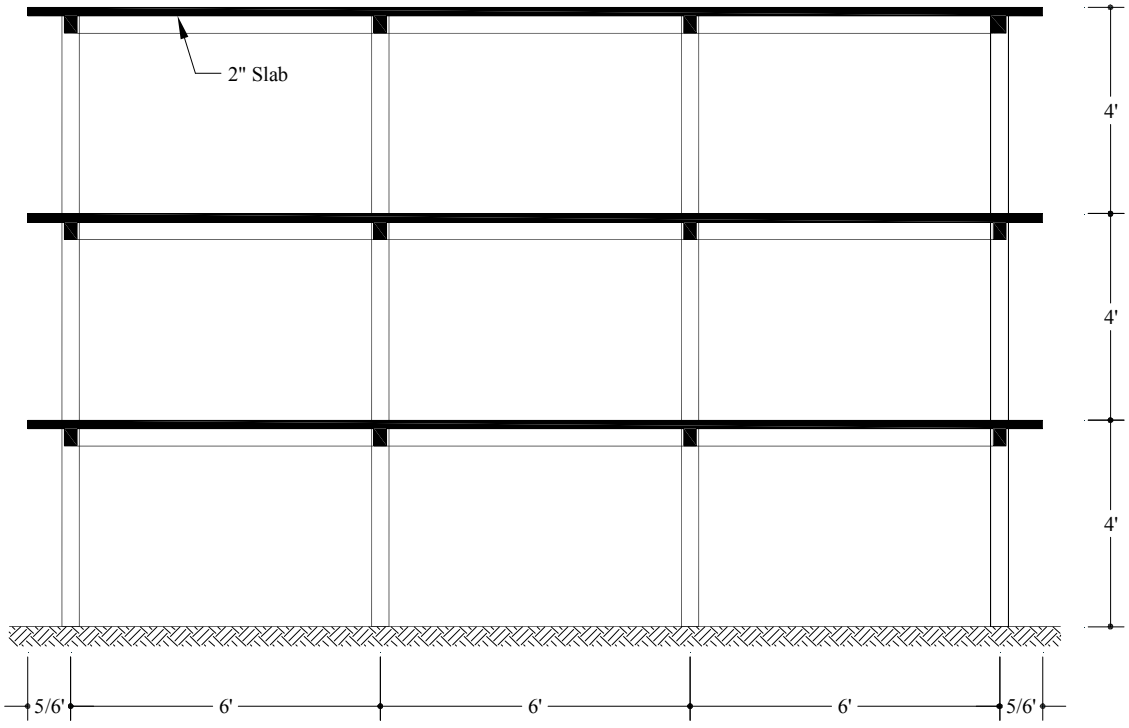

Fig. 9-1 Elevation View of Experimental Structure

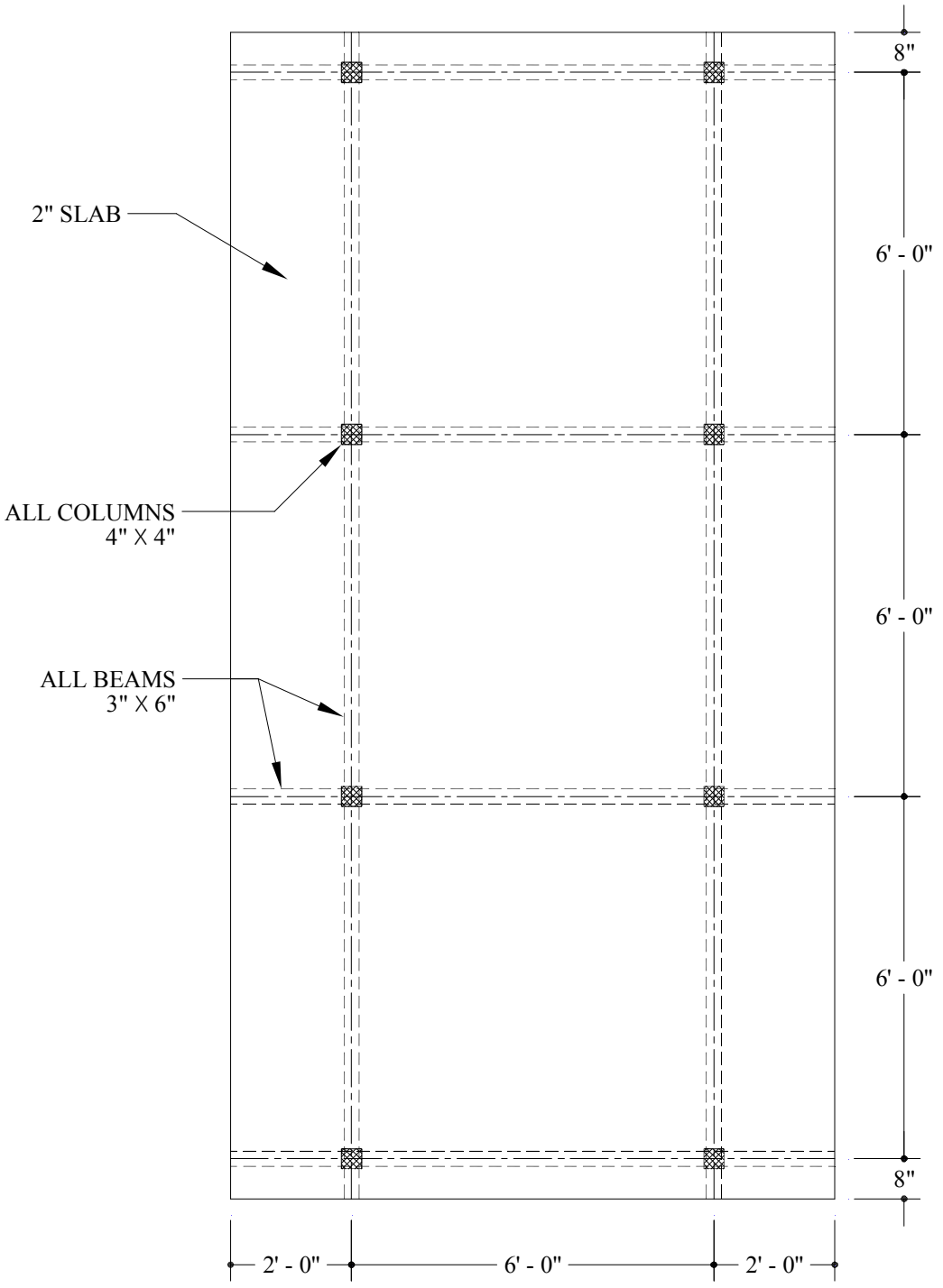

Fig. 9-2 Plan View of Experimental Structure

9.3 SUMMARY OF THE TESTING

The test structure was subjected to three levels of base motions: minor base motion, moderate base motion, and severe base motion. The N21E ground acceleration component of the July 21, 1952 Taft Earthquake at the Lincoln School Tunnel site in California was used as the base motion. For each level of base motion, Taft N21E was scaled to have the peak acceleration as 0.05g, 0.20g, and 0.30g ,respectively. After the structure was excited by each level of base motion, and before it was excited by the minor base motion, it was subjected to white noise base motion again to identify the structural parameters at each stage. The minor, moderate, and severe base motions were used to investigate the pre-yield behavior, the inelastic behavior, and the near collapse mechanism of the model structure (Bracci, 1997).

9.4 MODIFICATION TO THE SENSITIVITY METHOD TO ACCOMMODATE THE PROVIDED DATA

In this section, the proposed method which uses acceleration-structural parameters sensitivities is modified to use the mode shape vectors supplied by Bracci (1992) instead of the accelerations. Since the mode shapes are determined based on the mass and the stiffness of the structure, only the stiffness parameters not damping parameters at each step are identified. The process to identify the stiffness parameters with mode shapes is divided into two procedures:

(a) The first procedure determines the relative ratios of the story stiffness to reproduce mode shapes close to the measured mode shapes. (b) The second procedure scales the relative stiffnesses so that the structure has natural frequencies close to the measured natural frequencies.

The mode shape of the structure depends on the relative stiffness of each story. The relative stiffness of each story can be determined as outlined below.

a. Components of mode shape vectors at several pre-selected locations of the existing structure are measured.

b. A baseline structure, of which all stiffness parameters are 1, is generated, and the mode shape vectors at the same locations with the existing structure are numerically produced.

c. A sensitivity matrix F relating mode shape vectors to stiffness parameters is calculated. The sensitivity matrix F has the form :

$$\mathbf{F} = \begin{bmatrix} \frac{\partial \Phi_{11}}{\partial k_1} & \cdots & \frac{\partial \Phi_{11}}{\partial k_M} \\ \vdots & \cdots & \vdots \\ \frac{\partial \Phi_{mn}}{\partial k_1} & \cdots & \frac{\partial \Phi_{mn}}{\partial k_M} \end{bmatrix} \qquad \textbf{(9-1)}$$

Where Φ_{mn} =mth component of nth mode shape vector

k_M =Mth stiffness parameter

If n mode shapes are available at m locations, and M stiffness parameters are to be identified, the sensitivity matrix F will be of size mn? .

Each column of F matrix can be determined as follows: first, mode shapes are numerically produced at m locations for n mode from the FE model; second, the stiffness of the first element is modified by a known amount; third, the mode shapes are generated from the modified FE model; fourth, the fractional changes between the initial mode shapes and the mode shapes of the modified structure are computed; fifth, each column of the F matrix is computed by dividing the fractional changes in mode shape vectors by the magnitude of the modification at member one; sixth, the entire procedure is repeated for all members.

d. A difference column matrix Z of which each row is equivalent to the difference between the measured mode shape vectors of the existing structure and the simulated mode shape vectors of the baseline structure is built up. The difference column matrix has the form:

$$\mathbf{Z} = \begin{bmatrix} \tilde{\Phi}_{11} - \bar{\Phi}_{11} \\ \vdots \\ \tilde{\Phi}_{mn} - \bar{\Phi}_{mn} \end{bmatrix} \tag{9-2}$$

Where $\tilde{\Phi}_{mn}$ = measured mode shape vector at mth measurement location of nth mode shape

$\bar{\Phi}_{mn}$ = numerically generated mode shape vector at mth location of nth mode shape of the baseline structure

e. With the sensitivity matrix and the difference column matrix determined in Step c and Step d, the stiffness parameters are updated by solving the following system of equations.

$$\begin{bmatrix} \frac{\partial \Phi_{11}}{\partial k_1} & \cdots & \frac{\partial \Phi_{11}}{\partial k_M} \\ \vdots & \cdots & \vdots \\ \frac{\partial \Phi_{mn}}{\partial k_1} & \cdots & \frac{\partial \Phi_{mn}}{\partial k_M} \end{bmatrix} \begin{Bmatrix} \Delta k_1 \\ \vdots \\ \Delta k_M \end{Bmatrix} = \begin{bmatrix} \tilde{\Phi}_{11} - \bar{\Phi}_{11} \\ \vdots \\ \tilde{\Phi}_{mn} - \bar{\Phi}_{mn} \end{bmatrix} \tag{9-3}$$

Letting $\boldsymbol{\alpha} = \begin{Bmatrix} \Delta k_1 \\ \vdots \\ \Delta k_M \end{Bmatrix}$, Eq 9-3 can be expressed as

$\mathbf{F}\boldsymbol{\alpha} = \mathbf{Z}$

The modification of the stiffness parameters can be obtained by solving the equation,

$$\boldsymbol{\alpha} = (\mathbf{F}^T\mathbf{F})^{-1} \times (\mathbf{F}^T\mathbf{Z}) \tag{9-4}$$

f. The stiffness of each element is then updated and is scaled by the stiffness of Element 1.

g. Steps c, d, e, and f are repeated until $\mathbf{Z} \cong \mathbf{0}$ or $\boldsymbol{\alpha} \cong \mathbf{0}$

The natural frequencies generated from the structure whose stiffness parameters were scaled to one for Element 1 will show considerable errors when compared with the

measured natural frequencies. The scaling of the relative stiffness parameters to produce a closer agreement between generated natural frequencies and the measured natural frequencies can be done by utilizing the following procedure.

a. Natural frequencies of the existing structure are measured.
b. Based on the information about the as-built plans and field inspection, an initial estimate of the stiffness parameters is made.
c. The initial estimate of the scale factor is determined based on the estimated stiffness in Step b.
d. A sensitivity matrix F for natural frequencies to stiffness parameters is calculated. In this procedure, F will be a column matrix, because only one unknown, the scaling factor for the stiffness parameters is to be determined. The sensitivity matrix has the form of

$$\mathbf{F} = \begin{bmatrix} \dfrac{\partial \omega_1}{\partial s} \\ \vdots \\ \dfrac{\partial \omega_n}{\partial s} \end{bmatrix} \qquad \textbf{(9-5)}$$

Where ω_n = nth natural frequency

s = scaling factor

e. The difference column matrix Z in which each row is equivalent to the difference between the measured natural frequencies of the existing structure and the simulated natural frequencies of the numerical model are generated. The difference column matrix has the form:

$$\mathbf{Z} = \begin{bmatrix} \tilde{\omega}_1 - \bar{\omega}_1 \\ \vdots \\ \tilde{\omega}_n - \bar{\omega}_n \end{bmatrix} \qquad \textbf{(9-6)}$$

Where $\tilde{\omega}_n$ = measured nth natural frequency of the existing structure

$\bar{\omega}_n$ = simulated nth natural frequency of the numerical model

f. The scaling factor is updated by solving the following system of equations

$$\begin{bmatrix} \dfrac{\partial \omega_1}{\partial s} \\ \vdots \\ \dfrac{\partial \omega_n}{\partial s} \end{bmatrix} \Delta s = \begin{bmatrix} \tilde{\omega}_1 - \bar{\omega}_1 \\ \vdots \\ \tilde{\omega}_n - \bar{\omega}_n \end{bmatrix} \tag{9-7}$$

h. Steps d, e, and f are repeated until $\mathbf{Z} \cong \mathbf{0}$ or $\Delta s \cong 0$.

9.5 IDENTIFICATION OF THE RC FRAME BUILDING

The proposed method is applied to the measured mode shape vectors of the test structure before and after the test structure was subjected to the each level of base motion to identify the stiffness parameters. The stiffness parameters identified by the proposed method are compared with the stiffness parameters identified by Bracci(1992). Bracci identified the story stiffness of the test structure from the stiffness matrix constructed as follows:

$$\mathbf{K} = \mathbf{M}\boldsymbol{\Phi}_\mathbf{n}\boldsymbol{\Omega}\boldsymbol{\Phi}_\mathbf{n}^\mathrm{T}\mathbf{M} \tag{9-8}$$

Where $\mathbf{K}$ =Stiffness matrix

$\mathbf{M}$ =Mass matrix

$\boldsymbol{\Phi}_\mathbf{n}$ =Normalized modal shape matrix

$\boldsymbol{\Omega}$ =Diagonal natural frequency matrix $\left[\omega_1^2, \omega_2^2, \cdots \omega_n^2\right]$

ω_i =i-th natural frequency (rad/sec)

The test structure is modeled simply as the three story shear-beam building as shown in Fig. 9-3.

Based on estimated quantities, Bracci assessed the mass matrix as

$$\mathbf{M}_{ij} = \begin{bmatrix} 0.070 & 0.000 & 0.000 \\ 0.000 & 0.070 & 0.000 \\ 0.000 & 0.000 & 0.070 \end{bmatrix} \text{kip/in/sec}^2 \qquad \textbf{(9-9)}$$

This mass matrix is used in the proposed method. It is assumed that mass matrix remains constant even though stiffnesses may vary while the structure experiences damage.

The natural frequencies of the test structure at each step are listed in Table 9-1.

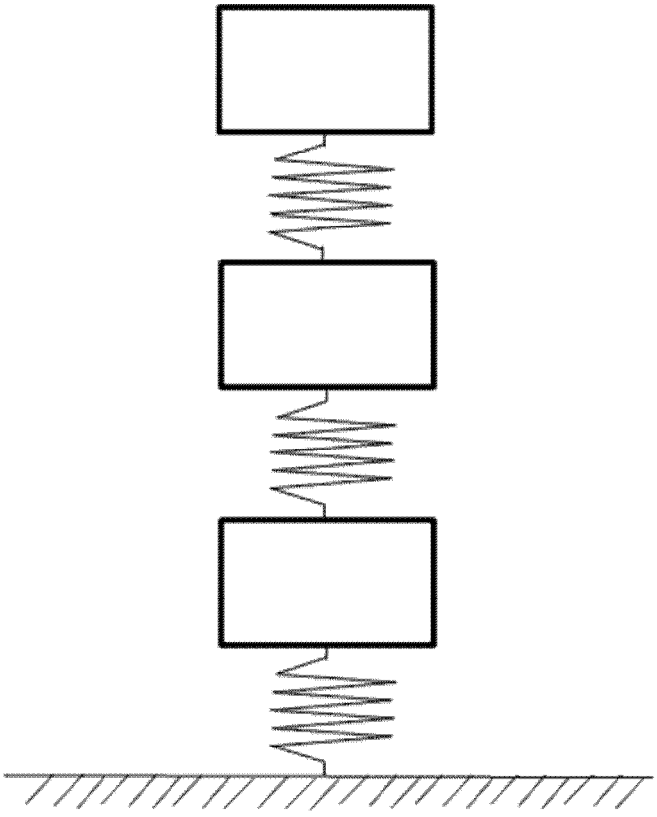

Fig. 9-3 Simplified Model of the Model Structure

Table 9-1 Natural Frequencies of the Test Structure at Each Step in Hz

	Undamaged	Minor Damage	Moderate Damage	Severe Damage
Mode 1	1.78	1.71	1.42	1.2
Mode 2	5.32	5.22	4.37	3.76
Mode 3	7.89	7.32	6.18	5.27

After the structure experienced the moderate base motion and severe base motion, the natural frequencies of the test structure were considerably decreased. Therefore it is obvious that the structure was damaged, but the decrease of the natural frequencies itself doesn't provide the information regarding the locations and the severities of the damage. The mode shapes of the test structure at each step are shown in Fig. 9-4.

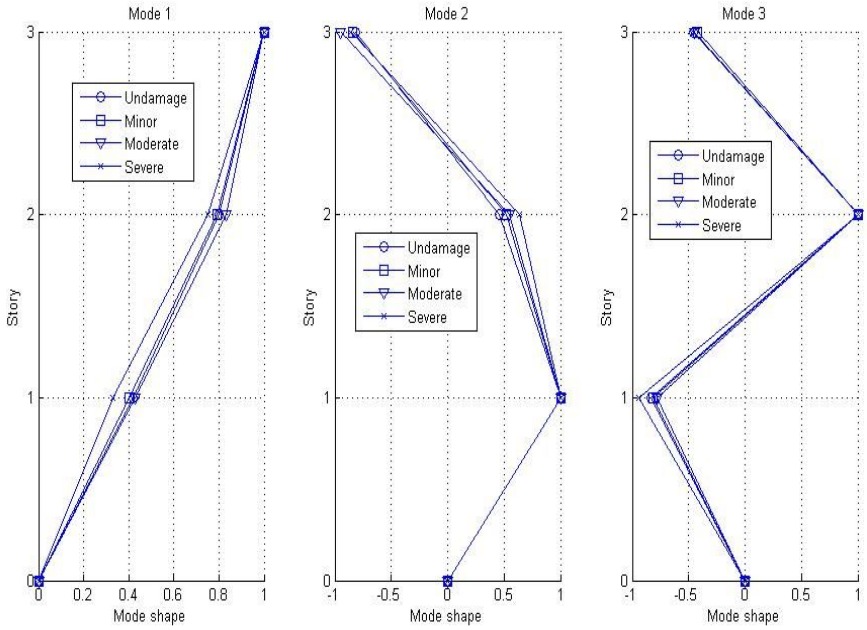

Fig. 9-4 Measured Mode Shapes of the Test Structure at Each Step

The mode shapes of the severely damaged structure show obvious deviation from the mode shapes of other cases. Based on the measured mode shapes, the relative stiffness at each story for each damage case was calculated by the first procedure

suggested in Section 9.4. The determined relative stiffness parameters are listed in Table 9-2 and the mode shapes produced with those stiffness parameters are compared with the measured mode shapes for each damage case in Fig. 9-5, Fig. 9-6, Fig. 9-7 and Fig. 9-8.

For the undamaged case, the story stiffnesses differ little from each other. However, in the severely damaged structure, the story stiffness of second story is 65% of the story stiffness of the first story.

Table 9-2 Relative Stiffness of Each Story for Each Damage Case

	Undamaged	Minor Damage	Moderate Damage	Severe Damage
1st	1	1	1	1
2nd	0.91	0.91	1.14	0.65
3rd	0.94	0.88	1.03	0.72

For the undamaged case and the minor damaged case, the mode shape from the FE model could be aprroximated to be very close to the measured mode shapes. However, for the moderately damaged case, and the severely damaged case, the numerically generated mode shapes show significant deviations from the measured mode shapes. These deviations are caused by the fact that the number of the stiffness parameters to be identified is less than the number of the measured mode shapes.

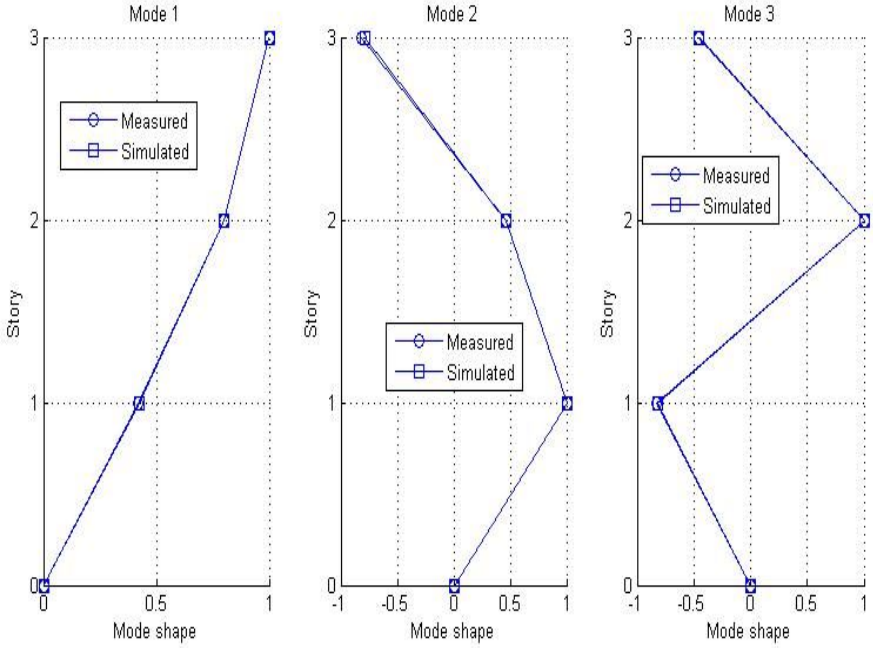

Fig. 9-5 Comparison of Mode Shapes for Undamaged Structure

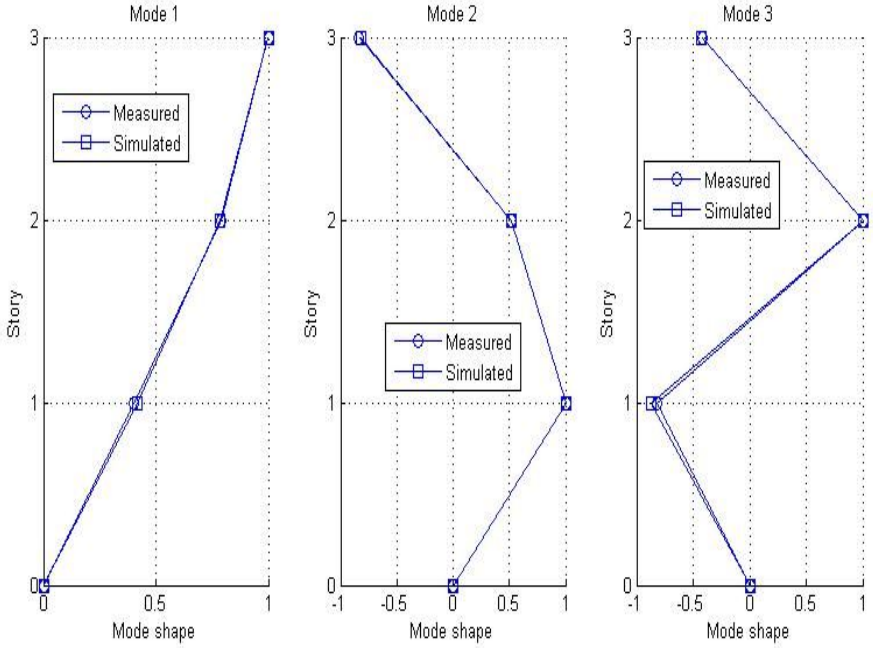

Fig. 9-6 Comparison of Mode Shapes for Minor Damaged Structure

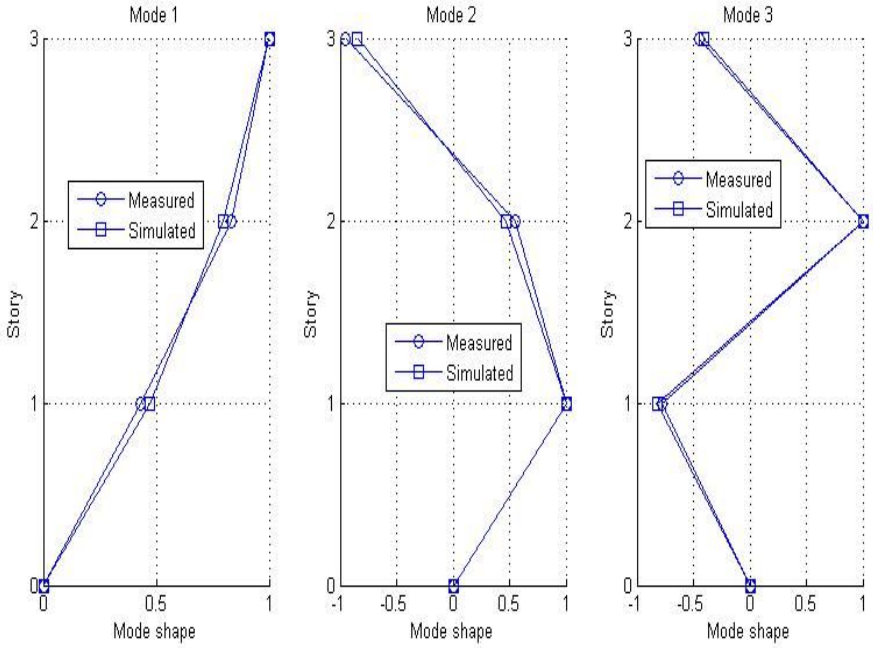

Fig. 9-7 Comparison of Mode Shapes for Moderately Damaged Structure

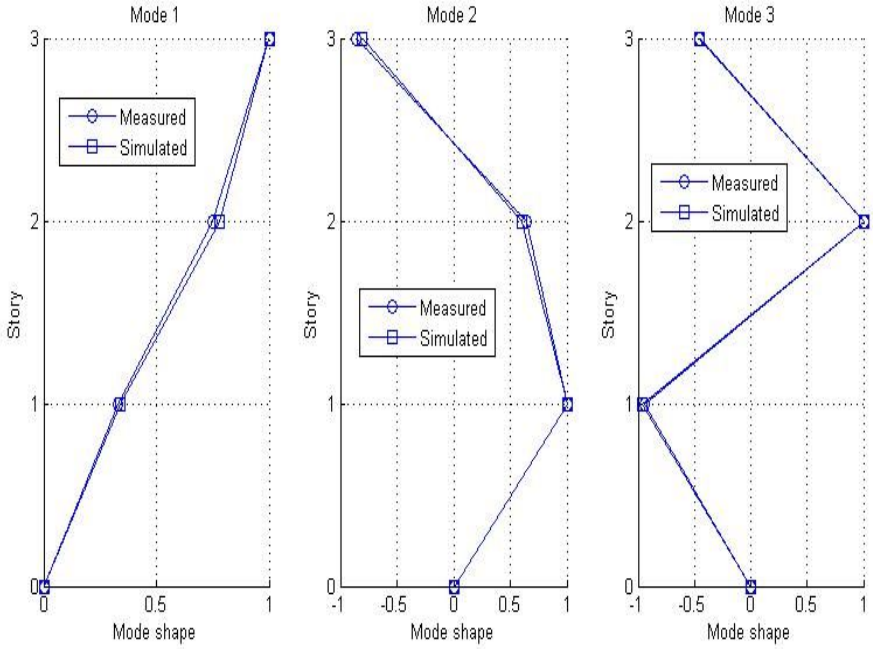

Fig. 9-8 Comparison of Mode Shapes for Severely Damaged Structure

The severities of the damaged elements can be assessed after the relative stiffness parameters are scaled so that the structure has the natural frequencies close to those listed in Table 9-1. The scaled stiffness parameters using the second procedure suggested in Section 9.3 are listed in Table 9-3; the natural frequencies with those stiffness parameters are compared with the measured natural frequencies in Table 9-4 and Table 9-5. For each and every case, the first natural frequency has the largest error and the numerically generated first frequency is larger than the measured one.

Table 9-3 Scaled Story Stiffness for Each Damage Case

	Undamaged	Minor Damage	Moderate Damage	Severe Damage
1st	51.53	47.68	29.79	29.36
2nd	46.91	43.44	33.89	18.97
3rd	48.45	42.13	30.58	21.19

Table 9-4 Comparison of Natural Frequencies I

	Undamaged			Minor		
	Measured	Simulated	Error (%)	Measured	Simulated	Error (%)
Mode 1	1.78	1.88	5.80	1.71	1.81	5.57
Mode 2	5.32	5.27	0.93	5.22	4.98	4.53
Mode 3	7.89	7.51	4.87	7.32	7.15	2.35

Table 9-5 Comparison of Natural Frequencies II

	Moderate			Severe		
	Measured	Simulated	Error (%)	Measured	Simulated	Error (%)
Mode 1	1.42	1.50	5.28	1.2	1.30	8.60
Mode 2	4.37	4.15	4.98	3.76	3.66	2.74
Mode 3	6.18	6.16	0.30	5.27	4.96	5.87

The story stiffness identified by the proposed method and by Bracci(1992) are compared in Fig. 9-9, Fig. 9-10, and Fig. 9-11.

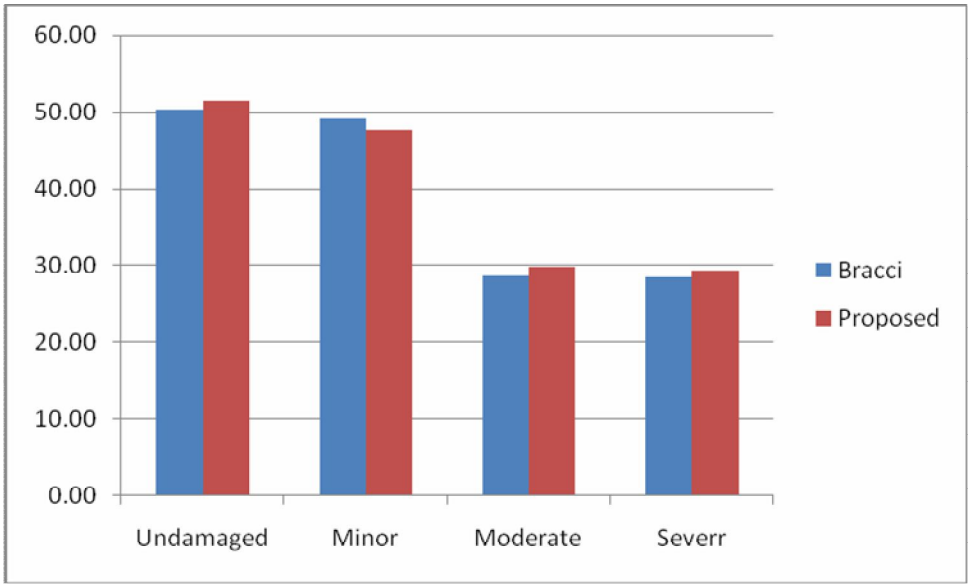

Fig. 9-9 Stiffness of the First Story for Each Damage Case

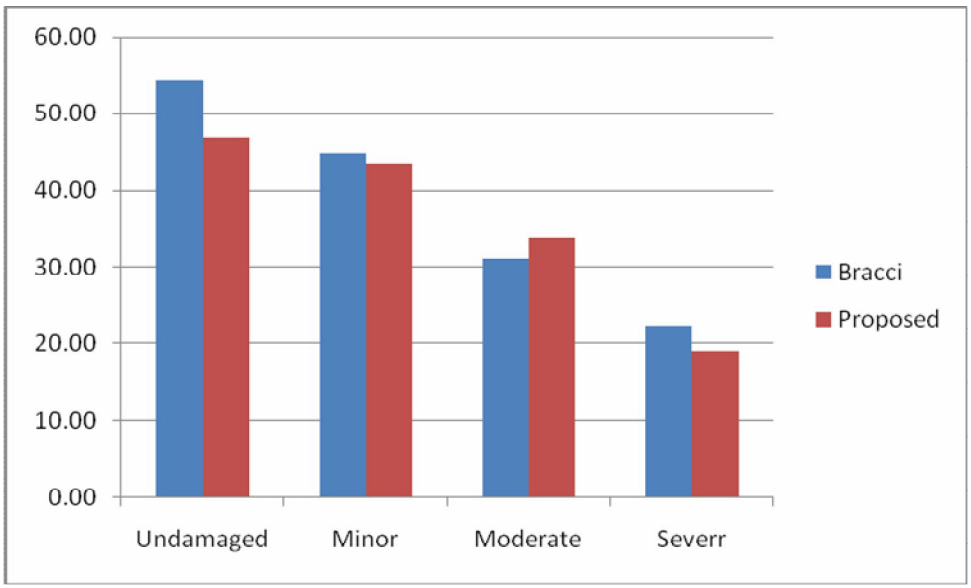

Fig. 9-10 Stiffness of the Second Story for Each Damage Case

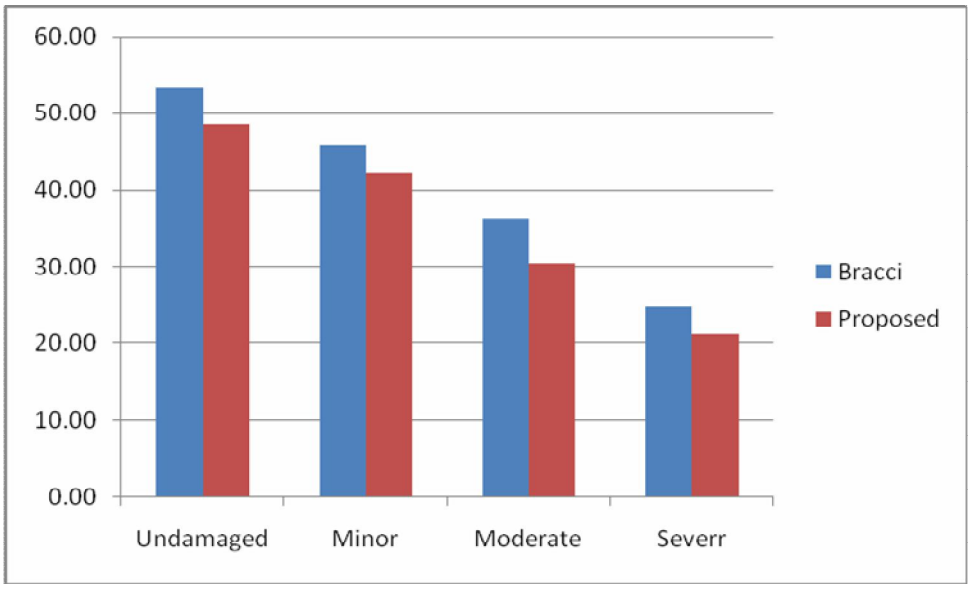

Fig. 9-11 Stiffness of the Third Story for Each Damage Case

9.6 SUMMARY

In this section, the sensitivity method was modified to identify the stiffness parameters using mode shapes instead of accelerations. The proposed method, with modification, was applied to a referenced structure and three damage cases: (a) an undamaged referenced case, (b) a minor damaged case, (c) a moderately damaged case, and (d) a severely damaged case. Similar mode shapes to the measured mode shapes were reproduced by the proposed method. The stiffness parameters identified by the sensitivity method were similar to those estimated via the stiffness matrix method, which utilized the mass matrix, mode shapes, and natural frequencies.

10 SUMMARY AND FUTURE WORK

10.1 SUMMARY

The objective of this study was to develop NDE techniques that can identify, simultaneously, both stiffness and damping changes in a structure. Two approaches were used to meet the stated objectives. First, a method was developed on the basis of the conservation of total energy; second, a method was proposed which utilized the acceleration-structural parameters (stiffness and damping) sensitivities.

In Section 2, the theoretical background of the approach based on the conservation of total energy was investigated. The governing equations for the identification of stiffness and damping were derived and expressed in matrix form.

In Section 3, the theoretical background of the approach utilizing acceleration-structural parameter sensitivities was investigated. The equations for the identification of stiffness and damping were derived in matrix form.

In Section 4, the performance of the developed NDE technique based on the conservation of total energy was numerically verified for a shear building.

In Section 5, the performance of the second proposed method, presented in Section3, which utilizes acceleration-structural parameter sensitivities, was verified for high-rise buildings modeled as shear beams.

In Section 6, a damping damage model for the beam structure was proposed. The performance of the second proposed method which uses acceleration-structural parameters sensitivities was verified numerically for a two-span continuous beam structure with known damage scenarios.

In Section 7, the performance of the developed NDE technique based on the conservation of total energy was numerically verified for high-rise buildings modeled as shear beams with noise-polluted data.

In Section 8, the performance of the second proposed method, presented in Section 3, which utilizes acceleration-structural parameter sensitivity, was verified for high-rise buildings modeled as shear beams with noise-polluted data.

Finally, in Section 9, the performance of the second proposed method was verified using experimental data for a three-story R/C frame building. The mode shapes, instead of the accelerations, were used for the identification of the story stiffness.

10.2 FINDINGS

In Section 4, in which the performance of the developed NDE technique based on the conservation of total energy was numerically verified for a shear building, the following major findings were made:

1. The influence of the sampling rate and the observation time on the identified values were numerically investigated and it was concluded that better identification results can be obtained with higher sampling rates. Observation time does not have as much influence as the sampling rate.

2. The performance of the energy based method was verified numerically using three damage scenarios.

In Section 5, in which the performance of the sensitivity method was verified for high-rise buildings modeled as shear beams, the following major findings were made:

1. Not only the spring constants but also dash pot constants of the baseline structure were identified using natural frequencies and modal damping values.
2. The performance of the sensitivity method was verified numerically using three damage scenarios.
3. Even with the accelerations measured at only one location, the structural parameters were identified accurately.

In Section 6, where the performance of the sensitivity-based method was verified numerically using a two-span continuous beam, the following major findings were made:

1. The proportional damping coefficients for the mass matrix and the stiffness matrix were identified using modal damping values and the bending stiffness of the baseline structure was determined using the natural frequencies.

2. The increased damping coefficient of the damping damaged element had an influence on the proportional coefficient for the mass matrix. The change in the proportional coefficient for the stiffness matrix was negligible.

3. The proposed method accurately identified both bending stiffness and damping coefficients for all damage scenarios.

In Section 7, the performance of the developed NDE technique based on the conservation of total energy was numerically investigated using a numerical model of a high-rise building modeled as a shear beam with noise-polluted data, the following major findings were made:

1. The identified values of the dash pot had larger standard deviations than the spring constant.

2. With 1% noise, the damaged elements were detected correctly, but there were some false-positive predictions.

3. With 3% noise, the damaged elements were not detected

4. Element 10 was detected as a false-positive prediction in almost every case.

In Section 8, in which the performance of the sensitivity method was analysed for a high-rise building modeled as shear beams with noise-polluted data, the following major findings were made:

1. When the structure had damping damage of 10% severity at a single location, 2 measurement locations were enough to accurately locate and size the damage for 1% noise.

2. When the noise level was increased to 3% and 5%, with 2 measurement locations, undamaged elements were falsely detected as damaged elements. To avoid false detection, an increase in the measurement locations was needed.

3. Stiffness damage was more detectable than the damping damage. With 5 measurement locations, stiffness damaged elements were detected correctly, however with respect to damping, some undamaged elements were falsely detected.

Finally, in Section 9, in which the performance of sensitivity method was verified using experimental data, the following major findings were made:

1. The proposed method was modified to identify the stiffness parameters with the mode shapes instead of the accelerations.

2. The stiffness parameters identified by the proposed method were similar to those estimated by the classical stiffness matrix formulation based on the mass matrix, mode shapes, and natural frequencies.

3. The similar mode shapes to the measured mode shapes were reproduced by the proposed method.

10.3 ORIGINALITY OF THIS WORK

There are three original aspects of this study. First, two new NDE techniques which can identify simultaneously both stiffness and damping changes were developed. With the NDE techniques developed in this study, the damping damaged element could be located and estimated in addition to the stiffness damaged element, while all current NDE techniques conducted to date can detect only stiffness damage. Second, the current baseline structure-identification technique was extended to include modal damping values. Current methods identify only the stiffness parameters using changes in the natural frequencies. However, in this study, the damping characteristics of the baseline structure were also identified using changes in the modal damping values. Finally, the damping damage model was proposed for a beam structure subjected to the assumption that the damping of the undamaged structure was modeled as proportional damping.

10.4 CONTRIBUTION OF THIS WORK

The damaged elements in the structure may be localized at an earlier stage with the NDE techniques developed in this study and, consequently, premature structural failure may be avoided at an earlier stage. Certainly, the correction of the damaged element when damage is very small may result in a significant reduction in repair costs and the other unwanted consequencies of failure. In addition, the result of this study can be extended to the problem of estimating the integrity of dampers that have been incorporated to control the motion of critical structures such as bridges.

10.5 FUTURE STUDY

On reviewing the findings in this work, future research may be directed in the following areas:

1. Improvement in the method such that the location and the severity of the damaged can be estimated when measurement points are sparsely spaced;

2. Improvements in the method that lead to practical estimates of the identified stiffness and damping changes;

3. Improvements in the method such that the proposed method are robust to noise; and

4. Development of damping damage models for more complicated structures (e.g., plates, shells, trusses, and frames).

REFERENCES

Adams,R.D., Cawley, P., Pye, C.J., and Stone, B.J.(1978) "A Vibration Technique for Non-Destructively Assessing the Integrity of Structures." *J. Mech. Engr. Science*, 20(2), 93-100.

Agbabian, M.S., Masri, S.F., Miller, R.K., and Caughey, T.K. (1991) "System Identification Approach to detection of Structural Changes." *ASCED J., Engineering Mechanics,* 117(2),370-390.

Aktan, .A.E., Lee, K.L., Chuntavan, C., and Aksel, ;. (1994). "Modal Testing for Structural Identification and Condition Assessment of Constructed Facilities." *Proc. Of the 12th Int. Modal Analysis Conf.*, Vol.1,462-468, Honolulu, Hawaii.

Banan, M.R., Bana, M.R., and Hjelmstad, K.D. (1994). "Parameter Estimation of Structures from Static Responses. II: Numerical Simulation Studies." *J. Structural Engineering,* ASCE,120(11),3259-3283.

Bracci, M.J. (1992). "Experimental and Analytical Study of Seismic Damage and Retrofit of Lightly Reinforced Concrete Structures in Low Seismicity Zones." Ph.D. dissertation, Dept of Civil Engineering, State University of New York.

Bray, D.E., and McBride, D. (1992). *Nondestructive Testing Techniques.* John Wiley & Sons, New York, New York.

Carrasco, C.J., Osegueda, R.A., Ferregut, C.M., and Grygier, M. (1997). "Damage Localization in a Space Truss Model Using Modal Strain Energy." *Proc. 15th IMAC,* Orlando, Florida, 2, 1782-1792.

Cawley, P., and Adams, R.D. (1979). "The Locations of Defects in Structures from Measurements of Natural Frequencies." *J. Strain Analysis*, 14(2),49-57.

Chance, J., Tomlinson, G.R. and Worden, K. (1994). "A Simplified Approach to the Numerical and Experimental Modeling of the Dynamics of a Cracked Beam." *Proc. 12th IMAC,* Honolulu, Hawaii,1, 778-785.

Chen, J.C., and Wada, B.K. (1975). "Criteria for Analysis – Test Correlation of Structural Dynamic Systems." *J. Applied Mechanics,* 6, 471-477.

Chen, Y., and Swamidas, A.S.J. (1994). "Dynamic Characteristic and Modal Parameters of a Plate with a Small Growing Surface Crack." *Proc. 12th IMAC,* Honolulu, Hawaii, 2, 1155-1161.

Collins, J.D., Har, G.C., Hasselman, T.K. and Kennedy, B. (1974) "Statistical Identification of Structures", *AIAA J.,* 12(2),185-190.

Cottin, N. (1998). "Model Updating and the Bias Problem." *International Workshop on Modeling and Reality – The Role of Learning and Self-organization,* Clausthal-Zellerfeld, Harz Mountain, Germany, 98-106.

Doebling, S. W. Farrar, C.R., and Prime, M.B. (1998). "A Summary Review of Vibration-Based Damage Identification Methods." *The Shock and Vibration Digest,* 30(2),91-105.

Dorn, L. (1982). "Correlation Between the Rate of Damage and Energy Absorption of Structural Steel During Fatigue Testing." *Materials Science and Engineering*, 53, 251-256.

Eykhoff, P. (1974). *System Identification : Parameter and State Estimation.* John Wiley & Sons, Inc. New York, N.Y.

Farrar, C.R., Cornwell, P.J., Doebling, S.W., and Prime, M.B. (2000). "Structural Health Monitoring Studies of the Alamosa Canyon and I-40 Bridges." *Report No, LA-13635-MS,* Los Alamos National Laboratory, Los Alamos, New Mexico.

Fox, C.H.J. (1992). "The Location of Defects in Structures: A Comparison of the Use of Natural Frequency and Mode Shape Data." *Proc. 10th IMAC,* Orlando, Florida,1, 522-528.

Hajela, P., and Soeiro, F.J. (1990). "Structural Damage Detection Based on Static and Modal Analysis." *AIAA J.,* 28(6), 1110-1115.

Jeary, A.P., and Ellis, B.R. (1984). "Non-destructive in-situ testing using dynamic techniques." *Proc. 3rd International Conference on Tall Buildings,* Hong Koan and Guanzhou, 76-81.

Juang, J.N. (1994). *Applied System Identification,* Prentice Hall, Englewood Cliffs, N.J.

Kim, B.H. (2002). "Local Damage Detection Using Modal Flexibility." PhD Dissertation, Texas A&M University, College Station, Texas.

Kawiecki G. (2001). "Modal Damping Measurement for Damage Detection." *Smart Mater. Struct*. 10(2001) 466-471.

Kramer, C., Smet, C.A.M., Roeck, G. (1999). "Z24 Bridge Damage Detection Tests." *Proc. 17th IMAC,*Orlando, Florida, 1, 1023-1029.

Lifshitz, J.M., and Rotem, A. (1969). "Determination of Reinforcement Unbonding of Composites by a Vibration Technique." *J. Composite Materials,* 3, 412-423.

Lin, R.M., and Ewins, D.J. (1994), "Analytical Model Improvement Using Frequency Response Functions." *Mechanical Systems and Signal Processing,* 8(4), 437-458.

Ljung, L.(1988), *System Identification Toolbox User's Guide.* The Mathworks, Inc., Natick, MA.

Mayes, R.L.(1995), "An Experimental Algorithm for Detecting Damage Applied to the I-40 Bridge over the Rio Grande." *Proc. Of the 13th Int. Modal Analysis Conf.,* Nashville, Tenessee, Vol.1,219-225.

Mottershead, J.E. (1990), "Theory for the Estimation of Structural Vibration Parameters from Incomplete Data." *AIAA J.,* 28(3), 559-561.

Natke, H.G. (1982). *Identification of Vibrating Structures*, Springer-Verlag, Wien, NewYork, NY.

Nicholson, D.W., and Alnefaie, K.A. (2000). "Modal Moment Index for Damage Detection in Beam Structures." *Acta mechanica,* 144, 155-167.

Nam, D.H. (2001). "Improvements in the Accuracy of System Identification and Nondestructive Damage Evaluation in Civil Engineering Structures." PhD Dissertation, Texas A&M University, College Station, Texas.

Pandey, A.K., Biswas, M., and Samman, M.M. (1991). "Damage Detection from Changes in Curvature Mode Shapes." *J. Sound and Vibration*, 145(2),321-332.

Pandey, A.K., Biswas, M., (1994). "Damage Detection in Structures Using Changes in Flexibility." *J. Sound and Vibration*, 169(1),3-17.

Petro, S.H., Chen S.-E., GangaRao, H.V.S., and Venkatappa, S. (1997). "Damage Detection Using Vibration Measurements." *Proc. 15th IMAC*, Orlando, Florida, 1, 113-119.

Reddy, J.N. (1984). *An Introduction to the Finite Element Method*, Mc Graw Hill, NewYork.

Rytter, A. (1993). "Vibrational Based Inspection of Civil Engineering Structures." PhD Dissertation, University of Aalborg, Aalborg, Denmark.

Sackman, J.L., Der Kiureghian, A., and Nour-Omid, B. (1983). "Dynamic Analysis of Light Equipment in Structures: Modal Properties of the Combined System." *J. Engineering Mechanics*, ASCE,109(1),73-89.

Salawu, O.S. (1997). "Detection of Structural Damage through Changes in Frequency: A Review." *Engineering Sciences,* 19(9),718-723.

Savage, R.J. and Hewlett, P.C. (1978). "A New NDT Method for Structural Integrity Assessment." *NDT International,* 11,61-66.

Shi, Z.Y., Law, S.S., and Zhang, L.M. (2000). "Structural Damage Detection from Modal Strain Energy Change." *J.Engrg. Mech.*, ASCE, 126(12),1216-1223.

Slastan,J. and Piegtrzko, S. (1993). "Changes of RC-beam Modal Parameters due to Cracks." *Proc. Of the 11th International Modal Analysis Conference,* Kissimmee, Florida, 1,70-76.

Stubbs, N. (1985). "A General Theory of Non-Destructive Damage Detection in Structure." *Proc. Of the 2nd Int. Sysmposium on Structural Control*, Waterloo, Ontario, Canada,694-713.

Stubbs, N., and Osegueda, R. (1990a). "Global Non-Destructive Damage Evaluation in Solids." *Int. J. Analytical and Experimental Modal Analysis*, 5(2),67-79.

Stubbs, N., and Osegueda, R. (1990b). "Global Damage Detection in Solids – Experimental Verification." *Int. J. Analytical and Experimental Modal Analysis*, 5(2),81-97.

Stubbs, N., and Kim,J.T., and Topole, K.(1992) "An Efficient and Robust Algorithm for Damage Localization in Offshore Platforms." *ASCE 10th Structures Congress '92,* San Antonio, Texas, 543-546.

Stubbs, N., Kim,J.T., and Farrar, C.R. (1995). "Field Verification of a Nondestructive Damage Localization in Offshore Platforms." *Proc 13th IMAC,* Nashville, Tennessee, 1, 210-218.

Stubbs, N., and Kim,J.T.(1996). "Damage Localization in Structures without Baseline Modal Parameters,", *AIAA J.*,34(8),1644-1649.

Tilly, G.P. (1977). "The Damping Capacity of Bridges." *Proceedings of Symposium in dynamic behavior of bridges.* TPRL, Department of Transport.

Toksoy, T., and Aktan, A.E. (1994). "Bridge-condition Assessment by Modal Flexibility." *Experimental Mechanics*, 34(3),271-278.

Tomlinson, G.R. (1985). "Dynamics of Nonlinear Systems." Report, Dept of Mechanical Engineering, Heriot-Watt University, Edinburgh, U.K.

Tsai, W.H, and Yang, J.C.S. (1988). "Non-destructive Evaluation of Composite Structures Using System Identification Technique." *J.Engineering Materials and Technology, Transactions of the ASME*, 110(2),134-139.

Wahab, M.M.A., and Roeck, G.D. (1999). "Damage Detection in Bridges Using Modal Curvature: Application to a Real Damage Scenario." *J.Sound and Vibration,* 226(2), 217-235.

Yao, G.C., Chang, K.C., and Lee, G.C. (1992). "Damage Diagnosis of Steel Frames Using Vibrational Signature Analysis." *J. Engrg. Mech.,* ASCE, 118(9), 1949-1961.

Yao, J.T.P.(1998). "On Structural Identification." *International Workshop on Modeling and Reality – The Role of Learning and Self-organization,* Clausthal-Zellerfeld, Harz Mountain, Germany, 126-134.

Zadeh, L.A. (1962). "From Circuit Theory to System Theory." *Proc., IRE.*, 50, 856-865.

VITA

Sang Su Hyung graduated from Mogye High School in February 1994. He entered Seoul National University in the following month. He received his B.S. in civil engineering in February 1998. He entered graduate school in Seoul National University in March 1998, and received a Master of Science degree in civil engineering in February 2000. After graduation, he joined Korea Military Academy as instructor. He gave lectures in the class of structural analysis, design of reinforced concrete structure, etc. He spent 3 years at Korea Military Academy, and he enrolled in the doctoral program in Texas A&M University and received his Ph.D. degree in December, 2007. His research areas of interest are solid mechanics, dynamic behavior of structure, nondestructive damage detection. His email address is greatcivil@hotmail.com and mailing address is 127-5 Samsung dong #102-104 Gangnamgu Seoul, Korea 135-090.